

1.0 FINAL SCIENTIFIC/TECHNICAL REPORT

**Prepared for
THE U.S. DEPARTMENT OF ENERGY**

**“INDUCED POLARIZATION WITH
ELECTROMAGNETIC COUPLING: 3D SPECTRAL
IMAGING THEORY: EMSP PROJECT NO. 73836”**

**Principal Investigator: F. Dale Morgan
Earth Resources Laboratory
Department of Earth, Atmospheric, and Planetary Sciences
Massachusetts Institute of Technology
Cambridge, Massachusetts 02139**

**Collaborator: David Lesmes
Boston College
Chestnut Hill, Boston, MA**

AWARD NO. DE-FG07-96ER14714

Project Duration: September 15, 1996–September 14, 2004

2.0 Table of Contents

3.0 Executive Summary	4
4.0 Research Objectives	6
5.0 Methods and Results	7
5.1 Field Method and Results	8
5.1.1 Instrumentation	8
5.1.2 Electrodes	8
5.1.3 Data acquisition geometry	9
5.1.4 Modeling and Inversion	10
5.1.5 Application of 2D IP inversion for Contaminant Mapping	12
5.1.6 Application of 3D IP inversion for Contaminant Mapping	15
5.1.7 Coupling problems	20
5.1.7.1 Inductive coupling	20
5.1.7.2 Capacitive couplings	21
5.2 Laboratory Method and Results	22
6.0 Relevance, Impact and Technology Transfer	23
6.1 Impact of the Project Result on DOE environmental management problem	
7.0 Project Productivity	24
8.0 Personnel Supported	26
9.0 Publications	27
9.1 Articles appearing in peer-reviewed journals	27
9.2 Articles in conference proceedings and unreviewed publications	27
9.3 Articles accepted/submitted for publication	28

10.0 Interactions	29
11.0 Transitions	30
12.0 Patents and Copyrights	30
13.0 Future Work	30
14.0 Literature Cited	31
15.0 Feedback	32
16.0 Appendices	
16.1 Copy of Publications	
16.1.1 Paper to be submitted to Geophysics (Sogade et. al.)	
16.1.2 Paper to be submitted to Geophysics (Sogade et. al.)	
16.1.3 Paper to be submitted to JGR (Sogade et. al.)	
16.1.4 Paper to be submitted to JEEG (Sogade et. al.)	

3.0 Executive Summary

The principal objective of the project was to develop a non-invasive imaging technique, based on spectral induced polarization (SIP), to characterize in-situ distribution of organic and inorganic contaminants. This was to be an advance over a similar technique offered by the DC resistivity method. The motivation for the choice of IP over resistivity is rooted in the fact that resistivity response is governed by volume distributions of electrical parameters and therefore is relatively insensitive to small changes contributed by the presence of contaminants. IP response on the other hand is governed by the electrochemical properties of the rock-grain pore-fluid interface, which can be significantly altered by the incoming contaminant (ions) over long residence times. Small concentrations of contaminants are the rule rather than the exception thus, the detection threshold for IP, which is more sensitive to small concentrations, is much lower than for resistivity (IP field threshold for PCE/TCE is about 1 μ g/g). Additionally, the observation that IP depends on the chemistry of the contaminants provided the motivation that a spectral IP response could lead to a database of identifying signatures by which contaminants can be discriminated.

The tasks designed to meet the preceding objectives were divided into field and laboratory work. The laboratory work was to extend on reported connections between spectral IP and the chemistry of contaminants, which eventually might lead to a database of identifying spectra. Laboratory IP response depends on the microgeometry of the rocks as well as the chemistry of the intervening pore fluids. A study of the relative contribution of each will involve a decomposition of the two effects. The laboratory work reported here was able to achieve this. Consequently, the spectral data, based on a microscopic physico-chemical model developed in this project were used to invert for the grain size and effective grain size distribution of sedimentary rocks. Inversion was also used to determine the formation factor, the porosity, the specific surface area, and the apparent surface fractal dimension. Furthermore, we established that the IP response changed with concentration of the same solution chemistry. In addition, solution chemistry, valence of the constituent ions, and ionic radius, were shown to affect the IP responses. However, during the lifetime of the laboratory component of the project

(September 1996 to September, 2000), a database of spectral IP signature was not achieved. Two main emerging problem areas remain outstanding with regards to laboratory models, the effect of microbial activities on polarization, and the effect of aging or long residence time of contaminants on the eventual polarization property of the media.

The laboratory component was to provide some of the tools necessary to accomplish our stated objectives in the field. The additional tools needed for field IP are the instrumentation for generating field data, and forward/inverse codes to understand the data and to create a physico-chemical image of the sub-surface. IP can be used for mapping polarization distribution in a dispersive earth media. In a heterogeneous earth media, the dispersive polarization property of constituent parts can achieve spectral amplitudes at different frequencies in the frequency domain or polarization or relaxation times in the time domain. Therefore field deployment of IP must of necessity be carried out within a spectral or time window that accommodates the extremes of characteristic frequencies or times related to contamination-produced polarization phenomena in the earth. To process the acquired data, we have developed 2D/3D time and frequency domain forward and inverse algorithm/codes that invert the data into chargeabilities and complex resistivities/conductivities respectively. The codes are based on a DC formulation, with the implication that inductive coupling problems have to be separately addressed. Additionally, the codes are fast, robust, and stable.

A number of experiments were designed to evaluate the possibility of mapping subsurface distribution of contaminants at the A-14 Outfall area of the Savannah River Site (SRS) using IP. The severe space limitations at SRS, and the intended target depths of the contamination (between surface and 85ft), precludes surface array deployment, and necessitated the deployment of cross-borehole acquisition geometries. In 2001 2D cross-borehole SIP measurements were carried out at a base frequency of 1/32Hz and its first four odd harmonics. The results were processed to successfully locate the contaminated region at the 1 to 3 $\mu\text{g/g}$ level. In March 2003, and June 2004, 2D and 3D cross-borehole SIP data were acquired at two base frequencies of 1/16 Hz and 1/4Hz, in another area of the A-14 Outfall where significant contamination had been earlier confirmed. After the

March 2003 data acquisition, five ground-truth boreholes were drilled in the area by SRS engineers (to depths of about 115ft), where PCE and TCE concentration data were sampled at 1ft interval. The March 2003 SIP data was processed by the 3D DC complex resistivity code developed for this project. The results show an outstanding log linear correlation of imaginary conductivity with the ground-truth PCE concentration data. Based on this correlation it was possible to create a 3D conceptual model of the contaminant concentration distribution at this site that showed considerably more detail than the one created by SRS engineers using the ground-truth data. In addition, the processing of the 2004 data revealed that significant contaminant mass had moved or depleted at this site during the period March, 2003 to June, 2004. The project was not able to perform ground-truth confirmations of the movements. However, some movements are expected based on the March 2003 ground-truth activities and nearby remediation activities using Soil Vapor Extraction.

The project therefore has been able to develop a 3D PCE/TCE mapping technology based on SIP, which can produce a fair estimate of the concentration distribution in 3D. This technology has not been applied to other contaminant types however. In addition, the project has produced documents which can guide field deployment of this technology, suggest areas for instrumentation improvements, and dealt with capacitive coupling problems. The aspect of the project which was to deal with inductive coupling was not completed because of re-directions to allow for field deployment of the already developed 3D DC processing algorithm, which can be safely applied at low enough frequencies (less than 1 Hz).

4.0 Research Objectives

The project was designed as a broad foundational study of SIP for site characterization. It encompassed laboratory and chemistry effects on Induced Polarization (IP), an investigation of electromagnetic coupling (emc) noise, and development of 3D modeling and inversion codes.

A systematic mathematical basis for the experimentally observed IP response of rocks and soil appeared in the 1950's. One of the most popular mathematical models developed during this time is attributed to Seigel (Seigel, 1959). It was observed that IP

could monitor the interface phenomena between electrolytes and conductive materials in the ground, such as metal bodies or metallic minerals (Angoran, 1975; Morgan, 1981). Until recently, induced polarization (IP) was exclusively used in the mineral exploration field. However, over the last two decades IP measurements have improved and new applications of IP have emerged in the environmental field. Recent applications of IP to environmental problems include Barker (1990), Shi (1998), Morgan et. al. (1999), Sogade et al. (1999) Briggs et al. (2003, 2004) and others. It has been established that spectral IP responses of contaminated rocks can be used to characterize and identify contaminants and in some cases provide information on interface chemistry (Olhoeft, 1985,1992), (Börner et. al,1993). Börner et. al. (1993) conducted laboratory studies of the effects of organic and inorganic contaminants on the complex conductivity responses of clay, and shaly sandstone samples, over the frequency range of 10^{-1} to 10^3 Hz. Their results showed that the frequency range of interest extends beyond 1 kHz. Soininen et al. (1994) showed from laboratory core samples that the ability to differentiate low grade dissemination and net-textured compact ore depends on the information derived from spectral IP phase above 1 kHz.. This project was designed to extend these mainly laboratory-based studies and provide a practical means of applying spectral IP to mapping and possible discrimination of contaminant types.

5.0 Method and Results

The tasks necessary to achieve the stated objectives can be divided into two main focus areas. These are field SIP and laboratory SIP. Field SIP involves instrumentation (Transmitters, Receivers, electrodes) and field methodologies (electrode acquisition geometry to produce optimal data, wiring layout, and logistics) required for the creation of spectral field IP data. It also involves the creation of forward and inverse codes to transform the field data into subsurface distribution of spectral IP parameters, which are then described or interpreted in terms of contaminant properties. The Earth Resources Laboratory (ERL) of the Massachusetts Institute of Technology undertook the field IP component of the project.

The laboratory IP component involves studies to establish a connection between the spectral IP parameters and the different physical and chemical mechanisms. This might eventually lead to a database, which will guide the interpretation of the field spectral IP parameters. This task was undertaken at the collaborating institution, Department of Geophysics, Boston College (BC).

5.1 Field Method and Results

5.1.1 Instrumentation

In the field experiments described in this report we have used two commercially available data acquisition systems, the IRIS ElrecT for time domain IP (TDIP) measurements and the Zonge ZT-30 and GDP 32-II for both time and frequency domain measurements. Field acquisition of SIP data is time intensive. Our analysis has shown that to perform spectral characterization with IP in a reasonable time budget of a day or two requires an order of magnitude increase in acquisition speed. Some consideration was therefore given to enhancements that can provide significant speed gains over currently available SIP instrumentation and is detailed in Appendix 16.1.4.

5.1.2 Electrodes

Current-bearing electrodes for IP field deployment can be metallic electrodes. However, potential electrodes must be non-polarizing and its spectral response must not overlap those of signals to be measured. Non-polarizing Ag/AgCl electrodes have this desirable property and have been designed and fabricated for use in our SIP field applications. In addition, some of the time-lapse field application results presented in this report required acquisition of cross-borehole spectral IP data at times separated by more than a year. This necessitated during the course of this project the design and fabrication of watertight potential electrodes that can be emplaced in boreholes for years.

Since watertight borehole potential electrodes with all the desirable properties - non-polarizable, low noise and long-term stability, low effective impedance - for spectral IP application were not commercially available, considerable project time was devoted to the design, fabrication and testing of these electrodes. The electrodes were made from Ag/AgCl meshes dipped in gelled agar-agar solution saturated with KCL, and the electrode was housed in a PVC tube with a porous cup plugging one end of it and permanently sealed at the other end. Figure 1 shows some samples of completed potential

electrodes, 28 of which were manufactured for deployment in the field boreholes. Also, 28 current electrodes were made from elemental copper pipes.

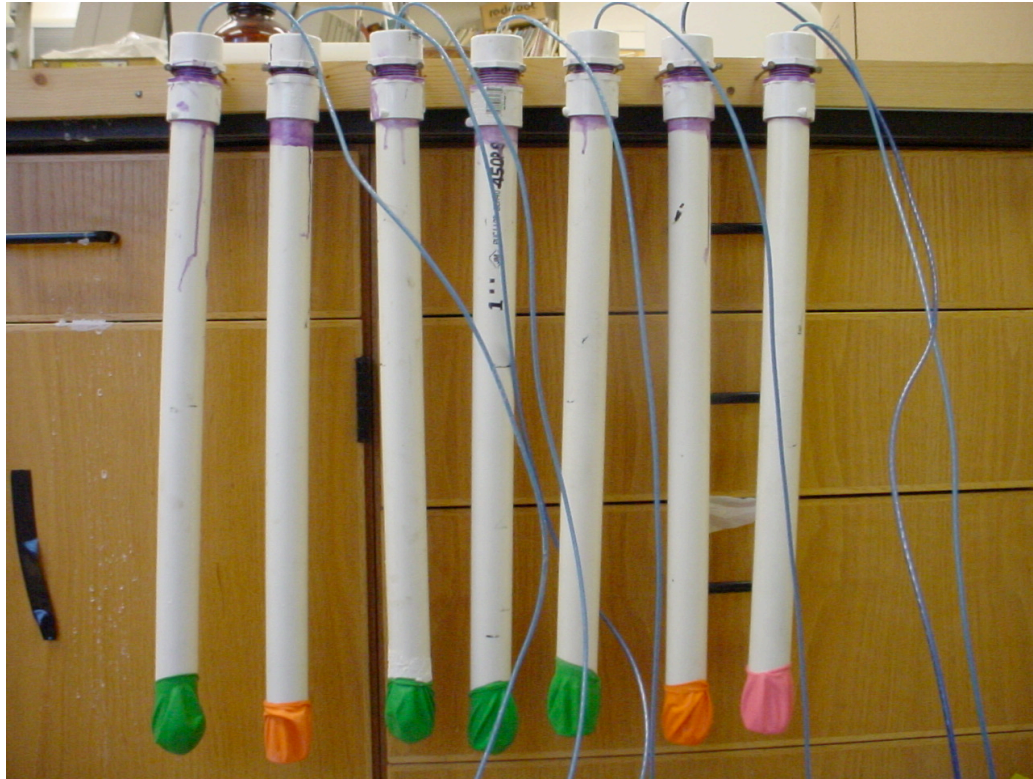


Figure 1: Example of completed potential electrodes shown with protective caps.

These electrodes were field deployed in September of 2002 and have been used successfully for measurements in March 2003 and June 2004.

5.1.3 Data acquisition geometry

Acquisition geometry involves the placement of transmitter and receiver electrodes in such a way that optimal datasets are acquired. Optimality in this context means that the acquired data uniformly samples the volume of interest and avoids some of the identified pit-falls. Designing optimal acquisition geometry can take a full project lifeline of its own. Thus, we have used heuristic and semi-empirical methods to design efficient data acquisition geometry for 2D and 3D cross-borehole spectral IP data. This acquisition geometry capitalized on diagonal pairs of current electrodes between boreholes and avoided using entirely horizontal pairs in order to avoid highly conductive horizontal channels that might act as current traps. By using only non-polarizing electrodes for potential measurements, it also avoided the electrode memory problem,

which arises when current-bearing (metallic) electrodes becomes polarized and used for subsequent potential measurements before full depolarization. Examples of the data acquisition geometries and further discussion can be found in appendices 16.1.2 and 16.1.3.

5.1.4 Modeling and Inversion

The project developed a 3D complex resistivity forward and inverse code (Shi, 1998) for inversion of frequency-domain IP data. The algorithms accommodate a general earth model with a complex electrical resistivity as a function of frequency and 3D spatial position. The forward problem is solved by a complex bi-conjugate gradient method, while the regularized inverse problem is solved by the complex nonlinear conjugate gradient method. In the initial phase of the development, synthetic data generated by a contaminated plume model shown in Figure 2 have been inverted using the complex resistivity codes. The synthetic data and the inversion results are shown in Figures 3 and 4.

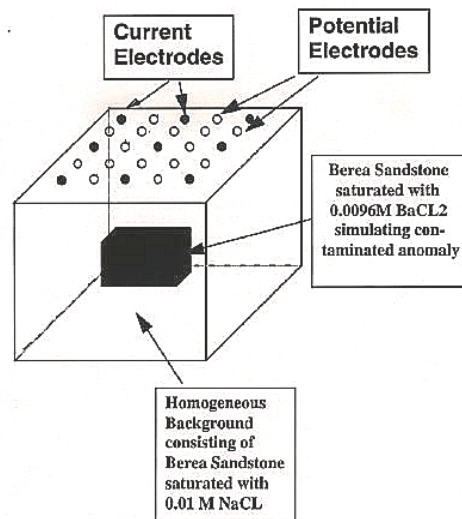


Figure 2: Model of a contaminated plume embedded in a homogenous background. The complex resistivity parameters as a function of frequency are based on the laboratory results. Synthetic IP data were computed for the electrode array at the surface.

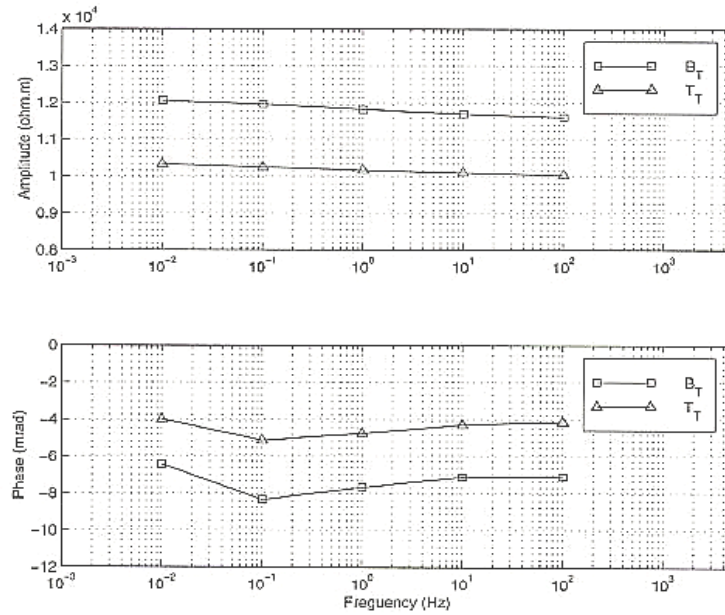


Figure 3: Frequency variations of amplitude and phase for two materials (Berea sandstone saturated with 0.01M NaCl, and Berea sandstone saturated with 0.0096M BaCl2). Data were taken from our laboratory studies.

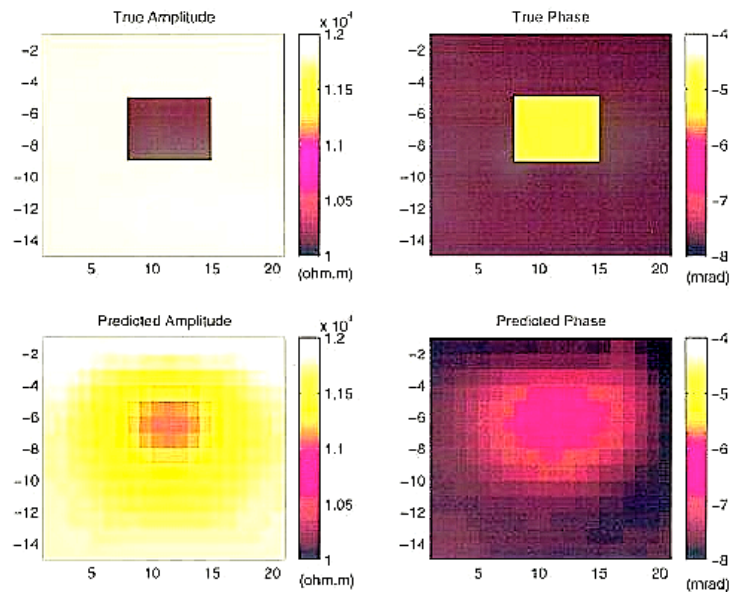


Figure 4: Inversion for $f=1\text{Hz}$ (bottom) are compared to the “true” model (top).

Each frame shows a cross-section through the center of the 3D model. The amplitude of the complex resistivity is shown on the left, and the phase is shown on the right. The inversion results are excellent compared to the “true” model. The amplitude almost exactly matches the model in location and shape. The phase was able to locate the zone of the target but not the shape. Other details can be found in Weiqun Shi’s thesis (Shi, 1998; appendix 16.3.2 of Morgan and Lesmes, 2001). Extensions to the inversion algorithms including cross-boreholes geometries were added later in the project and details can be found in appendices 16.1.3.

In addition, ancillary to the main focus of the project, 2D complex resistivity and TDIP forward and inverse codes were developed to evaluate the suitability of both 2D TDIP and SIP inversions for contaminant mapping (see Appendix 16.1.2).

5.1.5 Application of 2D IP inversion for Contaminant Mapping

The interest in 2D applications stems from the fact that 2D experiments are easier to plan and are faster both in data acquisition and processing times than 3D. During the initial part of the project, there was interest in establishing quickly that IP signals measured over contaminated subsurface can be inverted to produce a distribution of the polarized volume and that the resulting polarized volume is related to the contaminant distribution as expected from laboratory studies. To this end the developed 2D TDIP inversion was applied to process 2D time-domain data collected in a surface acquisition over a contaminated site at the OTIS air force base at the Massachusetts Military Reservation area. The 2D inversion algorithm recovers a 2D distribution of IP chargeability of the subsurface and is displayed as a ‘tomogram’ in figure 5. The results, when compared to the few well samples available on the survey line, show that the chargeability tomogram faithfully renders the subsurface distribution of the contaminants (Figure 5 below).

A more detailed description of this and the results of similar investigations using time-domain IP at two other sites can be found in appendix 16.1.2 of Morgan and Lesmes (2001).

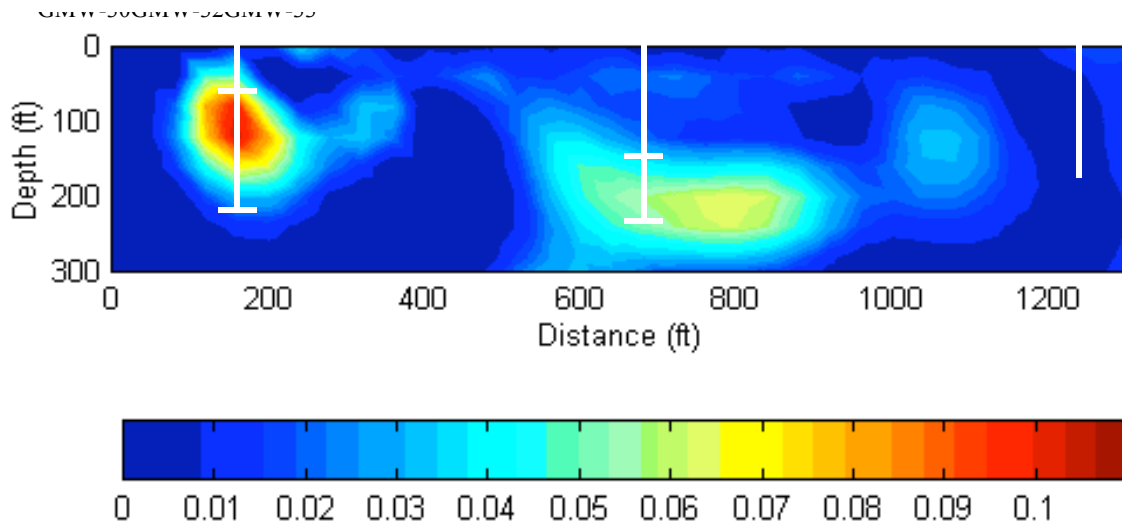


Figure 5: Chargeability tomogram showing the ground-truth wells (as white vertical bars) and the zones where significant contamination was recorded in each (between white horizontal bars).

We participated in a DOE-sponsored exercise (DOE Contract #DE-AM26-99FT4065 via Concurrent Technology Corporation) to assess the state-of-the-art in cross-borehole IP technology for delineating subsurface contaminants a project, which overlaps with this one. 2D cross-borehole spectral Induced Polarization (SIP) measurements were carried out at the two different PCE/TCE contaminated locations of the A-14 Outfall area of the Savannah River Site (SRS), in Aiken South Carolina in July 2001 (using 1/32Hz base frequency and first four odd-harmonics), and March 2003 (using 1/16Hz and 1/4 Hz base frequencies including the first four odd-harmonics for each) respectively, referred to henceforth as FY01, and FY03. The FY01 exercise also acquired a limited set of 2D time-domain cross-borehole IP data. Both the FY01 and FY03 results were ground-truthed by borehole sampling of contaminant concentration data (7 boreholes, CRS-1 to CRS-7 for FY01 and 5 boreholes, CR-1 to CR-5 for FY03). As part of the currently reported project repeat measurements at the FY03 site were carried out in June 2004, henceforth referred to as FY04, to evaluate suitability of using IP in monitoring mode.

The results of the FY01 measurements at 1/32 Hz processed by 2D Complex resistivity inversion are shown in figure 6 as panels of interpolated PCE concentration data (in $\mu\text{g/g}$), the IP phase (in mrad), imaginary conductivity (in S/m), and the IP chargeability (in V/V).

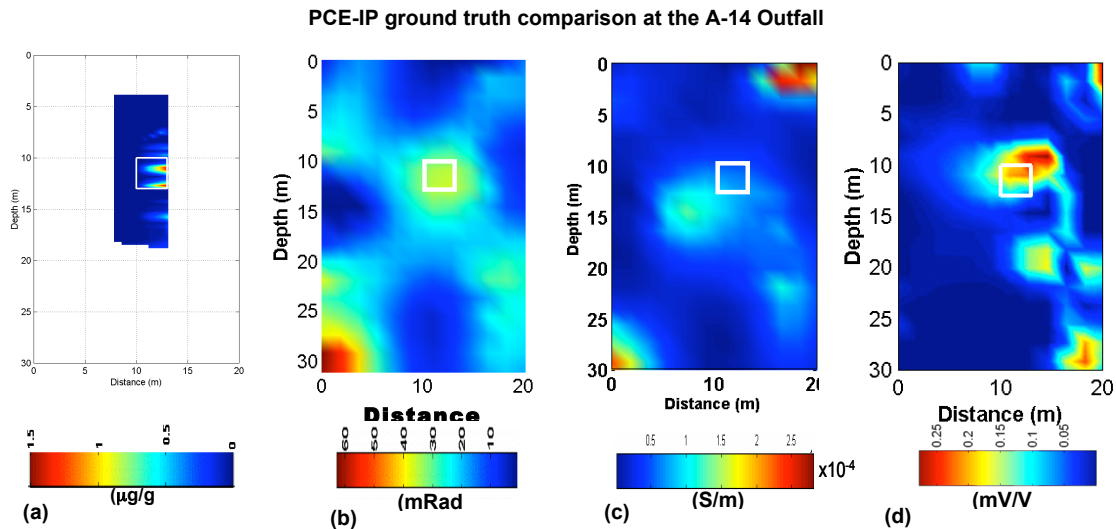


Figure 6: Comparison of the ground-truth PCE anomaly (a), the SIP anomaly (b), the imaginary conductivity anomaly (c), and the TDIP anomaly (d). Panel a has been generated by taking a slice along the imaged panel from the volumetric PCE concentration (interpolated from the CRS series of boreholes, taken during the FY01 ground-truth exercise). Panels b, c and d are the inversion results along the imaged panel.

It can be seen that the phase matched very well with the location of the contaminant anomaly, the chargeability anomaly agrees closely with the contaminant anomaly, but the imaginary conductivity is off-center to the left following a conductive feature revealed in the resistivity panel (not shown).

Figure 7 is an example result of the 2D SIP inversion of the 1/16 Hz FY03 data. It shows the result of one of the six inverted 2D panels and compares PCE concentration data (in mg/kg), with inverted resistivity magnitude (in Ω -m), SIP phase (in mrad), and imaginary conductivity (in S/m), respectively. It is seen that both the phase and imaginary conductivity anomalies correlate very well with the interpolated ground-truth PCE concentration data and the resistivity panel revealed that the contaminated zone is conductive. Details of the 2D experiments can be found in Appendix 16.1.2.

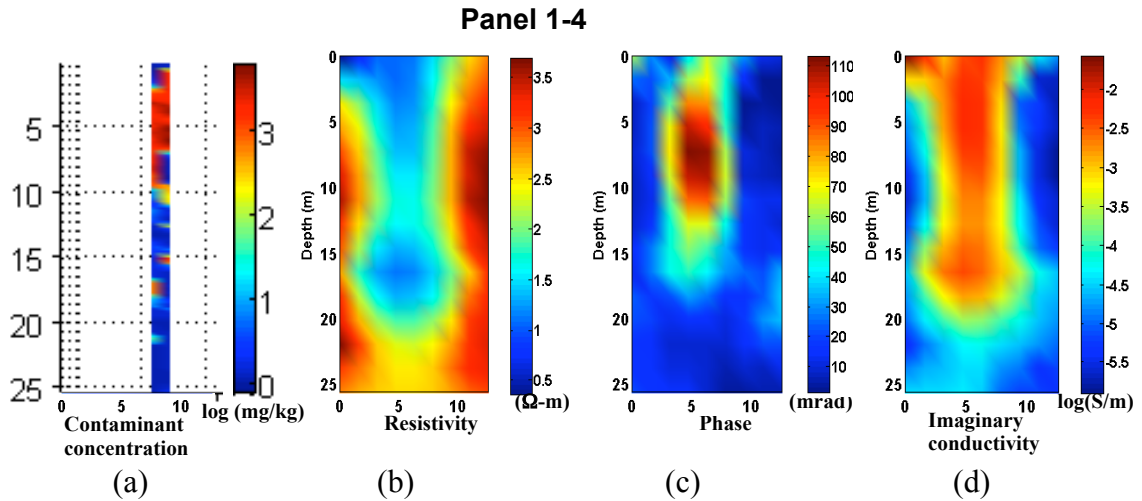


Figure 7: Comparison of the ground-truth PCE anomaly (a), the magnitude resistivity anomaly (b), the SIP phase anomaly (c), and the imaginary conductivity anomaly(d).Panel a is interpolated contaminant concentration data, and panels b, c, d, are the resistivity, phase, and imaginary conductivity produced by 2D inversion of the FY03 1/16 Hz data. Note the good visual correlation between the concentration panel and the phase.

5.1.6 Application of 3D IP inversion for Contaminant Mapping

Coincident with the FY03 and FY04 2D cross-borehole data described in section 5.1.4 above, 3D cross-borehole spectral IP data were acquired at a single location in the A-14 Outfall area of SRS, at base frequencies of 1/16 and 1/4 Hz respectively. Four boreholes, MIT-1, MIT-2, MIT-3, and MIT-4, drilled to 84 ft were equipped with the transmitter and receiver electrodes used for the measurements. The transmitter and receiver electrodes were placed intermittently 6ft apart in the four boreholes. The data were processed by the 3D complex resistivity code and the results are compared to measures of IP such as phase, as well as imaginary resistivity and conductivity. Imaginary conductivity provided the best correlation with $\log_{10}(\text{PCE})$ concentration data across all ground-truth boreholes, if it is scaled by a multiplicative scaling factor of about 20000. The result comparing $\log_{10}(\text{PCE})$ concentration with imaginary conductivity is

shown in figure 8 for the 1/16 and 1/4 Hz data, with the 1/16 Hz data showing better correlation with the concentration data. Note that only the CR-1, CR-2, and CR-3 borings were in the volume designed to be investigated by our SIP experiment. In addition, it can be noticed that the detection threshold for imaginary conductivity is about 1mg/kg (1 μ g/g), the zero point on the horizontal axis.

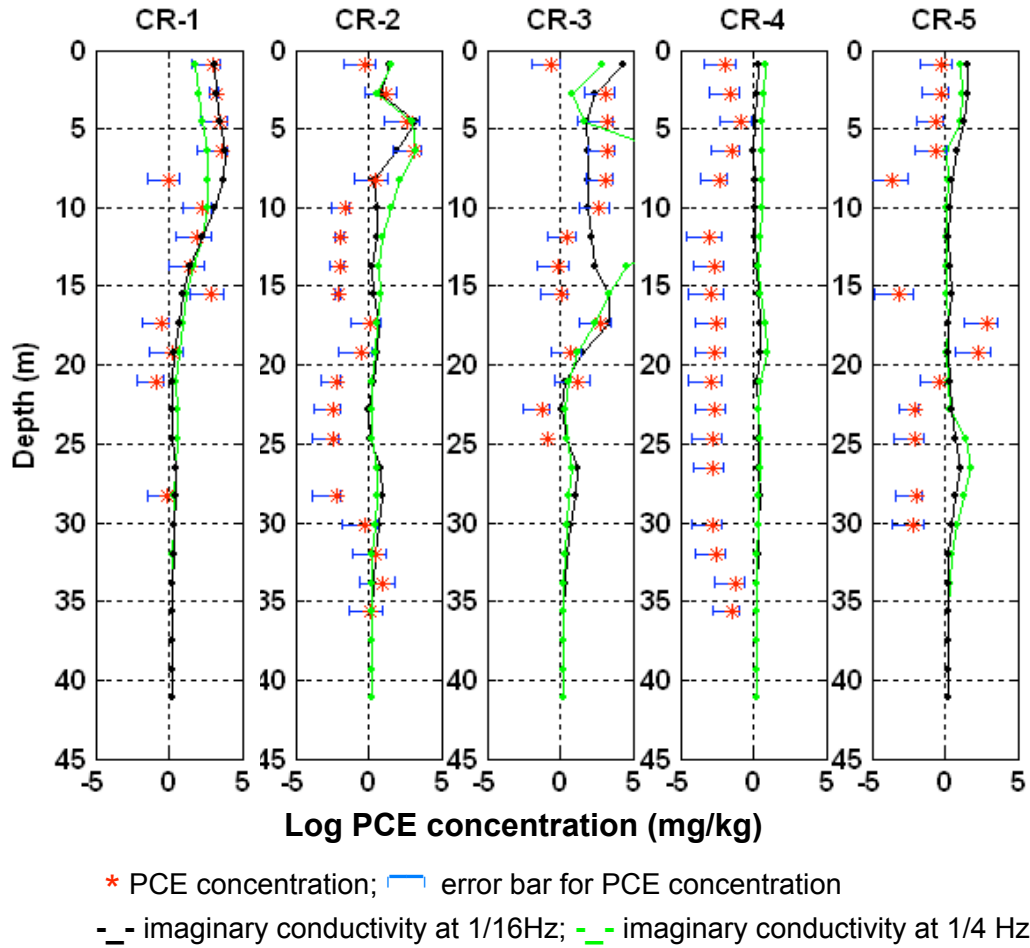


Figure 8: Imaginary conductivity from 3D SIP inversion of the March 2003 data, plotted against the concentration data from the five CR ground-truth wells. Note that the imaginary conductivity was scaled by a constant scalar multiplicative value of 20000 to bring all the data aligned as shown. Note also the remarkable correlation at 1/16 Hz.

Figure 9 shows a plot of log (PCE) concentration versus imaginary conductivity for the 1/16 Hz result. Apart from the two outlier points at the top left of the spot corresponding to a point each in boreholes CR-1 and CR-3, it is evident there is a log linear relationship

between the PCE concentration and imaginary conductivity. Outlier points might be related to the disparity between block volume averaging that the inversion performs on the imaginary conductivity data in its 5ftx5ftx6ft block and the average volume estimate derived few point samplings in a 3in borehole.

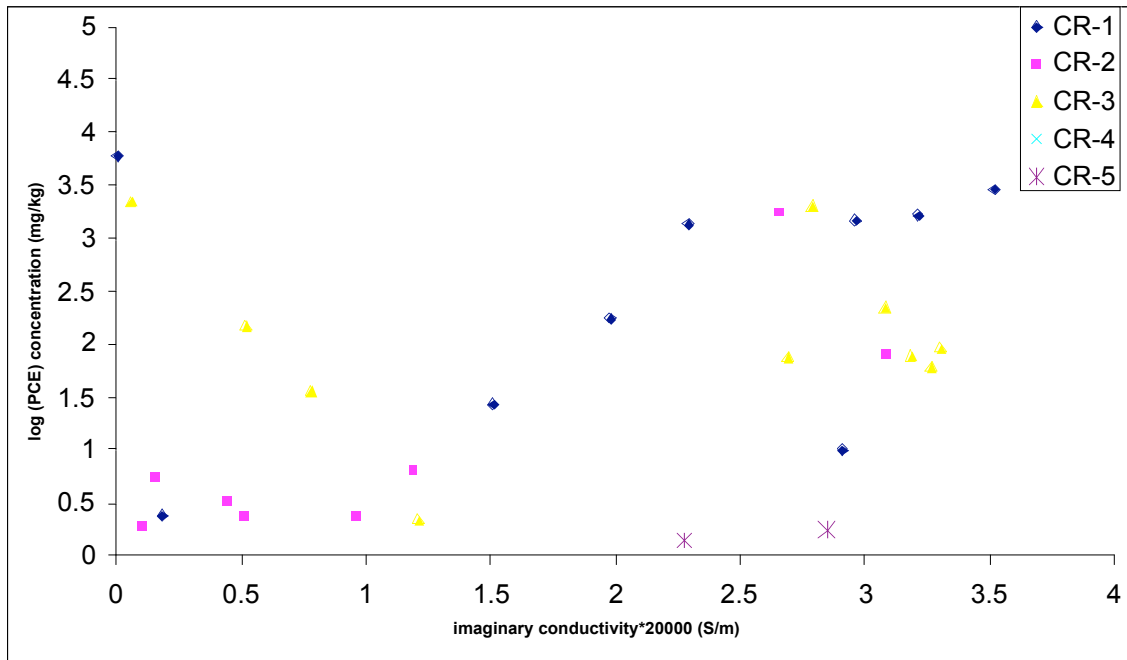


Figure 9: Scatter plot of log (PCE) concentration at the 1mg/kg level and above versus imaginary conductivity scaled by 20000, for the five boreholes CR-1 to CR-5. Note that there is no entry for CR-4 at this level, and the 2 entries for CR-5 appear as outliers.

Bolstered by the realization that for this site, imaginary conductivity is linearly correlated with the log₁₀(PCE) concentration we have created a 3D conceptual image of an imaginary conductivity derived contaminant mass at the investigated site for a concentration of 10mg/kg and above as shown in figure 10.

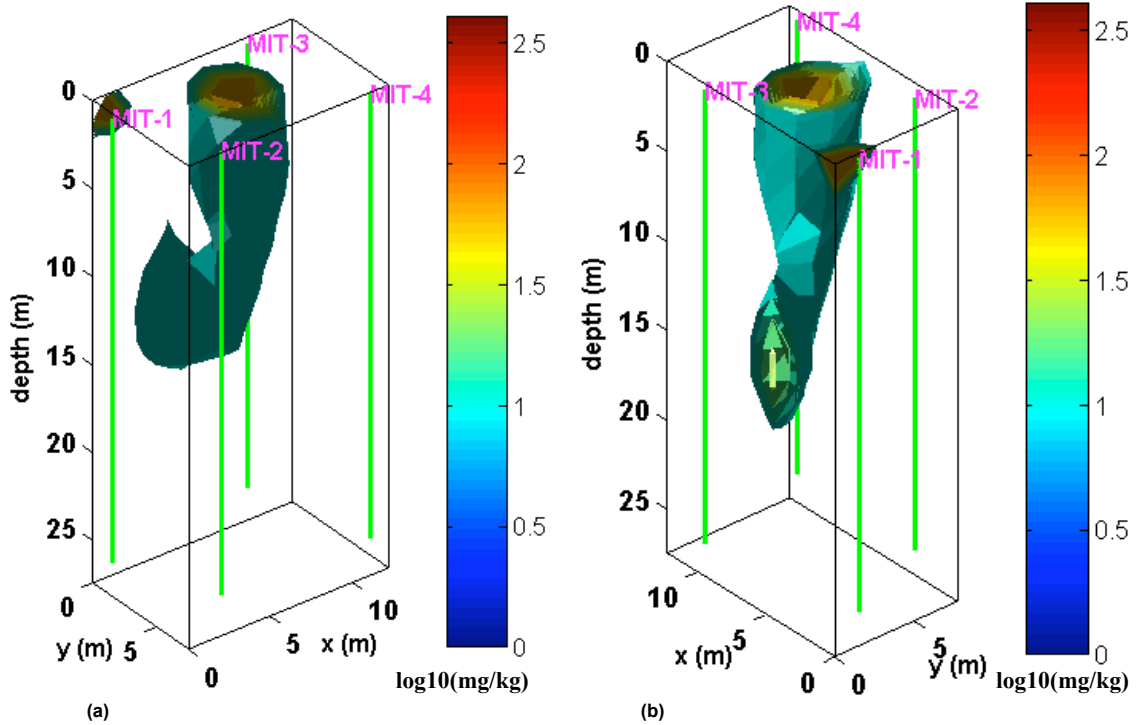


Figure 10: Two views of the 3D PCE concentration (10mg/kg level and above) distribution predicted by SIP at the investigation site near the A-14 Outfall area

The image in figure 10 reveals that the contaminant mass is heavily concentrated at the surface areas near the entry point between panels MIT-2/MIT-4 and MIT-1/MIT-3, and subsequently traveled downwards and turned in a horizontal direction to travel outside of this volume along panels MIT-1/MIT-3 in a SE-direction. This level of detail is not available from conceptual models derived from the five CR boreholes by Rossabi et al. (2004).

Using imaginary conductivity as a direct indicator of contamination, the repeat measurements carried out in FY04 showed that significant contaminant movements have occurred in the area since the measurements of FY03 as seen by the equivalent results in figure 11. Note the high near surface values of the imaginary conductivity in all CR locations except CR-2.

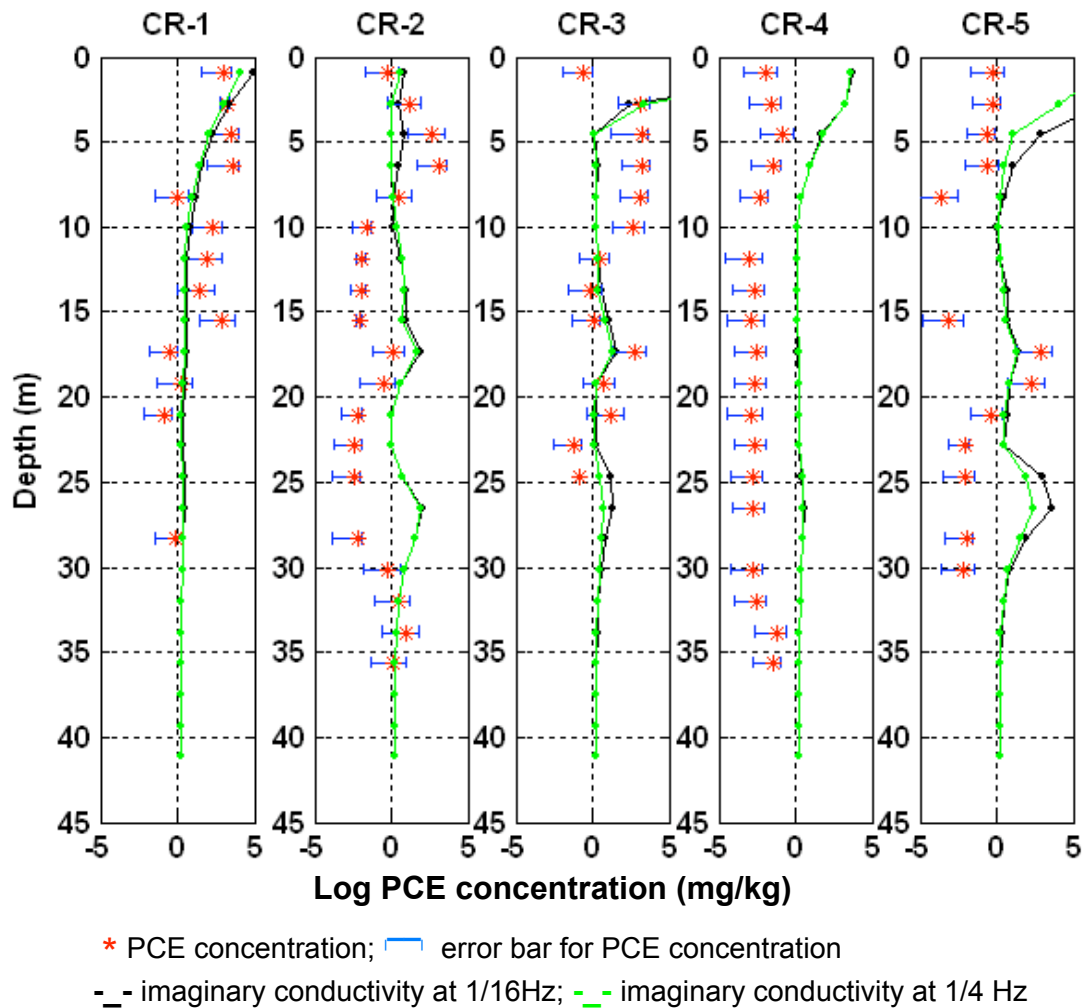


Figure 11: Imaginary conductivity from 3D SIP inversion of the June 2004 data, plotted against the concentration data from the five CR ground-truth wells. Note that the imaginary conductivity was scaled by a constant scalar multiplicative value of 20000 to bring all the data aligned as shown. Note also the significant loss of polarization at the concentration peaks of 2003 and the small increases at 17.5m depth on CR-2 and CR-3 that were not there in 2003.

Figure 12 shows a 3D volume plot of the predicted PCE concentration based on the imaginary conductivity of the inverted FY04 data. The plot is shown at the level of 1mg/kg and above because of the lower predicted concentrations in 2004.

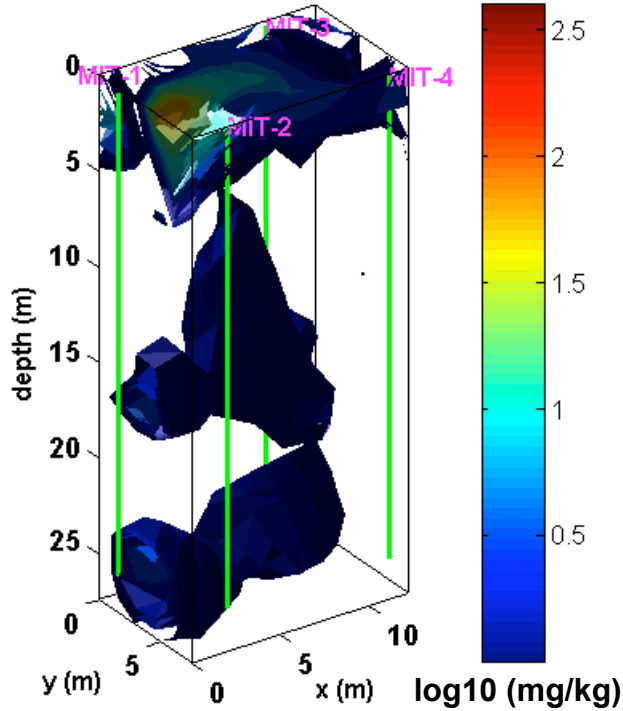


Figure 12: A view of the 3D PCE concentration (1mg/kg level and above) distribution predicted by SIP at the investigation site near the A-14 Outfall area based on June 2004 data

In conclusion, it can be seen that SIP has performed creditably at this site as a contaminant mapping tool that can provide significantly more detail than conventional borehole sampling. SIP has also shown evidence of significant contaminant movement in the interval between our two surveys in March 2003 and June 2004. Some of the movements are expected due to the ground-truth boring activities after the 2003 measurements and also nearby remediation activities targeted at capturing the target zones between 7ft and 21ft where the most movements have occurred. However, the movements predicted by our FY04 spectral IP experiment was not ground-truthed. Further details can be found in Appendix 16.1.3.

5.1.7 Coupling problems

5.1.7.1 Inductive coupling

For time varying systems such as SIP or time-domain IP (TDIP),

the transmitter and receiver circuits are coupled inductively like transformers with the earth and/or free space being the intervening medium between them. Thus, the accurate model for the transmitter-receiver-earth system should accommodate the inductive couplings. At DC, the inductive coupling action breaks down, and only galvanic couplings occurring through direct distribution of currents exists. The complex resistivity code developed at the end of the first project (September, 1996 to September, 2000) was based on the DC model. Our investigations at the end of that period revealed that inductive coupling would be a problem in the application of the DC model if the frequencies exceed about a 100 Hz for surface array deployments at environmental field sites. The case was made for accommodating inductive coupling in the modeling rather than treating it as data distortion. This aspect of the project was not completed during the second part of the project (September, 2000 to September, 2004). The reason is related to project re-directions to allow time for demonstrating the practical utility of the SIP methodology for contaminant mapping for the range of frequencies where the DC model will work i.e. below 100 Hz. For example, in attempts to use spectral IP at SRS, it was realized that severe spatial constraints would necessitate deployment of a cross-borehole acquisition system, which necessitated major programming alterations to the DC forward and inverse codes. The borehole acquisition systems also featured severe capacitive couplings and challenges with monitoring electrodes that were addressed as part of the project. If SRS is a good model for most sites where SIP might be deployed for contaminant mapping, then cross-borehole acquisition is likely to be a permanent feature of the spectral IP mapping technology.

5.1.7.2 Capacitive couplings

In field deployment of IP where cross-borehole acquisition geometries are needed, severe capacitive coupling problems show up, mostly due to the proximity of the transmitting and receiving wires. Studies were carried out to understand the capacitive coupling problem and to find ways to mitigate its effect. Our studies show that the most practical solutions are (1) increasing the input impedance of the receiver system front-end, (2) careful wiring layout that separates the transmitter and receiver wires going into the boreholes as much as possible, and (3) capitalizing on array geometries that will not aggravate the problem.

All these solutions were developed for our 3D acquisitions at SRS, and further details can be found in Appendices 16.1.2, 16.1.3, 16.1.4.

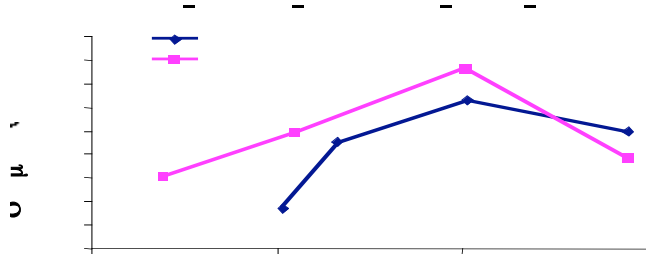
5.2 Laboratory Method and Results

The laboratory IP work involved fabrication of laboratory equipment to measure spectral IP response parameters over a frequency bandwidth ranging from 10^{-3} to 10^6 Hz. This frequency regime captures all the spectral IP parameters that may be of interest for contaminant discrimination.

David Lesmes and his group have conducted experiments at BC to study the effects of solution chemistry and microgeometry on the spectral IP response of sandstone. Results indicate that changes in chemistry affect the magnitude of the spectral IP response and changes in microgeometry affect the shape of the spectral IP response. Some of the results are shown below in figures 11 and 12.

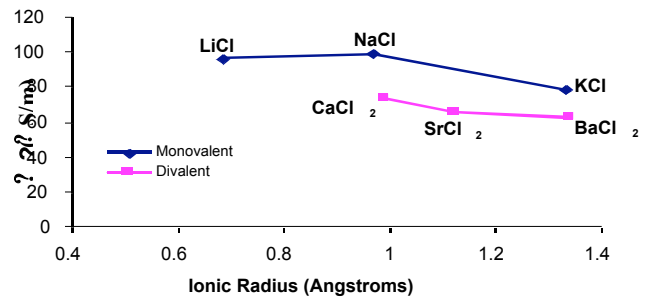
A physiochemical model, which was originally conceived by Professors Morgan and Lesmes (Morgan and Lesmes, 1994; Lesmes and Morgan, 1999), was extended (Lesmes and Morgan, 2001), and serves to interpret the spectral data both for the median grain size and effective grain size distribution of sedimentary rocks in the laboratory. Inversion was also used to determine the formation factor, the porosity, the specific surface area, and the apparent surface fractal dimension.

Response of Berea Sandstone at 1 Hz. to 100 ppm [NaCl] and 50 ppm



(a)

IP Response of Berea Sandstone at 1 Hz. pH = 8; constant solution conductivity



(b)

Figure 11: Spectral IP response with changing solution chemistry

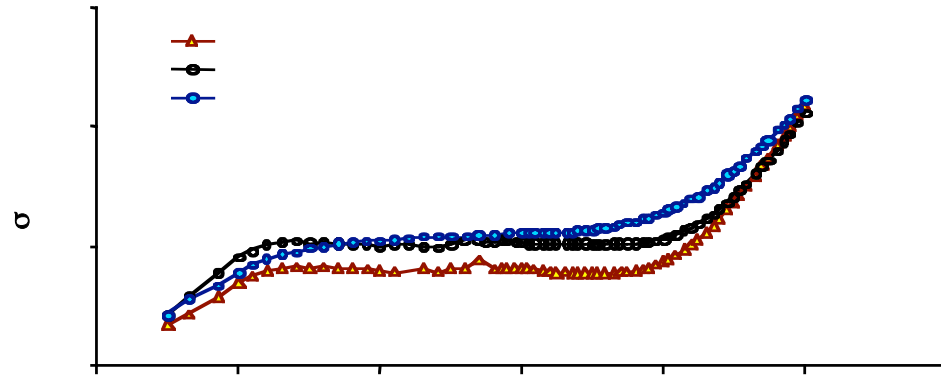


Figure 12: Spectral IP response with different solution chemistries

Further details can be found in the materials in appendix 16.1.1 of this volume, appendices 16.3.3, 16.3.4 of Morgan and Lesmes (2001) and the related publications (Frye, 1997; Sturrock, 1999; Lesmes and Morgan, 2001; Lesmes and Frye, 2001).

6.0 Relevance, Impact and Technology Transfer

6.1 Impact of the Project Result on DOE environmental management problem

The preliminary results of IP technology applied to data from a few sites showed positive results in mapping of contamination. If our experience at SRS extends to other sites it is now possible to map and directly predict the 3D volume distribution of contaminant concentration, at a level of spatial detail not easily achieved by conventional borehole sampling programs. The benefit of this technology to the DOE is the *cost reductions* from the *optimization* of well sampling achieved by integration of IP into site characterization and monitoring programs. IP has the potential to greatly reduce and

maybe eventually eliminate borehole samplings. This is borne out by the results of the SIP mapping of the contaminant plumes at SRS shown in figure 8 above and in appendix 16.1.3. This site was characterized by conventional well sampling and provides a comparison for our results. The boundary for the contaminants drawn by the few well samplings, we believe, is in good agreement with our IP predictions. In addition, our IP derived contaminant concentration shows a more realistic distribution of the contaminants, and has enough detail to develop a conceptual model.

Traditional site characterization techniques use a multi-phase approach of data collection on a statistical basis or grid to develop a conceptual model. Each phase focuses on locating the contaminant plume and follows a pre-approved work plan. Assume an hypothetical fuel leak of 20,000 gallons, a water table at 100 feet bgs, and investigation area of 50,000 ft². Assume the first phase involves drilling and sampling of 10 wells for a total cost of \$1,200,000. The use of IP as an initial investigation, before the commencement of a drilling program, could reduce the number of wells to 5. These wells would also be better placed to develop a more accurate conceptual model. The cost of the IP survey for the entire site and 5 wells would be \$700,000, a cost saving of 42% or \$500,000. Assuming the additional phases of the site characterization involved another 30 wells, a preliminary IP survey would completely eliminate the need for these wells, resulting in a savings of ~ \$3.6. Once the first five wells have been drilled, IP would be calibrated to data from these wells. The site could then be monitored entirely by IP for the remainder of its life and polarization tomograms of the earth will show the distribution and concentration of the contaminants and thus the progress of the remediation efforts. Additional wells could be drilled directed by the IP results. For this hypothetical example the savings for complete site characterization would be 70% or \$3.4 million, assuming that a total of 10 wells were drilled and three IP surveys performed whereas a traditional approach would have drilled a total of 40 wells.

7.0 Project Productivity

In the field IP part, we created a robust, stable and fast, 2D/3D code to process both time and frequency domain IP data. The codes have been used to invert data collected over a contaminated site with very good results. So, there is a technology in place that can map contaminated PCE/TCE sites and produce a 3D volume of the contaminant distribution in terms of contaminant concentration levels. This technology can be transferred as is. However, the technology has been applied only at two locations of the SRS, though successfully. The project raised the yet unanswered question about the most suitable way to ground-truth SIP predictions. For example, the ground-truth borings for the FY03 experiment used 3inch holes sampled at 1ft depth intervals with holes separated horizontally by up to 20ft, to compare to the predictions from IP inversion block sizes of 5ftx5ftx6ft, a volume ratio of 1:300. IP definitely averages over larger volumes than the small borings, and agreements between the two can only be expected if within an IP block, the ground-truth point samplings is representative of the distribution within the whole IP block. *Therefore, a carefully designed validation project with the aim to cleverly and extensively ground-truth SIP predictions is warranted.* This will increase confidence in the utility of SIP as a non- or minimally invasive contaminant mapping technology.

The aspect of the project that was to include electromagnetic coupling effects directly in the model has not been realized during the lifetime of the second part of this project. This was because of important re-directions to demonstrate the utility of spectral IP for the range of frequencies that the already developed 2D/3D codes are valid. It was realized then that to achieve targets depths at SRS a cross-borehole configuration is necessary. Substantial efforts were needed to re-tool the 3D complex resistivity code to fit this new scheme. In addition, it should be mentioned that the major utility of extending spectral IP to higher frequencies would be to accomplish discrimination of contaminant types. However, there is still paucity of laboratory evidence showing that discrimination of contaminant types is tenable.

In the laboratory IP part, which ended in September 2000, the project has made advances in understanding the complex interactions between microscopic physical and chemical properties and their contributions to the IP response. It is now possible to invert for certain physical properties like rock grain size distribution, which can lead to

hydraulic permeability predictions. Measurements have also revealed the connection between IP parameters and the chemistry of contaminants. However, the project did not provide an extensive database of signature SIP parameters that can be used for identification and/or discrimination of contaminant types. In addition the effects of microbial activity and residence time or aging on the polarization properties of contaminated soils/rocks are yet fully understood. *Further research studies along these lines are needed.*

A suite of 3D spectral IP data was acquired in June 2004 at five base frequencies spanning 1/16 Hz to 288 Hz. These have not all been analyzed in time for this report and processing all this data is likely to occupy a significant part of our research effort in the future.

The project produced one PhD thesis, three masters thesis, and one bachelor's thesis.

8.0 Personnel Supported

The following personnel including students were supported by funds derived from the project:

1. Professor F.D Morgan (Professor and PI, MIT)
2. Professor David Lesmes (Professor and Co-PI, Boston College)
3. Dr. William Rodi (Principal Research Scientist, MIT)
4. Dr. John Sogade (Postdoc, MIT)
5. Mr. Yervant Vichabian (research engineer, MIT)
6. Ms Weiqun Shi (student, MIT)
7. Mr. Philip Reppert (student, MIT)
8. Ms Amy Vandiver (student, MIT)
9. Mr. Kevin Frye (student, BC)
10. Mr. John Sturrock (student, BC)
11. Ms Lisa Lassner (student, MIT)
12. Mr. Michael Lambert (student, MIT)
13. Ms Victoria Briggs (student, MIT)
14. Mr. Darrell Coles (student, MIT)

9.0 Publications

9.1 Articles in peer-reviewed journals

9.1.1 Lesmes, D.P., and Morgan, F.D., 2001, Dielectric spectroscopy of sedimentary rocks, *J. of Geophys. Research*, **106** (B7): 13329-13346.

9.1.2 Lesmes, D.P. and Frye, K.M., 2001, Influence of pore fluid chemistry on the complex conductivity and induced polarization responses of Berea sandstone, *J. of Geophysical Research*, **106** (B3): 4079-4090.

9.2 Articles in conference proceedings and unreviewed publications

9.2.1 Briggs, V.A, Sogade, J., Minsley, B., Lambert, M., Coles, D., Reppert, P., Morgan, F.D, Rossabi,, J., and Riha, B., 3D induced polarization data from measurements to map subsurface contaminations of tetrachloroethylene and trichloroethylene, *Eos Trans., AGU, 84 (46)*, Fall Meet. Suppl., Abstract H31B-0461, 2003

9.2.2 Briggs, V.A, Sogade, J., Minsley, B., Lambert, M., Coles, D., Reppert, P., Morgan, F.D, Rossabi,, J., and Riha, B., Mapping of TCE and PCE contaminant plumes using 3-D induced polarization borehole data, presented at the Engineering and Geophysical Society, 2004 Symposium on the Application of Geophysics to Engineering and Environmental Problems, Colorado Springs, Feb. 2004.

9.2.3 Frye, K.M., 1997, The Effect of Pore Fluid Chemistry on the Spectral Induced-Polarization Response of Berea Sandstone, M.Sc. thesis, Boston College.

9.2.4 Frye, K.M., Lesmes, D.P., Morgan, F.D., 1998, The influence of pore fluid chemistry on the induced polarization response of rocks and soils, *SAGEEP Proceedings*, 771-781.

9.2.5 Lambert, M.B., 2003, Cross borehole induced polarization to detect subsurface NAPL at the Savannah River Site, South Carolina, M.Sc. thesis, Massachusetts Institute of Technology.

9.2.6 Morgan, F.D., Scira-Scappuzzo, F., Shi, W., Rodi, W., Sogade, J., Vichabian, Y., and, Lesmes, D., 1999, Induced Polarization Imaging of a Jet Fuel

Plume: Proceedings, SAGEEP, Oakland, CA, Environmental and Engineering Geophysical Society, Expanded, Abstracts, 541–548.

9.2.7 Shi, W., 1998, Advanced Modeling and Inversion Techniques for Three-dimensional Geoelectrical Surveys, Ph.D. thesis, Massachusetts Institute of Technology.

9.2.8 Shi, W., Rodi, W.L., and Morgan, F.D., 1998, 3-D induced polarization inversion using complex electrical resistivity, SAGEEP Proceedings, 785-795.

9.2.9 Morgan, F.D, Sogade, J., Lesmes, D., Coles, D., Vichabian, Y., Scira-Scappuzzo, F., Shi, W., Vandiver, A., Rodi, W., 2003, Noninvasive Contaminant Site Characterization Using Geophysical Induced Polarization, presented at the Environmental Management Science Program (EMSP) Symposium, Division of Environmental Chemistry of the American Chemical Society at the 225th ACS National Meeting, March 23-27, New Orleans, Louisiana.

9.2.10 Sturrock, J.T., Lesmes, D.P., and Morgan, F.D., 1998, The influence of micro-geometry on the hydraulic permeability and the induced polarization response of sandstones, SAGEEP Proceedings, 859-869.

9.2.11 Sturrock, J.T., Lesmes, D.P., and Morgan, F.D., 1999, Permeability estimation using spectral induced polarization measurements, SAGEEP Proceedings, 409-416.

9.2.12 Sturrock, J.T., 1999, Predictions of Hydraulic Permeability using Spectral Induced Polarization, M.Sc. thesis, Boston College.

9.2.13 Vandiver, A., 1998, Analysis of the Effects of Inductive Coupling in Induced-Polarization Surveys of Environmental Contaminants, B.Sc. thesis, Massachusetts Institute of Technology.

9.3 Articles accepted/submitted for publication

9.3.1 Sogade, J., Vichabian, Y, Scira-Scappuzzo, F., Shi, W., Rodi, W., Lesmes, D., and Morgan, F.D., 2000, Induced Polarization Detection and Mapping of Contaminant Plumes (submitted to Geophysics)

9.3.2 Sogade, J., and Morgan, F.D., 2004, Polarization Signatures for contamination: A critical Review (to be submitted to Geophysics)

9.3.3 Sogade, J., Minsley, B., Lambert, M., Vichabian, Y., Coles, D., Reppert, P., Rossabi, J., Riha, B., and Morgan, F.D., 2004, 2D Spectral induced polarization inversion of data acquired over a PCE/TCE contaminated site (to be submitted to Geophysics)

9.3.4 Sogade, J., Minsley, B., Lambert, M., Vichabian, Y., Coles, D., Reppert, P., Rossabi, J., Riha, B., and Morgan, F.D., 2004, Mapping TCE and PCE vadose zone contamination using 3-D complex resistivity borehole survey data (to be submitted to JGR)

9.3.5 Sogade, J., and Morgan, F.D., 2004, Instrumentation and coupling problems in spectral induced polarization field applications (to be submitted to JEEG)

10.0 Interactions

Participated in the following scientific meetings:

- 1) The Symposium on the Application of Geophysics to Engineering and Environmental Problems (SAGEEP) held in Chicago, IL, by the Environmental and Engineering Geophysical Society, March 22-26, 1998. Three papers were presented on results directly related to this project.
- 2) The Symposium on the Application of Geophysics to Engineering and Environmental Problems (SAGEEP) held in Oakland, CA, by the Environmental and Engineering Geophysical Society, March 14-18, 1999. One paper was presented on results directly related to this project.
- 3) Environmental Management Science Program (EMSP) Symposium, at the 225th ACS National Meeting, by the American Chemical Society, March 23-27, 2003, New Orleans, Louisiana. One paper was presented on results directly related to this project.
- 4) American Geophysical Union (AGU) 2004 Fall Meeting, by the American Geophysical Union, December 13-17, 2003. One paper was presented on results directly related to this project.
- 5) The Symposium on the Application of Geophysics to Engineering and Environmental Problems (SAGEEP) held in Colorado Springs, CO, by the

Environmental and Engineering Geophysical Society, February 22-26, 2004. One paper was presented on results directly related to this project.

11.0 Transitions

See 6.1 above.

12.0 Patents and Copyrights

Considering patent disclosure related to data acquisition geometry developed to enhance 2D/3D inversion results, and borehole long-term monitoring electrode design

13.0 Future Work

This project showed that more ground-truth data is needed to properly characterize SIP against all imaged polarization targets. In addition acquisition time will be prohibitive if SIP is to be engaged in a truly broadband mode for characterization. There is a need to determine the optimum frequency band for characterization as well as the optimum number of sampling points per decade. In a broadband mode the inductive coupling problem still remains unsolved.

We hope to be able to address these concerns/problems in our future work, and have started along that path in the area of inductive coupling. The need for instrumentation improvements were addressed by us in this project (see Appendix 16.1.4) and have suggested improvements to conventional instrumentation to allow significant gains in acquisition speed. We are currently talking to SRS engineers about a more extensive and detailed ground-truth exercise, and might pursue this, subject to availability of funds.

14.0 Literature Cited

Angoran, Y.E., 1975, Induced Polarization of Metallic Minerals: A study of its chemical basis, Ph.D. thesis, Massachusetts Institute of Technology.

Borner, F., Gruhne, M., and Schon, J., 1993, Contamination Indications Derived From Electrical Properties in the Low Frequency Range, *Geophysical Prospecting*, **41**, 83-98.

Briggs, V.A., Sogade, J., Minsley, B., Lambert, M., Coles, D., Reppert, P., Morgan, F.D., Rossabi, J., and Riha, B., 3D induced polarization data from measurements to map subsurface contaminations of tetrachloroethylene and trichloroethylene, *Eos Trans., AGU*, **84 (46)**, Fall Meet. Suppl., Abstract H31B-0461, 2003

Briggs, V.A., Sogade, J., Minsley, B., Lambert, M., Coles, D., Reppert, P., Morgan, F.D., Rossabi, J., and Riha, B., Mapping of TCE and PCE contaminant plumes using 3-D induced polarization borehole data, presented at the Engineering and Geophysical Society, 2004 Symposium on the Application of Geophysics to Engineering and Environmental Problems, Colorado Springs, Feb. 2004.

Frye, K.M., 1997, The Effect of Pore Fluid Chemistry on the Spectral Induced-Polarization Response of Berea Sandstone, M.Sc. thesis, Boston College.

Lesmes, D.P. and Frye, K.M., 2001, Influence of pore fluid chemistry on the complex conductivity and induced polarization responses of Berea sandstone, *J. of Geophysical Research*, **106 (B3)**: 4079-4090.

Lesmes, D.P., and Morgan, F.D. (2001) Dielectric spectroscopy of sedimentary rocks, *J. of Geophys. Research*, **106 (B7)**: 13329-13346.

Morgan, F.D., 1981, Electroics of Sulfide Minerals: Implications for Induced Polarization, Ph.D. thesis, Massachusetts Institute of Technology.

Morgan, F.D., Scira-Scappuzzo, F., Shi, W., Rodi, W., Sogade, J., Vichabian, Y., and, Lesmes, D., 1999, Induced Polarization Imaging of a Jet Fuel Plume: Proceedings, SAGEEP, Oakland, CA, Environmental and Engineering Geophysical Society, Expanded, Abstracts, 541-548.

Morgan, F.D., and Lesmes, D.P., 1994, Inversion for Dielectric Relaxation Spectra, *J. Chem. Phys.*, **100**, 671-681.

Morgan, F.D., and Lesmes, D., 2001, Topical Progress Report, 3-D Spectral IP Imaging: Non-Invasive Characterization of Contaminant Plumes, submitted to DOE - grant number: DE-FG03-96ER 14714.

Olhoeft, G., 1992, Geophysical Detection of Hydrocarbon and Organic Chemical Contaminants, SAGEEP proceedings, Oakbrook, IL, 587-594.

Olhoeft, G., 1985, Low Frequency Electrical Properties, *Geophysics*, **50**, 2492-2503.

Rossabi, J, Riha, B., and Jackson, D., 2004, Sediment Sampling at the A-014 Outfall for Comparison with Complex Resistivity Measurements, proceedings of the Symposium on the Application of Geophysics to Engineering and Environmental Problems, 22-26 February 2004, Colorado Springs, Colorado, Environmental and Engineering Geophysical Society, Denver, CO. p 484-495

Seigel, H. O., 1959, Mathematical Formulation and Type Curves for Induced Polarization, *Geophysics*, **24**, 547-565.

Shi, W., 1998, Advanced Modeling and Inversion Techniques for Three-dimensional Geoelectrical Surveys, Ph.D. thesis, Massachusetts Institute of Technology.

Sogade, J., Vichabian, Y., and Morgan, F.D., 1999, Induced Polarization in the Detection of Cave Systems: Proceedings, SAGEEP, Oakland, CA, Environmental and Engineering Geophysical Society, Expanded, Abstracts, 317 – 321.

Soininen, H., and Vanhala, H., 1994, Spectral Induced Polarization Studies of a Ni-Cu Ore Deposit, EAEG – 56th Meeting and Technical Exhibition – Vienna, Austria, 6-10 June, 1994.

Sturrock, J.T., 1999, Predictions of Hydraulic Permeability using Spectral Induced Polarization, M.Sc. thesis, Boston College.

15.0 Feedback

None.

16.0 Appendices

16.1 Copy of Publications

16.1.1 Sogade, J., and Morgan, F.D., 2004, Polarization Signatures for contamination: A critical Review (to be submitted to *Geophysics*)

16.1.2 Sogade, J., Minsley, B., Lambert, M., Vichabian, Y., Coles, D., Reppert, P., Rossabi, J., Riha, B., and Morgan, F.D., 2004, 2D Spectral induced polarization inversion of data acquired over a PCE/TCE contaminated site (to be submitted to *Geophysics*)

16.1.3 Sogade, J., Minsley, B., Lambert, M., Vichabian, Y., Coles, D., Reppert, P., Rossabi, J., Riha, B., and Morgan, F.D., 2004, Mapping TCE and PCE vadose zone contamination using 3-D complex resistivity borehole survey data (to be submitted to *JGR*)

16.1.4 Sogade, J., and Morgan, F.D., 2004, Instrumentation and coupling problems in spectral induced polarization field applications (to be submitted to *JEEG*)

Polarization Signatures for Contamination: A critical Review

by

John Sogade¹, Frank Dale Morgan¹

Abstract

This paper reviews the current understanding of induced polarization (IP) source mechanisms gained from laboratory studies as related to the polarization response of contaminated rocks and soils. This review takes the perspective of a prospective user of such information for development of an interpretation methodology for field applications.

The prospects for the application of time domain induced polarization (TDIP) or spectral domain induced polarization (SIP) to the problem of locating the subsurface distribution of contamination looked bright in the wake of published data claiming contamination produced measurable polarization response in rocks/soils. However, the literature today is dotted with conflicting reports of the polarization properties of contaminated rocks/soils. We have carried out a significant number of field experiments over contaminated soils and groundwater where inversion of the data successfully located the contaminated regions.

However, this review finds that an interpretation methodology that can be applied to field results based on laboratory studies of IP source mechanisms is still lacking. In addition, there is a general difference in the levels of polarization response of contaminated rocks/soils recorded in the field and in laboratory studies raising fresh concerns about the validity of a contamination related polarization signature. A field example is shown that supports significant polarization signature recorded over a site contaminated with Tetrachloroethylene (PCE) and Trichloroethylene (TCE).

1. Introduction

Induced polarization phenomena in earth media – rocks, soils, and sediments – has been known and studied both in the laboratory and field for over 80 years (Schlumberger, 1920; Bleil, 1953; Wait, 1959; Marshall and Madden, 1959). Early applications of induced polarization were to metallic mineral prospecting (i.e. see, Wait, 1959) and groundwater investigations (Vacquier, et al., 1957; Bodmer et al., 1968). Although there were references to logging applications in this period in the U.S.S.R. (Dakhnov et al., 1952, 1959), IP logging applications did not receive widespread serious considerations until later (Hoyer and Rumble, 1976; Snyder et al., 1977; Vinegar et al.,

¹ Earth Resources Laboratory, Department of Earth, Atmospheric and Planetary Sciences, Massachusetts Institute of Technology. e-mail: sogade@erl.mit.edu

1985). Subsequent applications were to environmental problems (Angoran, 1974; Olhoeft and King, 1991; Morgan et al., 1999; Slater and Lesmes, 2002; Briggs et al., 2003, 2004).

In recent times, laboratory studies (Olhoeft, 1986; Börner et al., 1993) suggested that chemical contamination introduced into rocks or soils produced measurable polarization response compared to clean samples. These observations, and similar ones published subsequently, led many researchers to develop field methodologies to map contaminated soils and aquifers using induced polarization. Despite all the promises of this methodology, there have been significant problems that militate against commonplace adoption of induced polarization for contaminant mapping. Some of these problems include: (1) speed and difficulty in processing data, (2) sometimes ambiguous results i.e. IP selectively maps contamination under certain favorable but often unpredictable site conditions, (3) lack of consensus on IP source mechanisms, and (4) a clear understanding of what constitutes IP signature for contamination.

This discourse arises out of a need to interpret IP data we have collected over contaminated soils and groundwater for several years, and the significant problems faced in synthesizing an interpretation methodology based on the available body of knowledge gained from laboratory studies. The discourse will review the existing literature on laboratory studies of IP source mechanisms and point out the problems faced in adopting an interpretation methodology based on these studies. A perspective on the problem from observations of field data will be provided and possible knowledge gaps to be filled will be suggested.

2. IP Theory

Induced polarization (IP) is a response of polarizable earth media – saturated or unsaturated rocks, soils, sediments - to electrical excitation. Polarization is a well-known phenomenon in physics and is characterized by spatial separation of charges under the action of an electric field. IP can be described phenomenologically, without consideration for the mechanisms that gave rise to it. The phenomenological description is useful in defining the appropriate constitutive equations, describing the relations between the electric displacement, D of polarizable media and the impending electric field (E).

To illustrate the general character of polarization responses, consider a vacuum capacitor with an electric field E applied across its metallic plates of unit cross-sectional area. An interfacial charge $Q_0 = \epsilon_0 E$ are developed on the plates, where

$\epsilon_0 = 8.854 \times 10^{-12}$ F/m is the dielectric permittivity of free space. For a monochromatic time varying field $E(\omega)$ at a frequency ω , the charge follows instantaneously because there is no ‘inertia’ in the vacuum response. If a dispersive dielectric medium -gaseous, liquid, or solid- fills the space between the plates then the induced charge is increased by the polarization $P(\omega) = \chi(\omega)E(\omega)$ of the medium which equals the dielectric induction or electric displacement, $D(\omega)$ i.e.

$$Q = Q_0 + P(\omega) = \epsilon_0 (1 + \chi(\omega))E(\omega) = \epsilon(\omega)E(\omega) = D(\omega) \quad (1.1)$$

and $\epsilon(\omega)$ is the permittivity. The susceptibility of the medium $\chi(\omega) = \epsilon(\omega)/\epsilon_0 - 1$ is a complex term with the real part $\chi'(\omega)$ related to the polarization property of the medium and the imaginary part $\chi''(\omega)$ accounting for dielectric losses. Due to ‘inertia’ of the material medium there is a delay between the variation of the field and the polarization response. For monochromatic signals, $E(\omega)$ the delay is recorded as a phase lag, and for arbitrarily time varying signals, $E(t)$ the delay is recorded as a time lag. Different mechanisms contribute to the polarization response at different regions of the frequency spectrum and the contribution of each can be described by the dispersive susceptibility term $\chi(\omega)$.

The permittivity of a multiphase medium like the earth which is comprised of any two or three combinations of rock matrix, pore spaces or pore fluids may be written in the form

$$\epsilon(\omega) = \epsilon_\infty + \epsilon_0 \sum_\alpha \chi_\alpha(\omega)$$

where the index α labels the various mechanisms, and ϵ_∞ is generally negligible compared with $\epsilon_0 \sum_\alpha \chi_\alpha(\omega)$ at lower frequencies (i.e. less than 1kHz). From the foregoing

a generalized Ohm’s law for a monochromatic source field, $E(\omega)$ at frequency, ω can be written as

$$J(\omega) = (\sigma_0 + i\epsilon(\omega))E(\omega) = (\sigma'(\omega) + i\sigma''(\omega))E(\omega) = \hat{y}(\omega)E(\omega) \quad (1.2)$$

where the inphase conductivity of the medium is

$$\sigma'(\omega) = \sigma_0 + \epsilon_0 \omega \chi''(\omega) \quad (1.3)$$

and its imaginary component, which can be seen as the lossless or quadrature conductivity, is

$$\sigma''(\omega) = \epsilon_0 \omega \chi'(\omega) \quad (1.4)$$

σ_0 is a non-dispersive conductivity, $\chi'(\omega)$ and $\chi''(\omega)$ are the real and imaginary susceptibility, and

$$\hat{y}(\omega) = \sigma'(\omega) + i\sigma''(\omega) \quad (1.5)$$

is often called the admittivity or complex conductivity of the medium.

The direct connection (1.4) between the imaginary conductivity and the polarization response of a media, $\chi'(\omega)$, is an important one, since it portends that at a given frequency a measurement of the imaginary conductivity provides the polarization response. However, because $\chi'(\omega)$ is a function of frequency, different regions of a heterogeneous earth might reach spectral polarization amplitudes at different frequencies, thus warranting that SIP investigations be carried out within a spectral window. The choice of such a window and the sampling frequency is not an easy one because of the large number of variables that affect polarization properties of earth media as discussed below.

3. IP Source Mechanisms

Several empirical or semi-phenomenological descriptions of $\chi(\omega)$ or $\hat{y}(\omega)$ for earth media at the low frequencies of interest in induced polarization (less than 1 kHz)

have been attempted (see Marshall and Madden, 1959; Sumner, 1976; Zonge, 1972; Pelton et al., 1978, Vinegar and Waxman, 1984, Samstag and Morgan, 1991, Börner et al., 1993). More recent investigators have attempted to describe $\chi(\omega)$ or $\hat{y}(\omega)$ by modeling the electrical properties of a distribution of mineral grains described by conducting or semi-conducting spheres/spheroids embedded in conducting fluids (Madden and Williams, 1993; Morgan and Lesmes, 1994; Sen et. al., 1996; Chelidze et. al., 1999a, Lesmes and Morgan, 2001). These descriptions attempt to express $\chi(\omega)$ or $\hat{y}(\omega)$ in terms of the rock/soil micro-geometry (pore-width, grain-size distribution), pore fluid properties (salinity, permittivity, major chemical species), or the nature of the grain-fluid interface (electrical characteristics affected by presence or absence of clay-sized particles with high ion-exchange capacity). It is expected that grain mineralogy will affect the mechanisms that produce polarization. The clearest distinction has been between electronically conducting metallic mineral grains, and semi- or non-conducting/non-metallic minerals.

The surfaces of most silicate minerals usually possess a net negative charge, by adsorption of essentially fixed ions (Pape et al., 1987). The net charge is one or a few molecular layers thick and constitutes what is called the fixed layer. At a solid-fluid interface, the net surface charge on the solid is a property measured by the ion exchange capacity (IEC), and it attracts charges of opposite polarity in solution to form a diffuse layer of ions next to the fixed layer. This electric double layer (EDL) of ions affects the surface electrical properties of most wet rock/soil systems in ways that will be shown below. Following the Debye-Hückel theory (see Hunter, 1993), most of the anomalous charge adsorbed adjacent to an interface is within a distance from the surface given by

$$d_{\text{surf}} = \sqrt{\frac{\epsilon \cdot k \cdot T}{2 \cdot n \cdot v^2 \cdot e^2}} \quad (1.6)$$

where n is normal ion concentration of electrolyte

v is valence of the normal ions

ϵ is dielectric permittivity of pore fluid

e elementary charge

k is Boltzmann constant

T is temperature.

Thus, the length of the EDL depends on chemical and dielectric properties of the pore fluid as well the temperature.

It is now very clear that at the low frequencies of interest in IP applications (i.e. less than 1 kHz) ionic conduction paths via the pore fluid electrolyte primarily control current conduction in resistivity. The IP effect, however, is linked to the build up of excess charge that results when the normal pore conduction path is blocked or the mobility of the normal ionic charge carriers is slowed.

There are three contemporary postulated mechanisms whereby charge separations and the resulting polarization phenomena are brought about in earth media at low frequencies, namely,

- (1) **Electrode Polarization:** Electrode polarization is due to the interface impedance that results when conducting mineral grains block pore paths. The mode of current conduction changes from ionic to metallic (electronic) at the mineral electrolyte interface, and current is carried across the interface either capacitively

via the EDL or by charge transfer reactions. The rate of these transfer reactions which is controlled by diffusion of redox active ions to reaction sites or by reaction kinetics determines whether there are local charge accumulations or polarization at the metal-fluid interface. If the rate-limiting step of these surface reactions is controlled by the diffusion of redox active ions, in conjunction with migration of inactive ions, normal to the metal-fluid interface, then the reaction impedance is usually described by the Warburg type with an inverse square root dependence on frequency (Madden, 1961; Angoran, 1977; Wong, 1979). It has been shown that adsorbed chemical species at the mineral surface, significantly affect polarization characteristics (Morgan, 1981).

- (2) **Membrane Polarization:** Membrane polarization is due to the interface impedance that results when, in certain regions of the normal conducting pore path, the diffuse layer is thick enough to block the path, therefore selectively passing ions of certain size and polarity, reducing the mobility of charge carriers, and causing charge build up. It rests on the assumption that these regions of sufficiently thick diffuse layers of ions, called membrane zones, exist and that the pore width is not too wide. One mechanism that can produce membrane zones is clay/clay-sized materials, with high IEC, partially blocking the ionic solution path (Marshall and Madden, 1959; Ward, 1990; Schön, 1996). Therefore, membrane polarization is of importance in rocks with a few percent clays distributed throughout the rock matrix, and dispersed among other larger mineral grains, for example, as a thin surface coating. It is very common for natural rock minerals including clay to be coated by organic matter which often times also has high IEC (Jenne, 1977), therefore presence of organic coating may also produce membrane polarization. As can be seen, the thickness of the EDL and the width of the pore-path are both factors that contribute to generation of the membrane effect. In cases where the length of the EDL is not enhanced by the presence of clay-sized materials with high IEC, constrictions in the pore-path might enable the reduced EDL layer to effectively create membrane zones. Therefore, a distribution of small and large pore radii can effectively create membrane zones (Schön, 1996; Titov, 2002). The spectral response due to the membrane mechanism is determined by the effective distances between membrane centers i.e. distribution of the dispersed clay-sized materials or pore-width constrictions (Marshall and Madden, 1959; Madden and Cantwell, 1967). The range of frequencies for which the membrane effect is expected to show up in the case of clay-bearing rocks/soils can be estimated to be between 0.024 to $2.4 \cdot 10^6$ Hz (Vinegar and Waxman, 1984). It has been observed that the membrane impedance is also Warburg type with an inverse square root dependence on frequency (Marshall and Madden, 1959; Madden and Cantwell, 1967; Vinegar and Waxman, 1984). Membrane polarization is a more likely mechanism for the IP effects observed in contaminant mapping.
- (3) **EDL Polarization:** On application of an electric field, the ions in the EDL migrate tangentially to the grain surface, leading to polarization. Other extensions that allow ionic migrations normal to the solid-fluid interface, or an exchange of ions between the open part of the EDL and the bulk of the solution, lead to polarization mechanisms controlled by ion diffusion over the grain lengths and

better explain polarization data at lower frequencies (i.e. see, Chelidze et al., 1999a, b). As can be expected, the dispersion characteristics of this polarization are closely tied to the grain sizes and the spectral response is determined by grain size distribution (i.e. see, Lesmes and Morgan, 2001). It should be noted however, that this type of polarization is expected to some extent in all fluid wet rocks/soils and as seen from laboratory data on clean clay free samples, the expected polarization is usually very small compared to contaminated samples or samples with some dispersed clay. In-situ rocks/soils coated with clays or organic matter might produce an enhanced EDL polarization or membrane polarization or both.

4. Factors that affect Polarization

The objective of our study is primarily linear IP effects, therefore we will exclude the consideration of non-linear effects. Additionally, the objective is to use IP for detection and mapping of rock/soil and aquifer contamination, and it is safe to assume that, except in zones of metallic mineralization, we can neglect electrode polarization. Therefore, subsequent considerations will be devoted primarily to membrane and EDL polarizations.

The chemical nature of the pore fluid and grain surface should affect both membrane and EDL polarizations. Similarly, grain microgeometry (size, shape), grain-grain interactions, possible correlation of grain size with the mineralogy, surface roughness, and the distribution of clay-sized membranes should affect polarization. If recent results (Lesmes and Morgan, 2001; Lesmes and Frye, 2001) are supported by further evidence, it appears that chemistry affects only the magnitude of polarization and geometry affects dispersion characteristics. Possible correlation of grain size with mineralogy might cause chemistry to affect the spectra in certain cases. In addition, the moisture content and clay-fraction of rocks/soils will affect polarization. The following sections will review available information to conform an understanding of the order of effects of the previously listed factors on polarization and point to new evidence suggesting that microorganisms play a role in polarization.

4.1 Effects of Chemistry

The effects of chemistry on polarization can be determined by variations of the valence of the component ions, the concentration of the component ions (active and inactive), and the fluid PH. There has been early evidence that polarization measured by chargeability is affected by the pore-water conductivity or salinity. Figure 1 show a plot of chargeability versus pore-water conductivity published by a number of authors.

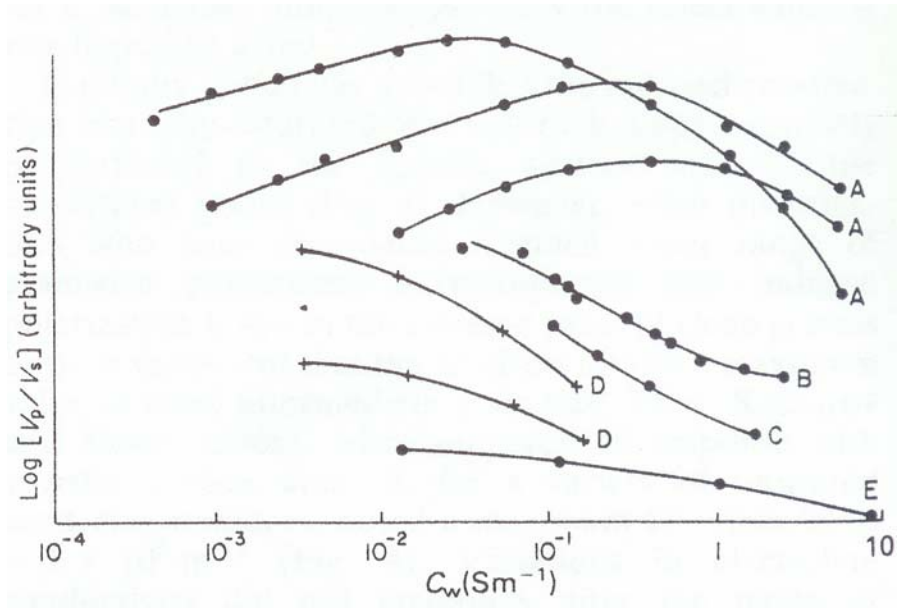


Figure 1: Reported variations of chargeability with electrolyte conductivity in water saturated sands (adapted from Worthington and Collar, 1983). A, Collar and Griffiths (1976); B, Henkel and Collins (1961); C, Komarov and Kotov, (1968); D, Vacquier et al., (1957); E, Sami Soliman Mohamed (1970). •, NaCl; + CaSO₄

This plot reveals that polarization initially increases with pore fluid conductivity, reaches a peak, and decreases thereafter. Similar results shown in figure 2, where polarization is measured by imaginary conductivity, further corroborate the earlier result.

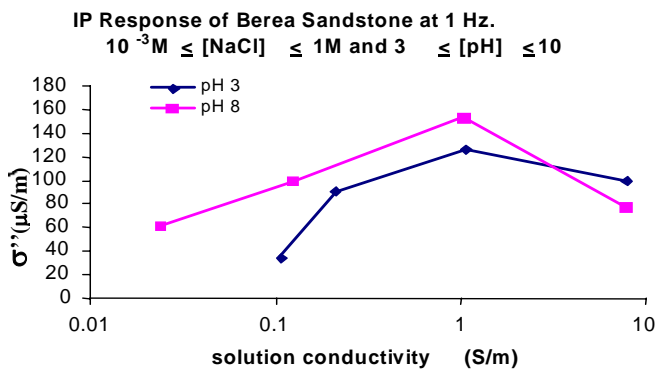


Figure 2: Variation of imaginary conductivity with solution conductivity for Berea sandstone sample at different PH values indicative of variation of polarization with changing solution chemistry (Lesmes, 1999).

Experimental data also reveal a dependence of polarization on ionic radius and ion valence as seen in figure 3.

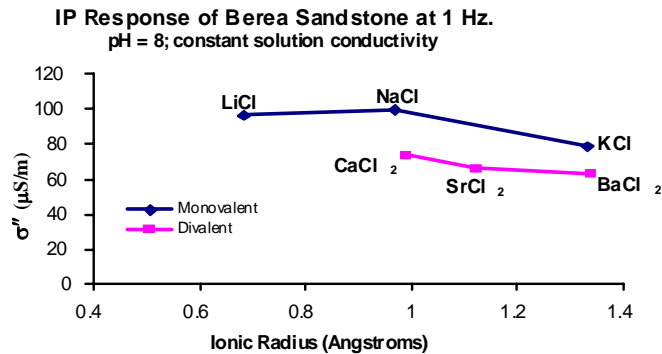


Figure 3: Variation of imaginary conductivity with ionic radius of monovalent and divalent ions at constant PH and solution conductivity (Lesmes, 1999).

The effect of the ionic components of pore fluids has been demonstrated in various experiments (Börner, et al, 1993; Garrouch et al., 1994; Glover et al., 1994; Chelidze et al., 1999; Lesmes and Frye, 2001, and others).

Lesmes and Frye (2001) concluded that based on broadband complex conductivity measurements made on Berea sandstone samples in which the specific surface area is fixed, the effects of chemistry measured by different pore fluid concentrations and PH values determines the magnitude of both parts of the conductivity response, and has negligible effect on the shape of the response. The second statement of this result contradicts those of Börner et al. (1993), who observed that contamination (which alters the chemistry) has measurable effects on the level of both parts of the conductivity response as well as the shape in some cases. This disparity might have arisen out of possible correlations between grain size and mineralogy, which has not been investigated in either study.

4.2 Effects of Non-Linearity

Non-linear polarization behavior manifests most strongly as a generation of higher order harmonics of a given monochromatic input signal. Therefore there is no longer a one-to-one correspondence between the input signal frequency and the output signal frequency.

Due to the work of Olhoeft and colleagues (Olhoeft, 1979, 1985, 1992; Sadowski, 1988; Jones, 1997), it has been recognized that passage of current in hydrocarbon contaminated clay-rich rocks/soils initiate clay-organic reactions that might lead to (1) non-linear polarization behavior (Sadowski, 1988; Jones, 1997) and (2) enhanced polarization in the presence of smectite clay types, and slightly enhanced, normal, or reduced polarization in the presence of other clay types (McKinley, 2003). However,

non-linear effects can also be initiated when the current density exceeds a given threshold (Madden, 1961; Sumner, 1976; Agunloye, 1980).

4.3 Effects of Microgeometry

Microgeometry can be measured by the geometrical characteristics of the mineral grains that make up the rock/soil matrix (shape, size, surface roughness). The distribution of these characteristics within the rock/soil matrix and the complex matrix-water interaction impart a geometrical character almost unique to each rock/soil.

To aid a conceptual understanding of clay free grain-water interactions however, laboratory and theoretical studies using simple models (i.e. mixtures of water and spherical glass/ceramic beads, and well characterized rocks/soil grains) have been carried out for several years (Lesmes and Morgan, 1994; Glover et al., 1994, and others). The models and theoretical considerations follow closely those of Maxwell-Wagner (Maxwell, 1891; Wagner, 1924), and their extensions (Hanai, 1935; Bruggeman, 1968) Maxwell-Wagner-Bruggeman- Hanai that we call the MWBH theory. The essential idea is that the dielectric or polarization properties of mixtures of materials can be different to their individual properties sometimes in remarkable ways. The essence of the results of these studies is that polarization in rock-water systems is a relaxation process and that the mineral grain size imparts a unique relaxation time or spectral peak to the polarization response (phase peak in frequency domain and relaxation time in time domain). However, a distribution of grain-sizes will produce a sum of relaxation processes and a significant spread in the relaxation spectra. These theories however, failed to satisfactorily account for the very low frequency dispersion of rock-water systems (i.e. below 100Hz). It has been observed that the specific surface area to porosity ratio of rock/soil materials increases the magnitude of the polarization contributions. Specific surface area also correlates closely with IEC and mineralogy.

Therefore distribution of clay-sized materials, within natural rocks/soils significantly impact on the resultant polarization behavior. Marshall and Madden (1959) and early workers recognized that the relaxation spectral peaks usually observed in the very low frequencies useful in induced polarization (less than 100Hz at that time) required a distribution of charge centers. Therefore, the conceptual idea of clay membrane centers distributed over larger grain surfaces or along pore walls offered a more plausible model for polarization of rocks/soils systems containing dispersed clays. The polarization mechanism is primarily controlled by the time it takes for diffusion of ions from adjacent membrane centers, which for most geologic materials, shows up strongly for frequencies less than 1Hz (Ward, 1990).

Recent extensions to the MWBH theory primarily accounts for the influence of the strong solid-fluid interface absent in the original theory. These extensions utilize an effective polarization of the EDL modeled by a conducting film around a non-conducting spherical grain (Schwarz, 1962), in which ionic migration is tangential to the interface. Further, extensions that allow ionic migrations normal to the solid-fluid interface, or an exchange of ions between the open part of the EDL and the bulk of the solution, lead to polarization mechanisms controlled by ion diffusion over the grain lengths and better explain polarization data at lower frequencies (Chelidze et al., 1999 a, b). As noted in Chelidze et al. (1999a) the effects of local electrical heterogeneities on grain surfaces account for significant low frequency dispersion characteristics of observed polarization

spectra. Similar surface effects, attributed to surface adhesion, have been observed for electrode polarization studies (Morgan, 1981). Grain surface roughness measured by a fractal exponent has been seen to affect the spectral polarization response as expected. What is more surprising is the coupling between surface roughness inferred from impedance spectroscopy and chemistry (Glover et. al, 1994).

4.4 Effects of Clay-Fraction

Since the work of Vacquier et al. (1957), clays have been shown to significantly affect polarization phenomena, and in particular clays or clay-sized materials play an important role in the membrane effect introduced by Madden and Marshall (1959). Because of the connection between polarization and clays there have been early attempts to explore IP as a means of the determination of in situ clay content of rocks and soils, with the ultimate aim of relating clay-fraction to permeability. The question then arises - what is the functional relationship between clay content, and polarization? Based on laboratory and field measurements, it appears that polarization grows with clay-fraction in saturated soils and rocks, reaches a peak, and subsequently decreases with further increase of clay-content (Ogilvy and Kuzmina, 1972; Collar and Griffiths, 1976; Worthington, 1984). Empirical relations connecting polarization and clay-fractions or permeability have been proposed (Collar and Griffiths, 1976; Worthington, 1984). Other studies proposed relations between polarization response and electrochemical properties of clays (IEC) in the presence of hydrocarbons (Vinegar and Waxman, 1984). Samstag and Morgan (1991) developed a multiphase model based on extensions of the Bruggeman-Hanai model that can be used to estimate clay fraction from polarization data. This is an ongoing study and other models and case histories exist in the literature.

4.5 Effects of Saturation

The effect of saturation on polarization response is important because some contaminants are trapped in the vadose zone and become secondary sources as most contaminants migrate through the vadose zone from surface source points to reach the aquifer. However, regardless of whether a contaminant pool has long residence time in the vadose zone or residual traces are left during transit, contamination of the vadose zone is an important one. Since vadose zones are unsaturated regions of the subsurface, it is useful to understand the effects of saturation or moisture content on polarization response.

Figure 4 shows the effect of saturation on polarization response for a montmorillonite-quartz sand mixture, where polarization initially increases with saturation, reaches a peak, and subsequently decreases. It appears that at an intermediate range of between 35% and 85% saturation, polarization response are kept near the peak, while outside this range polarization is severely attenuated by saturation. There are a number of studies of the effects of saturation on polarization response (Vinegar and Waxman, 1984; Chelidze et al., 1999b; Ulrich and Slater, 2004) and it appears that the effect is related to both the effective electrical properties of the EDL ions and the pore/pore-throat distribution.

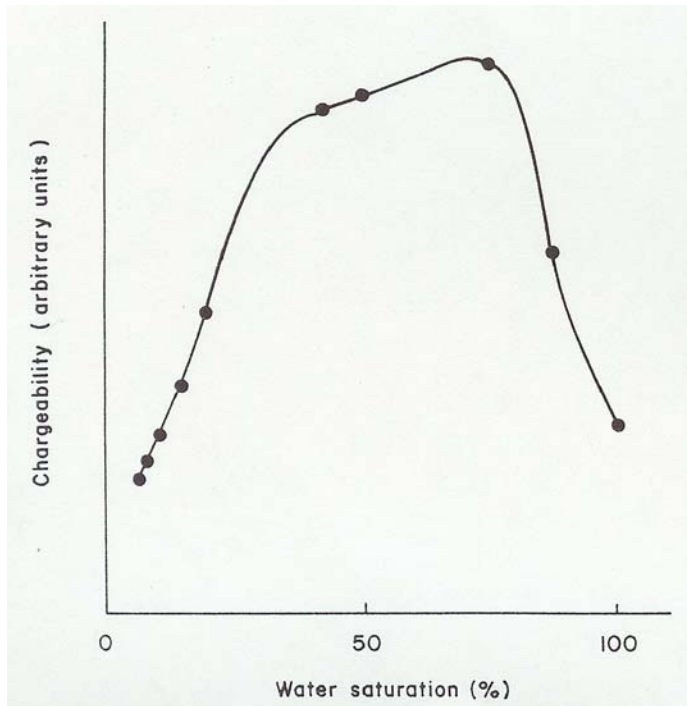


Figure 4: Variation of chargeability with water saturation for a montmorillonite-quartz sand mixture (after Ogilvy and Kuzmina, 1972).

4.6 Effects of Microbial Processes

Microorganisms (microbes) often use contamination as fuels for their energy supply and help in the chemical breakdown of contamination. Microbes populate mineral surfaces and often form as biofilms. In addition, the fact that bacterial cells have large surface areas, 30–100 m²/g (Van Der Wal et al., 1997a) and large wall counterion charge density, 0.5–1.0 Coulombs/ m², suggest that they might impact directly on polarization behavior of contaminated rocks/soils. The redox processes accompanying biodegradation activities may result in (1) secondary electrical potentials (measured as total or self-potentials) as suggested by Naudet et al. (2003), (2) (metallic) chemical byproducts that might affect both the pore-fluid electrolyte and interface electrical/electrochemical properties.

The initial efforts of Abdel Aal et al. (2004) have shown in a convincing set of carefully designed experiments that microbes affect both the electrolytic and interface properties of unconsolidated sediments contaminated with diesel. After sufficient time (about 14 weeks) for microbial activity to become effective, the study showed an increase in polarization response in contaminated areas with microbial presence and none in the contaminated areas without microbes. This increase was suggested to be either due to the biofilms formed by bacteria because of their large surface area, or linked to the byproducts of redox activities. In addition, if it is true that microbially mediated redox processes generates total or self-potentials, polarization response might be affected through a process of coupled flows (Marshall and Madden, 1959). The laboratory result

is consistent with those of field measurements made on hydrocarbon-contaminated sediments undergoing bio-degradation (Abdel Aal et al., 2003). The study also showed an increase in electrolytic conductivity in the contaminated areas populated by microbes consistent with the laboratory and field studies of Atekwana et al. (2004), where the increased fluid conductivity was shown to be strongly correlated with the dissolution of minerals resulting from the bio-degradation of the contaminant mass.

As a note, these investigations were carried out using LNAPL (Light Non-Aqueous Phase Liquids) contamination under mostly saturated conditions, and it is yet to determine whether the results will hold true for DNAPL (Dense Non-Aqueous Phase Liquids) such as PCE/TCE contamination of vadose zone sediments.

4.7 Effects of Aging

The solid mineral-fluid interfaces are often exposed to contamination for an extended period of time. During the long residence time of the contamination, various physical, chemical, and microbiological processes could affect the electrical nature of the interface. These processes are complex and often the exact processes cannot be determined. However, what is important to realize is that the length of exposure time of the solid-liquid interface to contamination and the consequent alterations due to complex bio-physicochemical interactions (aging) will impact the polarization response of the affected media.

A number of authors have noted the change in polarization response with time in contaminated samples. For example, Vanhala (1992) noted a change in polarization response for oil contaminated glacial till sample during a period of about 40 days. While this is not a good indicator of aging effects, it is an indicator that further studies should be directed at quantifying this effect. Horner (2001) noted that physical adhesion of contaminants to clays in sediments is a very fast process but that chemical adhesion is a very slow process. If surface alteration brought about by chemical adhesion is a strong contributor to the resulting polarization properties of contaminated rocks/soils, then laboratory contaminated rocks might not be measuring the same response as aged rocks/soils with contaminant residence time of decades.

A study worthy of mention is that of Moss and Jing (2003) who performed broadband (10Hz to 1MHz) complex resistivity measurements on aged samples. The samples were oil reservoir pore plugs of different lithologies, permeabilities, and wettabilities. The aging process involved wetting the samples with dead crude oil, which are then loaded in a pressure vessel, and pressure of 200Psi applied. Finally the samples were heated in an oven at 85 °C for 40 days. The samples were subsequently cooled to room temperature, and the pressure reduced to 0 Psi. The complex resistivity measurements indicated effects of aging on polarization response at the low frequencies. However, most of the important results were given as impedance amplitudes and it was not possible to quantify them in terms of phase changes.

5. Contamination indications by IP

We have earlier discussed the currently postulated mechanisms that give rise to the induced polarization response of geologic materials. The principal mechanism that is expected to explain the polarization behavior of contaminated rocks/soils is the

membrane effect. Ward (1990) suggested that contamination is expected to affect the effective length of the EDL by changing some of the variables in (1.6). If contamination increases the length of the EDL then membrane effect is more prominent in contaminated areas and can lead to enhanced polarization. In addition, the effects of different surface physical and electrochemical processes dominate the effective polarization response of rocks/soils. Adsorbed charges on grain surfaces appear to play a controlling role in explaining the low frequency character of the polarization response. When contamination enters the pore spaces within the rock/soil matrix, surface reactions between the rock/soil grain surface and surface reactive contaminant solutes are expected to affect the grain surface electrical characteristics of the rock/soils. Such surface reactions or sorptive processes include adsorption (solute sticks to solid surface by physical or chemical means), ion exchange (attraction between ions in the pore fluid and clay/clay-sized minerals in the soil), chemisorption (solute is incorporated in the structure of a sediment/rock), absorption (solute diffuses into the sediment/rock/organic matter).

These processes tend to remove the contaminants from the free phase in the soil and are affected by the saturation of the soil. In groundwater, adsorption is a very important and common sorptive process (Drever, 1997). Usually the dissolved components of aromatic and chlorinated hydrocarbons, which are usually hydrophobic, are strongly adsorbed by the solid phases in the subsurface. The important substrate here is the organic coating on rock minerals, and the consequent adsorption, usually hydrophobic driven, has been recognized to probably be the most important mechanism for groundwater contaminant transport of aromatic and chlorinated hydrocarbons (Drever, 1997). The linkage between the IP response and adsorbed species has long been known (Morgan, 1981; Olhoeft, 1986); therefore, because the adsorbed species include the contaminant solutes, the induced polarization method could in principle detect and map soil and aquifer contamination.

The IP literature suggests that the most important contributions of the surface impedance to IP effect exist at frequencies below 1kHz (Madden and Cantwell, 1967; Klein et al., 1984; Vinegar and Waxman, 1984; Boener et al., 1993; Vanhala, 1997a,b), although there is evidence that useful information exists beyond 1kHz (Börner et al., 1993; Soininen et al. (1994). For membrane polarization, the reduction in ion mobility and therefore the IP effect is most easily observed for potential variations (<1Hz) much slower than the time of diffusion of ions between adjacent membrane zones. To avoid induction coupling problems and based on the results of field-tested signal-to-noise ratios we have found it preferable to choose frequencies below 32Hz for most of our field studies involving application of spectral IP for mapping and detection of contamination released into the subsurface.

To answer the question of whether laboratory or field studies exist that show significant effects of contamination on polarization response, we offer a synopsis of examples garnered from the literature and our own measurements.

5.1 Laboratory signatures

A number of authors have published data indicating polarization response signatures for contaminated rocks/soils. The chemical character of the contamination has ranged from inorganic to organic, weakly acidic to strongly acidic, and volatile to non-volatile. Because sites contaminated with DNAPLs, especially the chlorinated solvents

such as PCE and TCE, are amongst the most common and the most difficult to characterize, we will focus mostly on organic contamination. The works of Olhoeft and his colleagues seem to have awakened interest in the use of SIP as a diagnostic tool for contaminant detection and mapping. However, Olhoeft's work has been mostly concerned with the non-linear aspects of polarization response, where significant currents might need to be exercised to obtain non-linearity. Our own efforts and those of many investigators have been limited to linear polarization response, thus the laboratory data presented here are mostly concerned with linear polarization response.

The first serious look at linear polarization signatures for contamination is the work of Börner et al. (1993), who investigated the effects of different types of contamination (organic and inorganic), their concentrations, and the different rock types on the magnitude and shape of complex conductivity spectral response. He came up with the general conclusion that the complex conductivity behavior of the rocks he studied at frequencies below 1 kHz is measurably influenced by the contamination, with a change in the amplitude of both real and imaginary conductivity, and in some cases a change in the shape of the imaginary parts. In addition he concluded that the imaginary part of conductivity in certain cases provide additional diagnostic information that enables a differentiation of the various substances in the pore space to be made. Figure 5 from Börner (1993) shows a spectral polarization phase plot of a shaly sandstone sample (sample E14) contaminated with different types of contaminants.

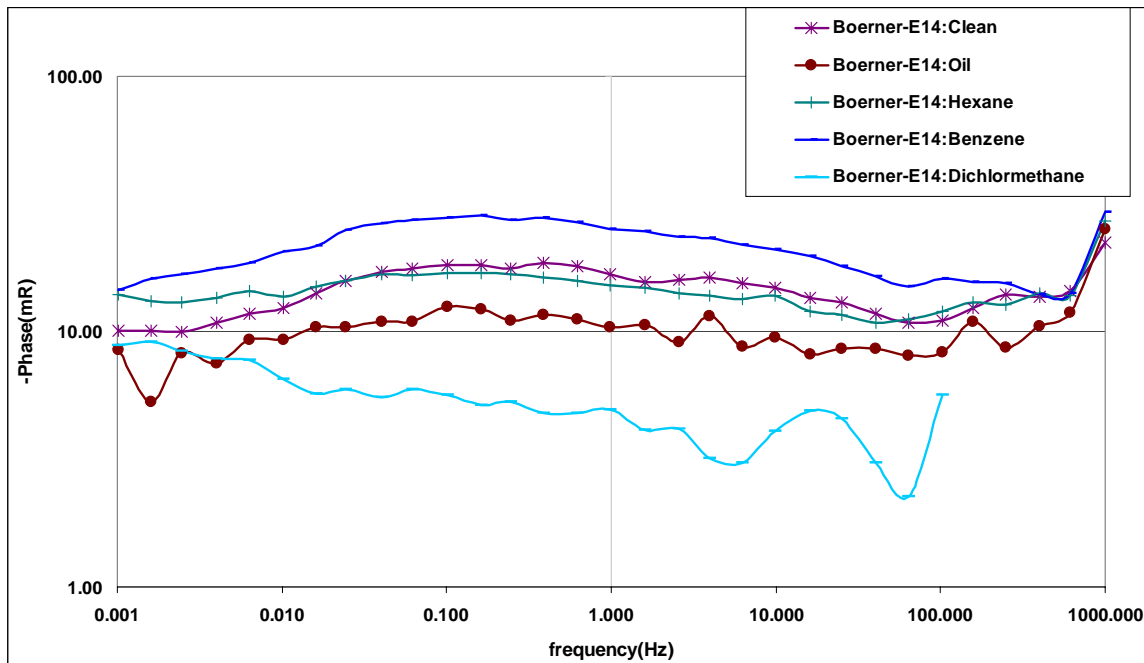


Figure 5: Spectral response of a shaly sandstone sample contaminated with different contaminants. The properties of the sample are: Porosity = 0.2403, Surface area = 1.31, Clay type = Kaolinite, (adapted from data on sample E14, Börner et al., 1993).

The plot clearly reveals that contamination, depending on type, can raise or lower the level of the phase spectra from that of the clean sample. Vanhala (1997) also obtained lowering of levels of phase spectra on oil contaminated glacial tills.

Ramirez et al. (1996) conducted complex resistivity measurements in a controlled scaled model experiment where PCE contamination was released into a tank where saturated layers of sand, bentonite, and sand/bentonite mixtures were installed. Borehole measurements of conductivity and phase at 1 and 64Hz were carried out regularly from the onset of the spill until about 30 days afterward. Tomogram images were created for resistivity and phase. Independent monitoring of the PCE revealed that it sank downward in the sand column until it reached the boundary of the sand-bentonite layer where it was stopped. The result indicated that the free phase PCE showed up as a resistive anomaly above a baseline. At the sand-bentonite layer boundary where the PCE finally settled, there was a net phase increase of about 60 milliradians (mrad) at 64Hz above a baseline value, indicating increased polarization of this zone. Jones (1997) performed broadband (10^{-3} to 10^6 Hz) spectral polarization measurements on natural and prepared clay-bearing samples contaminated with a variety of organic contaminants including TCE, tetrachloroethylene, ethylene glycol, and phenol. His focus however was on non-linear polarization effects. Roberts and Wildenschild (2001) carried out spectral polarization measurements on TCE and ethanol contaminated clay-sand mixtures, with the result that TCE slightly increased the resistivity of the samples but has marginal effects on the phase. They reported that the loss tangent, related to the imaginary conductivity, produced the greatest change in the electrical properties. McKinley (2003) performed broadband (10^{-3} to 10^3 Hz) spectral polarization data on clean and TCE/PCE contaminated clay-bearing and sand core samples acquired from the A14 outfall area of the Savannah River Site (SRS). The level of the resistivity spectrum of sand core samples was raised by more than 50% with the addition of PCE, but with marginal changes in the phase spectrum. The level of the resistivity spectrum of Kaolinite and montmorillonite clay-bearing samples was raised, but not as significantly as those of the sand. However, both showed more pronounced phase increases than the sand samples, the montmorillonite sample showing more pronounced phase level shifts than the Kaolinite sample.

Brown et al. (2004) performed broadband (10^{-2} to 10^3 Hz) measurements on Toluene contaminated sand and montmorillonite clay-bearing samples in order to validate an earlier work of Olhoeft and his student. Their result indicated that the earlier work of Sadowski (1988) could not be reproduced with two different apparatus designed after those of Olhoeft and colleagues (Olhoeft, 1979a, b, 1985; Sadowski, 1988; Jones, 1997) and Vanhala and colleagues (Vanhala et al., 1992; Vanhala and Soininen, 1995; Vanhala, 1997). Vanhala (1992) also made measurements on glacial till samples contaminated with Toluene with an increase in phase levels above 50 Hz and a decrease at lower frequencies. Their measurements on washed till contaminated with Toluene however showed a consistent lowering of the phase level at all frequencies. Brown et al. (2004), concluded that that spectral polarization measurements could not be a valid detection tool for all organic contamination. This conclusion was based on the inability to reproduce Sadowski's (1988) more significant shifts in phase levels at low frequencies for Toluene contaminated montmorillonite clay-bearing sample, and the consequent low phase level changes observed in their own measurements. However, in making this claim no

consideration was given to the fact that naturally contaminated rock/soil samples have in many cases exposure times of decades, the rock/soil grains might be coated by organic matter, only toluene was considered, and that complex bio-physicochemical interactions impact the polarization behavior of in-situ contaminated rocks/soils.

Field applications of spectral polarization are time intensive and it would be beneficial if published polarization data on different rock types was to identify a particular frequency bandwidth where significant polarization exists. To answer this question a histogram plot of all the data available is shown in figure 6. This plot reveals that no clear pattern can be identified to locate the bandwidth of significant polarization.

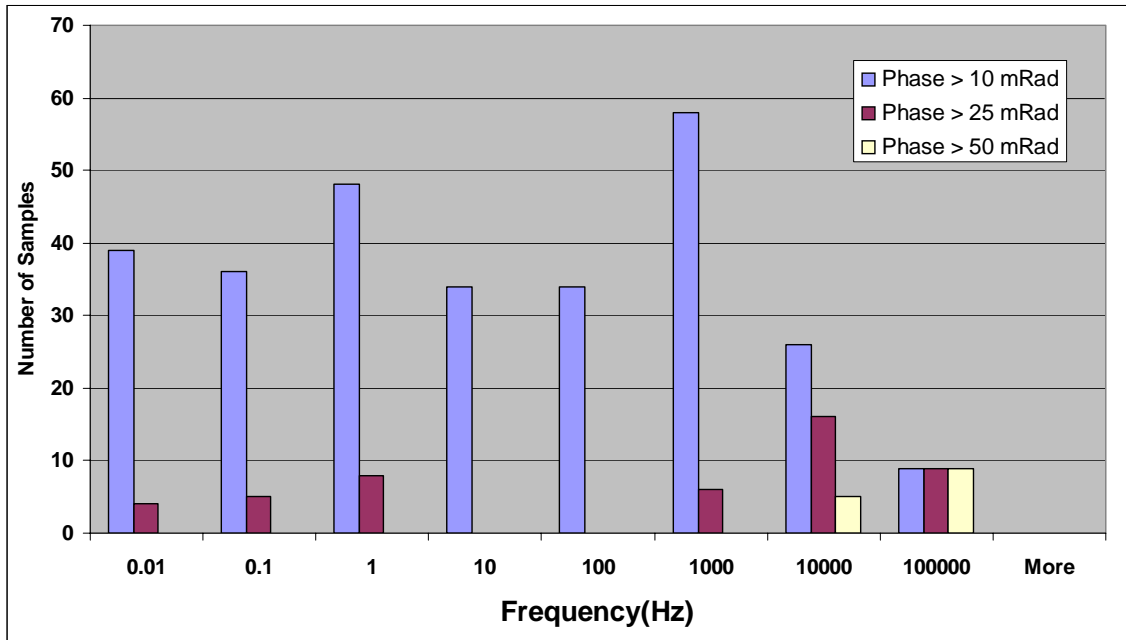


Figure 6: Histogram plot of spectral IP phase data from several sources organized into frequency bins.

5.2 Field based signatures

Sternberg (1991) had carried out an extensive set of surface field measurements over areas with significant hydrocarbon reserves. He showed clear examples where close correlation existed between shallow IP anomalies and deeper hydrocarbon production. His result also revealed that anomalies which occurred over the producing fields have significantly greater amplitudes than variations in the surrounding background response. Sternberg also had some IP logs to confirm that the IP anomalies are related to hydrocarbon sources. The peak IP measured in his logs are about 40mrad. He cautioned about the need for the right geologic conditions for the IP response to be observed. His results are relevant to the contamination discussion because similar factors play important roles in areas contaminated with chlorinated and non-chlorinated hydrocarbons. However, the sources of the hydrocarbon distributions are usually much deeper than those for environmental contamination problems.

Based on the fact that currently available spectral polarization laboratory data cannot account for all the factors that will affect polarization behavior of natural contaminated rocks/soils, we have attempted to determine what information can be obtained by field data collected over a site contaminated with PCE/TCE. The site is the A14 outfall area of the SRS, and has been characterized by ground truth borehole sampling, measuring significant amounts of PCE/TCE DNAPL pool within the first 40ft. A total of 10206 amplitude and phase measurements were made at two frequencies of 1/16Hz and 1/4Hz using surface and borehole electrodes (potential electrodes were only placed in boreholes). We will only show data for the lower frequency of 1/16Hz where electromagnetic and capacitive coupling are minimal. To enable a determination of whether there was significant phase polarization above the background, synthetic data emulating our field data geometry was created using a model of polarizable ground with 3 target anomalies (200Ωm, -5mrad; 50Ωm, -60mrad; 2000Ωm, -30mrad) emplaced in a 500Ωm, -17mrad host medium. The calculation was carried out using a 3D complex resistivity forward code developed at the earth resources laboratory (Shi, 1998; Appendices 16.1.2, and 16.1.3, this report). A plot of the real versus imaginary parts of the impedance is shown in figure 7. An estimate of the background phase, can be inferred from the slope, using

$$\phi_{\text{background}} = \tan^{-1}(\Delta Z_I / \Delta Z_R) \quad (1.7)$$

where $\Delta Z_I / \Delta Z_R$ is the imaginary versus real impedance slope. Using (1.7) the background phase was estimated to be about 19mrad. Furthermore, the possibility of determining background phases using raw data suggests that extensive effects of the host material overshadow the effects of the anomalies on the data trend.

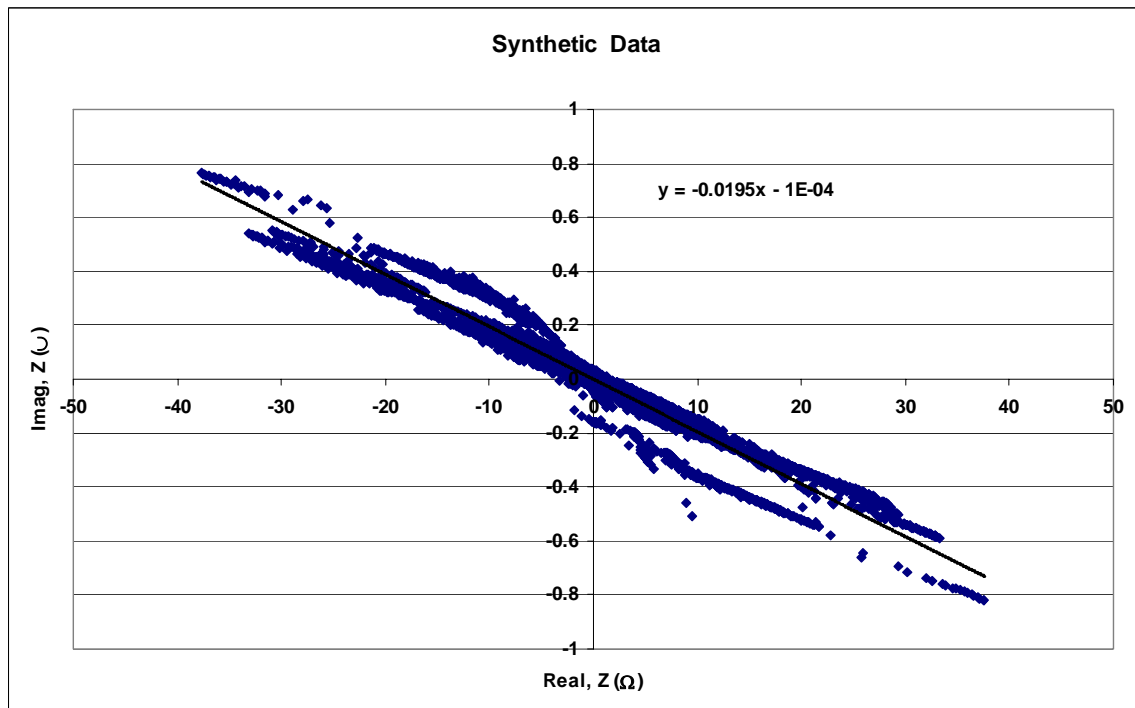


Figure 7: Plot of imaginary versus real impedance for the synthetic model described in the text. The trend line and equation are shown on the plot.

This is a particularly important observation since knowledge of the background material properties provides the ability to determine if there are anomalies. A distribution of data fractions (in %) within a given frequency bin is shown as a histogram plot in figure 8. This plot shows that the significant fractions of the phase (amplitude) for synthetic data lie between bins 0 and 17mrad (36%), 17 and 30mrad (48%) and 30 and 60mrad (12%). Thus, a large fraction of the data (60%) lies between our two anomalies of 30mrad and 60mrad, both greater than the background value, and a large fraction (35%) reflect the presence of the 5mrad anomaly, confirming that the data tracks the anomalies within the volume of interest.

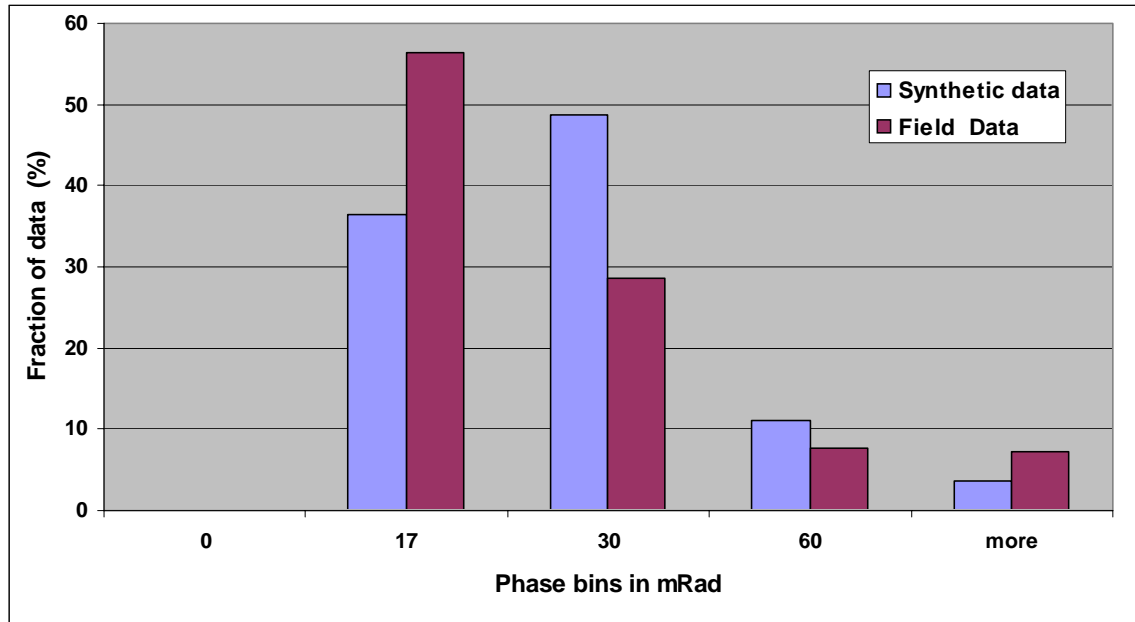


Figure 8: Histogram plot of spectral IP phase data from several sources organized into frequency bins.

Armed with this knowledge we have plotted a similar histogram of actual field data collected at 1/16Hz, also shown in figure 8. This plot reveals a background phase value of -15.8 mrad, which is supported by laboratory data on clean samples measured at the A14 outfall area (McKinley, 2003). The data distribution suggests that significant fractions lies between 0 and 17mrad (56%), as well as between 17 and 30mrad (28%). This result further suggests that there are targets with phase values less than the background in this site and also targets with phase values between 17 and 30mrad. Note that the fraction that lies between 30 and 60mrad (7.5%) as well as more than 60mrad (7.5%) suggest that a target with a phase value more than 30mrad exists somewhere at the site. It is left to determine whether the significant phase anomalies between 17 and 60mrad is suggestive of polarization from clean clays dispersed in the rock/soils or from contaminated rocks/soils with significant clay fractions. This determination cannot be made accurately. However, guided by spectral polarization measurements on clean clay bearing samples at this site at different depths and locations (McKinley, 2003), an estimated average phase value at 1/16Hz is about 20mrad. Therefore we are left to

conclude that the phase anomalies depicted in the significant phase bins in figure 8, especially for phases greater than 30mrad, is due to the presence of contamination within the volume constrained by our data.

5.3 Possible Interpretation methodology for PCE/TCE contamination

A more thorough interpretation methodology might have to await a better understanding of the several factors that influence the electrical polarization data determined by the IP inversion process. However, it is possible to offer a somewhat tentative interpretation methodology for determination of PCE/TCE contaminant presence or absence from interpretation of IP data. Other contaminants apart from TCE/PCE appear to have provided confusing IP signatures, and sometimes provide very little property contrast to the background. Based on the field data we looked at in the last section, it is possible to see that sufficient data exist for measuring the effect of PCE and TCE on spectral polarization characteristics of rocks and soils.

As shown earlier TCE, have negligible effect on spectral polarization phase response of contaminated rocks and sands, but has a significant effect on the amplitude spectra (Roberts and Wildenschild, 2001). PCE appears to increase the resistivity of sand and sand-clay mixtures (Ramirez et. al, 1996; McKinley, 2003), produce small polarization phase response in sands (McKinley, 2003), and produces significant polarization phase response in sand-clay mixtures (Ramirez et al., 1996; McKinley, 2003). As a general rule resistivity amplitude and phase as well as real and complex conductivity image sections should be produced. An increase of the resistivity of sandy areas will be produced from both the presence of PCE and TCE, but with small phase enhancements due to the PCE and probable microbial presence. PCE/TCE being both DNAPLS will tend to flow through permeable sand layers and pool in the junction between permeable sand and impermeable clay layers or trap zones. Enhanced phase response will be produced in these areas, and the junction areas should show up as contrasts in the resistivity section. The conductivity section should show up areas with interesting property contrast that should be further investigated. Examples of such contrasts could be their significant imaginary conductivity. Image sections produced using normalized IP parameters (Lesmes and Frye, 2001) can be introduced to accentuate areas of significant polarization that might have been masked by the high pore fluid conductivity, however we recommend this as an additional step. Figure 9 is an interpretation chart outlining some of the considerations just listed.

	low phase	medium phase	high phase
high resistivity	Clean sands with low water saturation	Possible Contaminant	Very likely Contaminant
low resistivity	Clean sands with high water saturation	Clay or Clay-disseminated sand. Possible contaminant	Likely Contaminant

Figure 9: Simple chart for interpretation of complex resistivity or induced polarization results in terms of contaminant presence or absence.

In the figure, low and high phases refer to phase values significantly lower or higher than background values, and medium refers to values just slightly higher than background.

6. Discussions and Conclusion

There is some difficulty in assessing the effects of contamination on measured polarization data based on laboratory studies carried out thus far, and whether such data can then be used as a diagnostic for contamination detection. It appears that amplitude enhancement of the polarization response (i.e. phase or imaginary conductivity) seem to offer the best diagnostic guide for contaminant detection. However, many of the contaminants seem to either increase or decrease polarization spectral amplitudes without affecting the shape. The published data seem to have different types of characteristic shapes and amplitudes that might be distortions introduced during the measurement process (Brown et al., 2004), or a general lack of standardized test platforms and samples.

There appears to be some inconsistency in the range of amplitudes measured in the field and those reported in the laboratory. We provided evidence from field data that helps to confirm that contamination does impart measurable effects on polarization data. There are a number of important factors that might significantly impact on the amplitude and shape of polarization responses that are not being carefully investigated and that might explain the difference in laboratory and field samples. Some of these factors include (1) the effects of microbial degradation processes (Abdel Aal et al., 2004), (2) presence of organic matter and consequent preferred adhesion of hydrophobic contaminants on organic substrates, (3) the effect of length of exposure (aging) of the solid-liquid interface to contamination and the consequent alterations due to complex biophysicochemical interactions (for examples of these effects see, Vanhala, 1997; Man and Ming, 2000; Abdel Aal, 2004). While there are reported initial efforts to address some of these problems considerable concerted efforts are needed to systematically investigate polarization phenomena under near field conditions.

Acknowledgements

The authors wish to express their gratitude to Mr. Paul Wang of Concurrent Technologies Corporation (CTC), and the Environmental Management Science Program (EMSP) of the US Department of Energy (DOE), for the funding of parts of this work via the projects CTC project 004846/DOE project DE-AM26-99FT40465DOE and EMSP project DE-FG07-96ER14714.

References

- Abdel Aal, G. Z., Atekwana, E. A., Slater, L. D., and Ulrich, C., 2003, *Induced polarization (IP) measurements of soils from an aged hydrocarbon contaminated site*, paper presented at Symposium on the Application of Geophysics to Engineering and Environmental Problems, Environ. and

- Eng. Geophys. Soc., San Antonio, Tex., April 6– 10, 190– 202.
- Abdel Aal, G. Z., Atekwana, E. A., Slater, L. D., and Atekwana, E. A., 2004, *Effects of microbial processes on electrolytic and interfacial electrical properties of unconsolidated sediments*, *Geophys. Res. Lett.*, **31**, L12505, doi:10.1029/2004GL020030
- Agunloye, O.A., 1980,
- Angoran, 1974;
- Angoran, 1977;
- Bleil, D. F., 1953, *Induced polarization: A method of geophysical prospecting*. *Geophysics*, **18**:636–661.
- Börner, F., Gruhne, M., and Schön, J., 1993, *Contamination Indications Derived From Electrical Properties in the Low Frequency Range*, *Geophysical Prospecting*, **41**, 83-98.
- Briggs et al., 2003, 2004
- Chelidze, T.L., Gueguen, Y., 1999, *Electrical spectroscopy of porous rocks: a review - I. Theoretical models*, *Geophys. J. Int.*, **137**: 1-15.
- Chelidze, T.L., Gueguen, Y., and Ruffet, C., 1999, *Electrical spectroscopy of porous rocks: a review - II. Experimental results and interpretation*, *Geophys. J. Int.*, **137**: 16-34.
- Dakhnov, V. N., 1959, *The application of geophysical methods; electrical well logging*: Moscow Petroleum Institute; trans. by G. V. Keller (1962). Colorado School of Mines Quart., 57.
- Dakhnov, V. N., Latishova, M. G., and Ryapolov, V. A., 1952, *Investigation of wells by the induced polarization method (electrolytic well logging)*: Sb. Promislovaya Geofizika, Vnetoneft; trans. by G. V. Keller: The Log Analyst, November-December 1967: 4682.
- Hoyer, W. A., and Rumble, R. C., 1976, *Dielectric constant of rocks as a petrophysical parameter*: Soc. Prof. Well Log Analysts 17th Ann. Logging Symp., Denver, paper 0.
- Hunter R.J., 1993, *Introduction to modern colloid science*, Oxford science publications, Oxford university press.
- Lesmes, D.P., 1999, personal communication.
- Lesmes, D.P. and Frye, K.M., 2001, *Influence of pore fluid chemistry on the complex conductivity and induced polarization responses of Berea sandstone*, *J. of Geophysical Research*, **106** (B3): 4079-4090.
- Lesmes, D.P., and Morgan, F.D., 2001, *Dielectric spectroscopy of sedimentary rocks*, *J. of Geophys. Research*, **106** (B7): 13329-13346.
- Marshall, D.J., and Madden, T.R., 1959, *Induced Polarization, a Study of its causes*, *Geophysics*, **24**, 790-816.
- Madden, 1961;
- Madden, T. R., 1976, *Random networks and mixing laws*, *Geophysics*, **41**, 1104-1125.
- Madden, T.R., and Williams, E.R., 1993, *Role of size distribution on physical properties: Real size renormalization group*, *J. Geophys. Res.*, **98**, 15,951-15,955.
- Morgan, 1981,
- Morgan, F.D., and Lesmes, D.P., 1994, *Inversion for Dielectric Relaxation Spectra*, *J. Chem. Phys.*, **100**, 671-681.

- Morgan, F.D., Scira-Scappuzzo, F., Shi, W., Rodi, W., Sogade, J., Vichabian, Y., and Lesmes, D.P., 1999, *Induced Polarization Imaging of a Jet Fuel Plume*, paper presented at Symposium on the Application of Geophysics to Engineering and Environmental Problems, Environ. and Eng. Geophys. Soc., Oakland, CA paper presented at Symposium on the Application of Geophysics to Engineering and Environmental Problems, Environ. and Eng. Geophys. Soc., San Antonio, Tex., March, 541
- Olhoeft, G.R., 1986, *Direct detection of hydrocarbon and organic chemicals with ground penetrating radar and complex resistivity*, Proc. National Water Well Assoc. Conf. on Hydrocarbons and Organic Chemicals in Groundwater, Houston, Texas, November 12– 14, 1986, 284-305.
- Olhoeft, G.R., and King, T.V.V., 1991, *Mapping subsurface organic compounds noninvasively by their reactions with clays*, U.S. Geological Survey Toxic Substance Hydrology Program, in Proceedings of technical meeting, Monterey, California, March 11–15, 1991, edited by G.E. Mallard and D.A. Aronson, USGS Water Resources Investigation #91-4034, 552-557.
- Pape et al., 1987
- Pelton, W.H., Ward, S.H., Hallof, P.G., Sill, W.R., and Nelson, P.H., 1978, *Mineral discrimination and removal of inductive coupling with multi-frequency IP*, Geophysics, **43**, 588-609.
- Samstag, F.J., and Morgan, F.D., 1991, *Induced polarization shaly sands: Salinity domain modeling by double embedding of the effective medium theory*, Geophysics, **56**, 1749-1756.
- Sen et al., 1981;
- Slater, L., and Lesmes, D., 2002, *IP interpretation in environmental investigations*, Geophysics, **67** (1): 77-88.
- Snyder, D. D., Merkel, R. H., and Williams, J. T., 1977, Complex formation resistivity—the forgotten half of the resistivity log: Sot. Prof. Well Log Analysts 18th Ann. Logging Symp., Houston, paper Z.
- Sumner, J.S., 1976, *Principles of Induced Polarization for Geophysical Exploration*, Elsevier Scientific Publishing Company.
- Vinegar, H. J., Waxman, M. H., Best, M. H., and Reddy, I. K., 1985, *Induced polarization logging--tool development, borehole departure curves and field test results*: Sot. Prof. Well Log Analysts, 26th Ann. Logging Symp., Dallas, paper AAA.
- Wait, J.R., 1959, (Ed.) *Overvoltage research and geophysical application*, Pergamon Press.
- Vinegar, H. J. and Waxman, M. H., 1984, *Induced polarization of shaly sands*, Geophysics, **49**, 1267-1287.
- Wong, 1979,
- Zonge, K.L., 1972, *Electrical Properties of Rocks as Applied to Geophysical Prospecting*, Ph.D. Thesis, University of Arizona.

2D Spectral Induced Polarization Inversion of Data Acquired Over a PCE/TCE Contaminated Site

by

John Sogade, Burke Minsley, Michael Lambert, Yervant Vichabian, Darrell Coles,
Phillip Reppert, Frank Dale Morgan¹

and

Joseph Rossabi, Brian Riha²

¹ Earth Resources Laboratory, Department of Earth, Atmospheric and Planetary Sciences, Massachusetts Institute of Technology, Cambridge, MA, E-mail: sogade@erl.mit.edu

² Savannah River Technology Center, Westinghouse Savannah River Company, LLC, Savannah River Site, Aiken, SC

Abstract

This study is focused on evaluating the suitability of 2D Complex Resistivity inversions to model spectral induced polarization (SIP) data acquired over contaminated soils and aquifers. The concern is that 2D inversions might introduce significant distortions to the inversion results because of model errors attending the use of 2D models in truly 3D environments which are common in environmental applications. This is important for the strongly non-unique inverse problems encountered when the problem is solved in complex arithmetic. The interest in 2D stems from the fact that 2D experiments are easy to plan and the inversions are fast enough even in the complex domain that they can be carried out in the field. This study concluded that in certain cases 2D inversions produce error free results, which are judged by both the comparisons to transects of a synthetic 3D model and by ground-truth data in field applications. However, in certain cases significant distortions occur that can produce false or misleading results. Based on these findings, 2D is offered as a fast tool useful for reconnaissance surveys, but its predictions should be supplemented by additional information as much as possible.

1.0 Introduction

The increased public concern within the last two decades that many of the groundwater reserves in the US were contaminated provoked remedial actions. Effective remediation requires development of conceptual models aided by adequate characterization of contaminated sites in terms of the distribution of the contaminant mass. The traditional method of characterization is multi-phase sampling of the subsurface by drilling sampling wells. However, characterization by sampling wells has proven difficult at many contaminated sites, primarily because of the heterogeneous character of near-surface geologic formations and the preferred mode of transport or behavior of certain contaminant types in these formations. For example it has been found that in unsaturated soils, i.e. the vadose zone, DNAPLs (Dense Non-Aqueous Phase Liquids) have a tendency to finger down into sandy areas giving high concentrations in localized areas and then spread over less permeable clayey zones. In addition, it often disperses in heterogeneous media as microglobules (Fennstra et al, 1996). Other characterization methods have been developed but are still limited.

Interest in the Induced Polarization (IP) method for characterization started since the work of Olhoeft (1979; 1984), who showed that organic contaminated clay-bearing rocks/soils present distinct complex resistivity (CR) or spectral Induced Polarization (SIP) signatures. A number of laboratory and field studies have since been directed at further development of the IP method for detection and mapping of mostly organic contamination (Olhoeft and King, 1991; Borner, et al., 1993; Ramirez et al., 1996; Morgan et al., 1999, and others). While 3D inversion facilities for processing SIP data have existed for some time (Shi, 1998; Weller et al., 1999), most of the reported studies have been carried out in 2D. This is probably a reflection of the difficulty of planning 3D experiments coupled with the slow speed of SIP data acquisition. Time domain IP (TDIP) data acquisition are often faster than IP, and can provide essentially the same data to constrain the polarization behavior of the investigated targets, but there are formal problems in posing an adequate solution to the forward and inverse problems that can process the acquired data.

Traditionally, 2D inversions of geophysical data have been used for cases where the third dimension of the earth model can be assumed not to affect the measured data. The most common earth model of this type arises when line measurements are made over earth structures where the target bodies are assumed to extend indefinitely in a direction perpendicular to the survey line. In environmental problems, where the extent of both models and survey length are restricted to much smaller sizes, and heterogeneities exist in all directions, a look at the utility of 2D inversions in environmental problems is warranted.

The present study is primarily aimed at evaluating the use of 2D SIP inversion for contaminant mapping. Two sets of measurements were carried out in 2001 and 2003, respectively referred to as FY01 and FY03 henceforth. The FY01 measurements were carried out at a site believed to have been contaminated with DNAPLs (primarily PCE and TCE). Subsequent ground-truth borehole sampling revealed that the levels of contamination was very low. However, both SIP and TDIP together showed polarization anomalies at an area with the maximum residual DNAPL concentration. There are two

other anomalies, one that is partially correlated with ground-truth contaminant concentration data, and the other not well constrained by the borehole-sampling program. The FY03 measurements were carried out at the same site, but in another area known to have been significantly contaminated with TCE/PCE DNAPL. In trying to answer questions on the accuracy of 2D SIP models in truly 3D environments, the second measurements were designed so that 2D data were extracted from 3D data, and therefore allowed a comparison of 2D with 3D predictions.

2.0 Background

2.1 Site Description

The study area is the A14 Outfall area of the Savannah River Site (SRS), Aiken, SC and was used as a discharge point for chlorinated solvents between the 1950's and 1980's, including PCE (Tetrachloroethylene) and TCE (Trichloroethylene), both of which are DNAPLs. Migration of the contaminants is complicated by subsurface structure, which consists of several clay layers interbedded with sand and silt. The A-14 outfall leads to a tributary of Tims Branch, which eventually discharges into the Savannah River and into local water supply. The FY01 and FY03 measurements were carried out at different areas of the A-14 outfall area. The target contamination in our study is located in the vadose zone, and is expected to be as shallow as 5ft below ground and as deep as 80ft or more.

Figure 1, which will be referred to often, lists different borings in the A14-outfall area and includes the boreholes used for the FY01 (MES-1, MES-2, MES-3, MES-4) and FY03 (MIT-1, MIT-2, MIT-3, MIT-4) measurements.

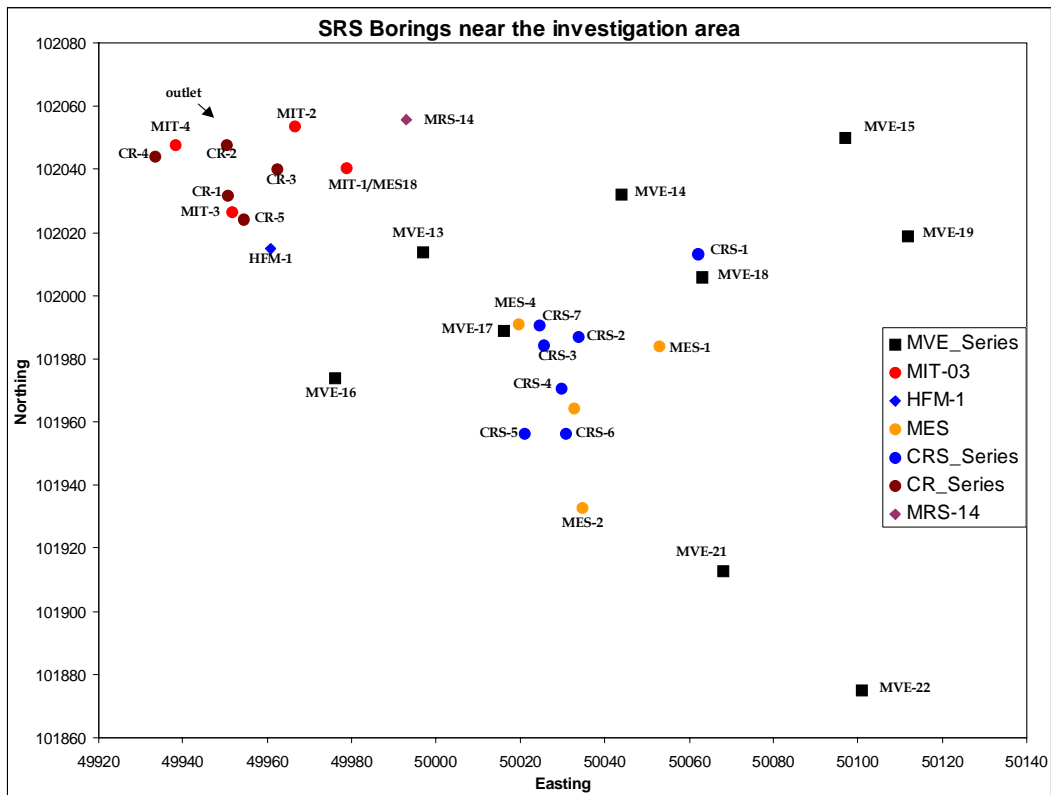


Figure 1: Location map of the borings in the vicinity of the A-14 Outfall area of SRS. In particular the FY01 measurements used the MES series with the CRS series serving as ground-truth borings. The FY03 measurements used the MIT series with the CR series serving as ground-truth borings.

2.2 Data acquisition and pre-processing

2.2.1 Survey Geometry

2.2.1.1 General

The raw data for both sets of experiments were acquired in a cross-borehole configuration, as potential magnitude, phase, and current magnitude. The borehole acquisition geometry was used because space limitations force the lateral (surface) profile length to be too short for the intended depth of investigation of 85ft. The data acquisition used the Zonge GDP-32 II receiver, and a Zonge ZT-30 EM/Resistivity Transmitter energized the ground. The GDP-32 is capable of acquiring data simultaneously at the first four odd-harmonics of the base frequency. The FY01 data sets were acquired at a base frequency of 1/32Hz, which with the harmonics span a total of 5 frequencies. In addition, a partial (i.e. not as large in size and coverage as the SIP) TDIP dataset was acquired along the panel between MES-2 and MES-4. The FY03 data were acquired at two base frequencies of 1/16 and 1/4Hz, which, with the harmonics span a total of 10 frequencies.

2.2.1.2 2001 Measurements

The 2001 data were acquired in 2D cross-borehole geometry along panels MES-1/MES-4 and MES-2/MES-4, both henceforth referred to as MES-14 and MES-24 respectively. Each borehole carried a total of 16 electrodes, in an alternating sequence of receiver and current bearing electrodes. This arrangement avoids the electrode memory problem, which arises when current-bearing (metallic) electrodes becomes polarized and subsequent potential measurements with the same electrodes before full depolarization. In addition, data acquisition capitalized on diagonal pairs of current electrodes between boreholes and avoided using entirely horizontal pairs in order to avoid highly conductive horizontal channels that might act as current traps. Both current and receiver electrodes were already emplaced before our occupation of this site and they were made of a special metal alloy, whose capacitive response appeared to have introduced significant data distortion. **Figure 2** shows the configuration of current and receiver electrodes used for the measurements along each panel, some of which will be referred to later.

To give a sense of the data distribution and quality, Figure 3 shows a trend plot of imaginary impedance against real impedance for MES-24 and figure 4 shows a histogram plot of the data fraction (in %) within certain phase bins for MES-14 and MES-24. From figure 3, an estimate of the background phase can be made using $\phi = \arctan(\Delta Z_I / \Delta Z_R)$, where $\Delta Z_I / \Delta Z_R$, is the slope of the imaginary versus real impedance plots respectively. This estimate gave

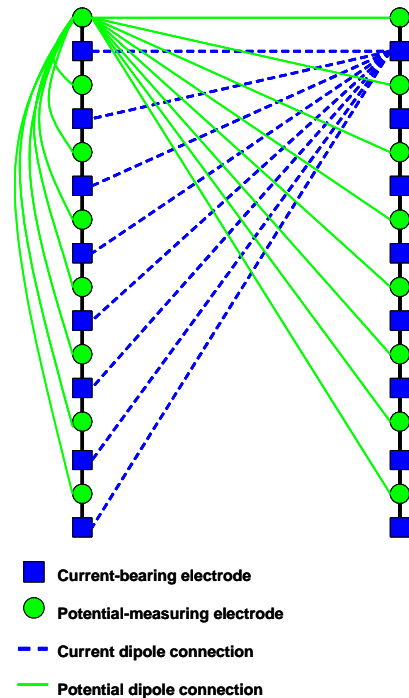


Figure 2: Schematic of a 2D cross-borehole electrode deployment

-19.0 and -16.2mrad for the background phase using MES-14 and MES-24 data respectively. Using synthetic models with complex heterogeneous structures, this technique has been demonstrated to be useful in providing a reasonably good estimate for the background phase.

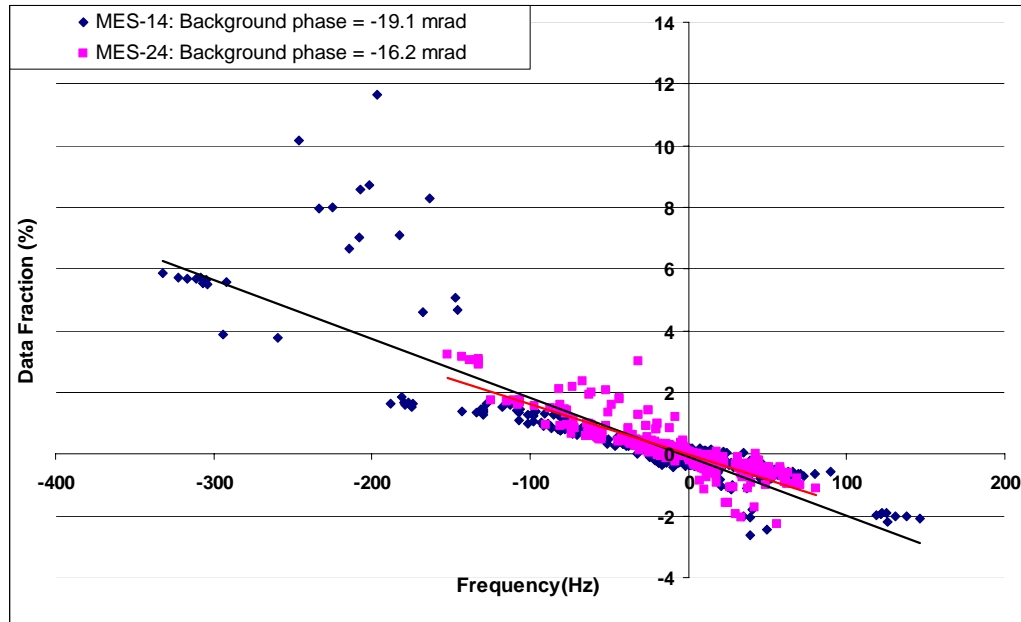


Figure 3: The scatter plot of imaginary versus real impedance for the MES-14 and MES-24 at 1/32 Hz. The regression lines are shown on the plot.

From figure 4, the fraction of data lying between 0 and -100 mrad (milliradian) is 70% for MES-14 and 85% for MES-24. Based on Laboratory measurements of clean and contaminated core samples in this area (McKinley, 2003), the expected background phase is about -16mrad, and the average phase for clean sand-clay mixture about -20mrad, while the phase for contaminated samples can range between background and -550mrad. Induced Polarization is a capacitive phenomenon and negative phases are expected if there are no data distortions arising from electromagnetic or geometric coupling. Based on simulations we have carried out, using the same data configuration, and for different heterogeneous structures, the average fraction of positive phase values due to geometric effects is about 2.5% maximum. However, the fraction of positive phase values in the data shown in figure 3 is about 25% for MES-14 and 10% for MES-24. This is interpreted to mean that there is significant data distortion at this site, and it is worse for MES-14 measurements. Therefore, data with positive phase values were edited out.

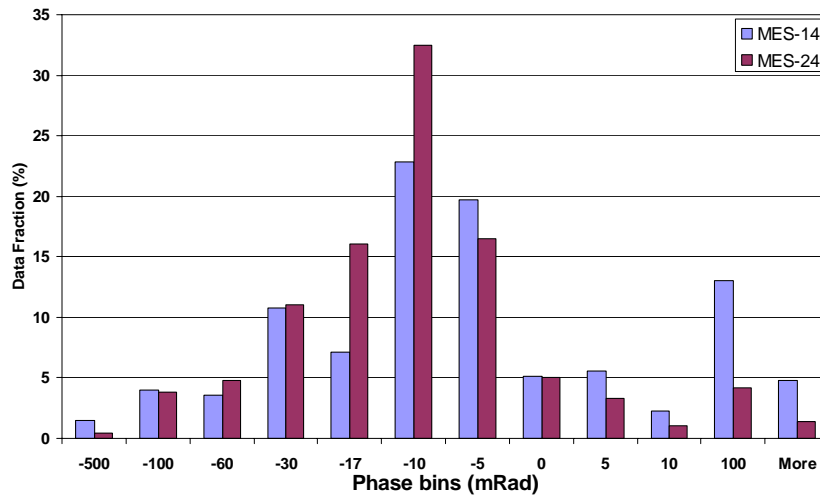


Figure 4: SIP phase data for MES-14 and MES-24 arranged as histogram plot. This plot reveals in which phase bins significant fractions of the data lie.

2.2.1.2 2003 Measurements

The 2003 measurements used four new boreholes (MIT-1, MIT-2, MIT-3, and MIT-4 in figure 1), and each carry seven current and seven non-polarizing potential bearing electrodes arranged as an alternating sequence of potential-current pair, each electrode separated by 6ft. The first and top-most electrode in each borehole is a potential electrode located 6ft below ground surface and the last is a current electrode located at a depth of 84ft. Halfway between each pair of boreholes is a surface current bearing electrode, making a total of 5 surface current electrodes 4 in the perimeter and 5 in the center. Current is injected across two boreholes or from a surface to a borehole electrode. The potential and phase are recorded between a reference electrode, the topmost electrode in borehole MIT-1 (referred to henceforth as the universal electrode), and all other 27 potential electrodes. Thus for each current pair 27 potential measurements are collected.

The data collection scheme is organized in terms of six 2D panels, which are the six planes through each pair of boreholes, and the bounded region is the 3D region of interest. Thus, for each panel there are a total of 63 cross-borehole plus surface electrode current electrode pair configurations. Inherently the data acquisition scheme just described is 3D from which the 2D dataset is extracted. In order to invert data for 2D panels the data has to be referenced to an electrode within that panel and this entails re-referencing in situations where the two boreholes of the panels do not include the universal electrode. In this way data for six 2D panels were acquired (MIT-12, MIT-13, MIT-14, MIT-23, MIT-24, and MIT-34). The schematic in Figure 2 aptly depicts the measurement geometry for panel MIT-12, except that the centrally located surface current electrode is not shown.

Figure 5 shows a plot of imaginary versus real impedance for MIT-14 at 1/16 and 1/4 Hz with estimated background phase values of 16.9 and 17.3 mrad, respectively.

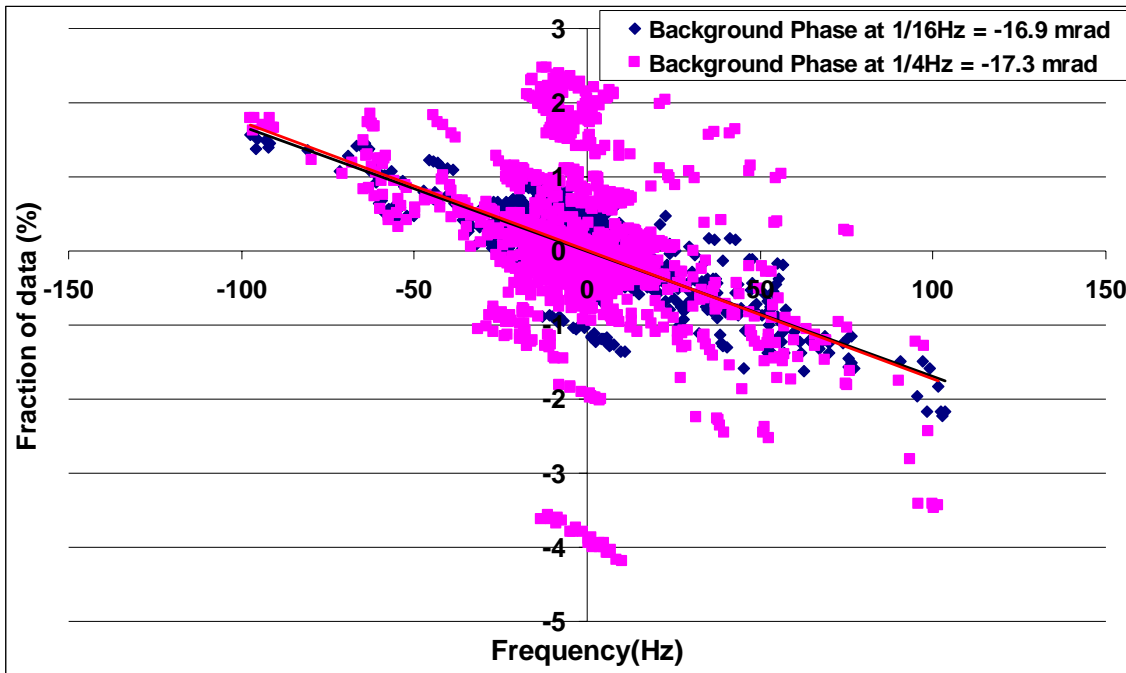


Figure 5: The scatter plots of imaginary versus real impedance at 1/16 Hz and 1/4 Hz for panel MIT-14. The regression lines are shown on the plot.

3.0 Possible Mechanisms of Polarization

The study of the mechanisms that give rise to polarization behavior in rocks/soils will aid in the interpretation of the inverted models in terms of the cause. In order to use IP for detection, it is necessary that the underlying processes of the IP mechanisms are affected by contaminations that have resided in the soils for up to decades. The mounting body of knowledge of IP source mechanisms suggests that IP phenomena are closely tied to processes active at the interface between the solid (rock/soil grain) and the fluid (electrolyte) that partially or completely fills the pore space. This can be contrasted to resistivity, which is primarily controlled by the electrical properties of the bulk electrolytic fluid that fills the pore space. Therefore, normal conduction in rocks/soils under near surface conditions is ionic.

The surfaces of most silicate minerals possess a net surface charge by adsorption of essentially fixed ions called the fixed layer (see Pape et al., 1987). This fixed layer attracts a cloud of charges of essentially opposite sign in solution to form a diffuse second layer of ions that span some distance into the solution from the solid surface. This electric double layer (EDL) affects the electrical characteristics of most solid-liquid interfaces directly or indirectly and lies behind most of the observed polarization behavior of rocks/soils. The ability of a solid surface to create strong EDL is measured by the ion-exchange capacity (IEC), which varies inversely with the grain size. There are three postulated causes of polarization behavior of rocks/soils at the low frequencies of interest in IP (i.e. less than 100Hz). They are electrode polarization, membrane

polarization, and EDL polarization. Electrode polarization takes place when metallic mineral grains partially or fully blocks the normal ionic conduction path and changes the mode of conduction from ionic in the pore fluid to electronic in the metal. The transfer of charge from solution to metal happens across the interface by charge transfer reactions or capacitively via the interface capacitance. The effective reduction in carrier mobility either due to reaction rate or the time for diffusion of ions to reaction center causes localized charge build up and polarization. Except in mineralized zones, electrode polarization is not expected to be important in most polarization processes at environmental sites.

Membrane polarization occurs when clays or clay sized materials with high IEC form coatings on grain surfaces or are dispersed in the pore walls in such a way that the thick EDL layer selectively passes ions of certain polarity, thereby causing ionic charge redistribution, charge accumulation and consequent polarization. It is important to note that both the electrical properties of the interface as well the geometrical characteristics of the pore-space/pore-wall are important for the establishment of a membrane polarization effect. At membrane centers (i.e. positions of the clay/clay-sized islands), the larger the pore-width the less is the membrane effect. The membrane effect could also arise not because of the distribution of clay or clay-sized membrane centers, but because of a distribution of pore radii (pore-throats/pore-wall distribution).

EDL polarization is due to the migration of ions in the EDL tangential and/or normal to the grains surface (i.e., see Chelidze, et al., 1999a,b; Lesmes and Morgan, 2001) and is expected to some extent in all water-wet rocks/soils.

4.0 Inversion

The SIP data were inverted by a 2D complex resistivity inversion. The forward problem can be written as

$$\nabla \left(\frac{1}{\rho(\mathbf{x})} \nabla V(\mathbf{x}) \right) = \sum_{\alpha} I(\mathbf{x}_{\alpha}) \delta(\mathbf{x} - \mathbf{x}_{\alpha}) \quad (1)$$

where $\rho(\mathbf{x})$ is the distribution of complex resistivities at spatial locations \mathbf{x} in the earth, and $V(\mathbf{x})$ are the distribution of complex potentials during the injection of the currents at locations \mathbf{x}_{α} (In our case, $\alpha = 1, 2$, and $I(\mathbf{x}_1) = -I(\mathbf{x}_2)$). Note that the above formulation assumes a DC formulation, and therefore does not account for electromagnetic coupling effects. Note also that the forward problem in (1) describes a 3D problem. The 2D problem actually solves a 3D problem arranged so that an odd numbered 2D grid of blocks is replicated along the symmetry direction. The 2D grid used is the centrally and symmetrically located grid. The 3D space of the forward problem can be discretized into a grid of blocks and solved as a transmission network problem, a concept introduced into geophysics by Madden (1972). The solution to the 3D complex resistivity forward problem is already aptly described in Weiqun Shi's thesis (Shi, 1998) and will not be repeated here. The solution to the 3D forward problem for real resistivities using the transmission network model can also be found in Zhang et al. (1995). However, certain pertinent aspects of the inverse problem not described by Shi follow.

The inverse problem can be posed as an optimization problem for an objective functional $\Phi(\mathbf{d}, \mathbf{x}, \tau)$ given by

$$\Phi(\mathbf{d}, \mathbf{x}, \tau) = (\mathbf{W}(\mathbf{d} - \mathbf{g}(\mathbf{x})))^H (\mathbf{W}(\mathbf{d} - \mathbf{g}(\mathbf{x}))) + \tau(\mathbf{L}\mathbf{m})^H \mathbf{L}\mathbf{m} + \tau(\mathbf{m} - \mathbf{m}_0)^H (\mathbf{m} - \mathbf{m}_0) \quad (2)$$

where H stands for the Hermitian and data and model lengths of N and M are assumed respectively. The measured data is represented by a complex vector valued function \mathbf{d} ($d_i, i = 1 \cdots N$), and the inversion parameters \mathbf{m} ($m_i, i = 1 \cdots M$), is a complex vector valued function whose components are log-rescaled resistivities of the model blocks according to $m_i = \log(\rho_i)$. Note that for both \mathbf{m} and ρ the location \mathbf{x} in parentheses has been dropped for convenience. The data weighting matrix, \mathbf{W} , is given

by $\mathbf{W} = \text{diag} \left[\frac{1}{\sqrt{\sigma_{ii}}} \right]$, for $i = 1$ to N , where σ_{ii} is data variance at the i th measurement

point. The Zonge GDP 32II system records only a standard error of the mean for the phase, which we call $\Delta\phi$. This can be converted to the data variance used in \mathbf{W}

by $\sqrt{\sigma_{ii}} = i\Delta\phi$.

\mathbf{L} is a first or second order difference operator; $\mathbf{m}_0 = \log(\rho_0)$ represents an a priori model, and τ acts as a Lagrange multiplier or a regularization parameter. The optimization problem defined in (2) attempts to minimize the data misfit with the first term, enforce smoothness between close neighbor cells with the second term, and ensures the closeness of the constructed model to a priori specification with the third term.

The inversion is iterative; it starts with an initial guess $\mathbf{m}_{\text{orig}} = \log(\rho_{\text{orig}})$, calculates updates $\Delta\mathbf{m}$, and then constructs a new model $\mathbf{m}_{\text{new}} = \mathbf{m}_{\text{orig}} + \Delta\mathbf{m}$ that moves in the direction of decreasing $\Phi(\mathbf{d}, \mathbf{x})$. Subsequent iterations replace \mathbf{m}_{orig} with \mathbf{m}_{new} , and repeat the update process. The parameter τ starts with an initial guess value and is updated based on considerations similar to the Levenberg-Marquadt algorithm (Levenberg, 1944; Marquardt, 1963). The parameter τ is decreased (division by a factor) when the data misfit decreases from the previous iteration and increased (multiplication factor) otherwise. A cursory explanation for the τ update algorithm can be seen by noting that τ moves the inversion in $\Phi(\mathbf{d}, \mathbf{x})$ space. The larger τ gets, the inversion biases the constructed solution towards smoother character and the a priori specification. Contrarily, the smaller τ gets, the inversion is biased to construct models that preferentially reduce data misfit. Thus, increasing or decreasing τ at a given iteration based on feedback from the inversion, adjusts to the competing demands of the optimization problem. It should be noted in terms of execution time, this algorithm should always do better than the OCCAM linear search algorithm of deGroot-Hedlin and Constable (1990), and in many cases better than the constant τ algorithm of Sasaki (1989).

5.0 Results

5.1 FY01 Results

Both the MES-14 and MES-24 dataset were processed by the 2D inversion code described above to produce amplitude and phase plots for each panel at the first five

harmonics. Ground-truthing was carried out using point sampling inside five borehole locations, the CRS-series in figure 1 (CRS-1, CRS-2, CRS-3, CRS-4, and CRS-5).

Figures 4 (a), (b), (c) and (d) shows the result for MES-14 as an interpolated panel of PCE concentration measured in the CRS boreholes and alongside the inverted resistivity (figure 4b), SIP phase (figure 4c), and imaginary conductivity (figure 4d) distributions. Similarly for MES-24, figure 5 (a), (b), and (c) shows an interpolated panel of PCE concentration as well as the phase and imaginary conductivity respectively. The result of the 2D inversion of an independent TDIP measurement carried out along MES-24 is shown in figure 5(d) as a chargeability distribution. Figure 6 shows the inverted resistivity along panel MES-24.

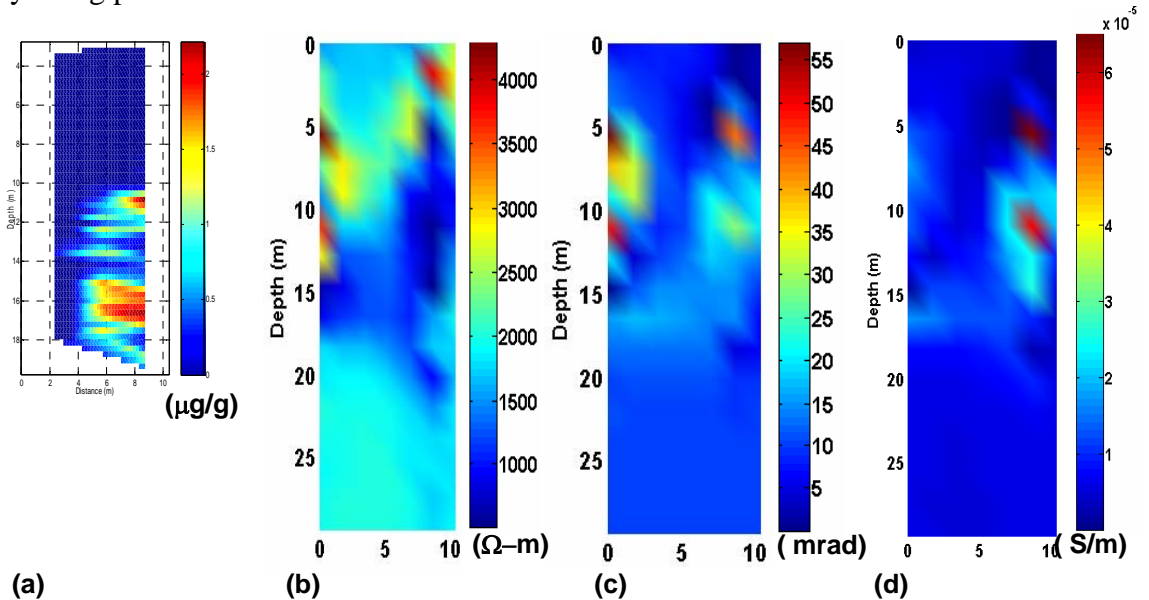


Figure 4: Comparison of the ground-truth PCE anomaly (a), the resistivity anomaly (b), the SIP phase anomaly (c), and the imaginary conductivity anomaly (d). Panel (a) has been generated by taking a slice along the MES-14 panel from the volumetric PCE concentration (interpolated from the CRS series of boreholes, taken during the FY01 ground-truth exercise). Panels b, c and d are the inversion results along the MES-14 panel. MES-4 is located on the right-hand side of all three panels.

In figure 4, the region of anomalous PCE concentration only spatially agrees with the anomaly locations around 10m depth near MES-4 on the right for both phase and imaginary conductivity. The concentration anomaly at 16m depth appeared as negative anomalies (i.e. decrease with respect to background values) on both phase and imaginary conductivity. It is not clear whether this is real, an inversion error, model error, or due to the significant data distortion reported earlier for MES-14. Notice however that the resistivity panel shows a conductive zone for the 10m polarization and a relatively more resistive zone at 16m.

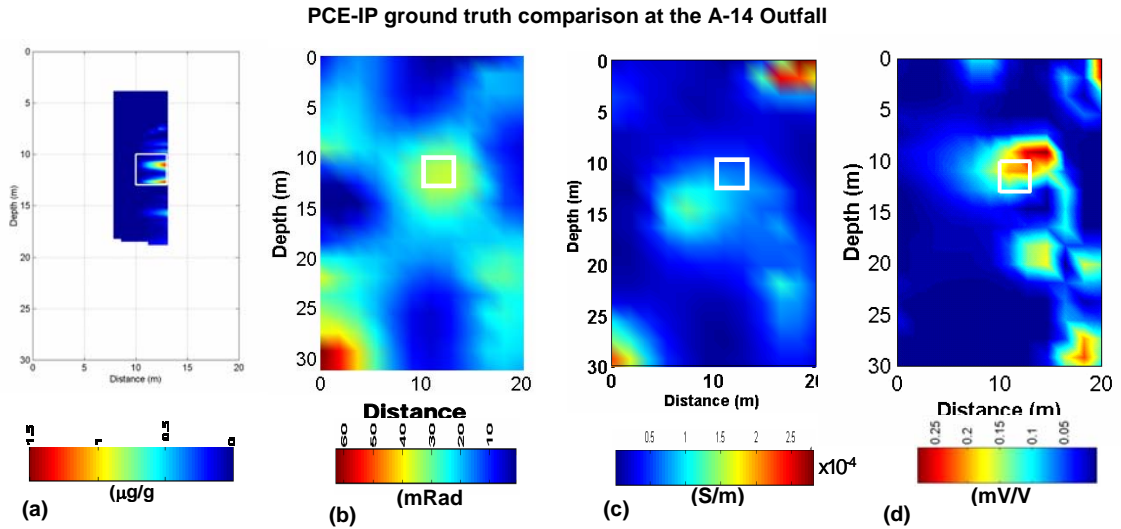


Figure 5: Comparison of the ground-truth PCE anomaly (a), the SIP anomaly (b), the imaginary conductivity anomaly (c), and the TDIP anomaly (d). Panel a has been generated by taking a slice along the MES-24 panel from the volumetric PCE concentration (interpolated from the CRS series of boreholes, taken during the FY01 ground-truth exercise). Panels b, c and d are the inversion results along the MES-24 panel. MES-4 is located on the right-hand side of all three panels.

In figure 5, the small region of anomalous PCE concentration spatially agrees very well with the anomaly locations as derived using SIP phase and TDIP chargeability. The agreement with the PCE concentration anomaly and the two independent confirmations of polarization at this location by both SIP and TDIP increased confidence that the contamination at this location has caused the polarization anomaly. It appears that center of the imaginary conductivity is offset to the left to match closer with the conductive anomaly seen in figure 6.

However, the results of this exercise were considered inconclusive because the ground-truthing phase of the operation failed to detect any concentration of NAPL above a requisite threshold of 40-50µg/g. It is our understanding that this threshold level is based upon analytic chemical partition analysis, which is dependent upon the physicochemical properties of the soil, its pore-fluid, and organic constituents (Cohen and Mercer, 1993), and therefore represents a necessary and sufficient condition to confirm the presence of NAPL.

Therefore, since the ground-truthing phase never found PCE concentrations in excess of ~3µg/g, there is no irrefutable evidence of NAPL; hence, the objective of the

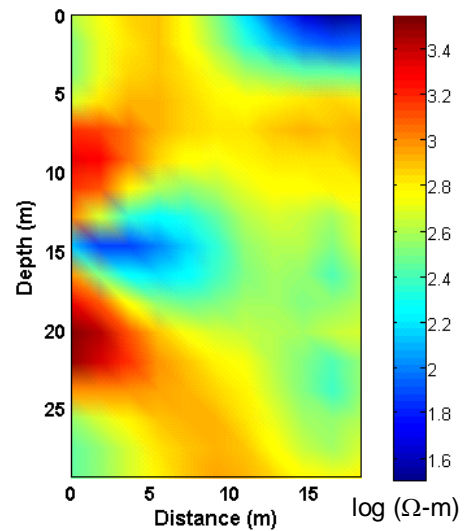


Figure 6: Resistivity for panel MES-24

FY01 exercise could not be completed. Nonetheless, the inversion results agree well with the ground truth, considering the sparseness of the CRS boreholes, low concentrations of 'PCE' ($< 3\mu\text{g/g}$), and despite poor electrodes.

5.2 FY03 Results

The six panel data at 1/16 and 1/4 Hz have been inverted using the 2D complex resistivity inversion algorithm. Each panel is labeled by the two boreholes lying on it i.e. 12 for the plane between boreholes MIT-1 and MIT-2. The inversion outputs a spatial distribution of the complex resistivity within each panel. Equivalent electrical parameters such as amplitude/phase and complex conductivity can be calculated from the complex resistivity result. Below in figures 6 – 10 are the set of six 2D panel results at the 1/16 Hz frequency showing the distribution of amplitude resistivity, phase, and imaginary conductivity respectively. PCE/TCE concentration data were acquired at 1ft sampling intervals in 5 ground-truth boreholes shown in figure 1 as CR-1 to CR-5. The PCE/TCE concentration data from the boreholes were interpolated into a 3D volume from which transects that fall along each of the six panels were created. Only 4 of these transects, shown in figures 7, 8, 9, and 11 could be created this way, the remaining are not near enough to any of the ground-truth wells for the interpolation to work.

The locations of concentration anomalies on panels MIT-14 and MIT-23 agree closely with the corresponding phase anomalies. This is encouraging since these are the only two panels that are located near two or more ground-truth boreholes. The locations of concentration anomalies on panel MIT-14 are not strongest where the phase anomalies are. However, there are two faint anomalies at about 7.5m (30mrad) and 18m (20mrad) depths, respectively, that match with the locations of the ground-truth concentration anomalies. Both of these anomalies are above the estimated background anomaly of about 17 mrad for this location and both correspond closely with a resistive to conductive boundary as seen from the resistivity panel. There is a chance that the significant phase anomaly between 12.5 and 20m depth to the left is a highly contaminated region, but it is not constrained by the ground-truth borehole. Panels MIT-12 and MIT-24 are not constrained by ground-truth information. The inversion results are however shown in figures 6 and 10, respectively. Figure 6 shows a long and narrow centrally located phase anomaly running from about 12.5m all the way to 25m, but it is not clear what this feature corresponds to. In addition, on panel MIT-24 there are two significant phase anomalies at 15 to 22m near borehole MIT-2 to the left and 15 to 20m near borehole MIT-4 to the right.

Panel 1-2

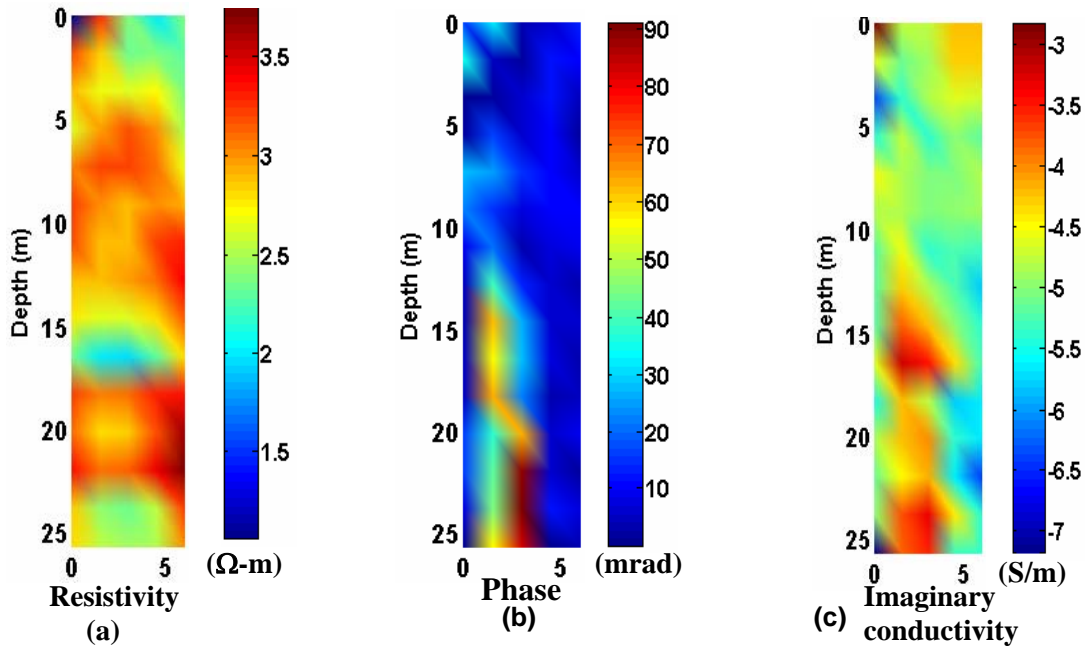


Figure 6: Inversion results for panel MIT-12 shown as the resistivity anomaly (a), the SIP phase anomaly (b), and the imaginary conductivity anomaly (c). MIT-4 is located on the right-hand side of all three panels.

Panel 1-3

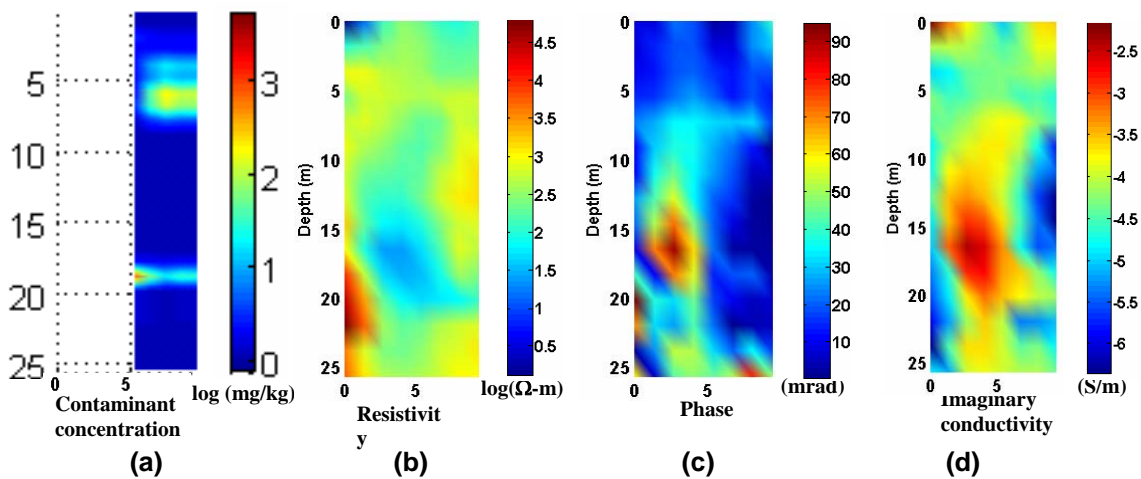


Figure 7: Comparison of the ground-truth PCE anomaly (a), the resistivity anomaly (b), the SIP phase anomaly (c), and the imaginary conductivity anomaly (d). Panel (a) has been generated by taking a slice along the MIT-13 panel from the volumetric PCE concentration (interpolated from the CR series of boreholes, taken during the FY03 ground-truth exercise). Panels b, c and d are the inversion results along the MIT-13 panel. MIT-3 is located on the right-hand side of all four panels.

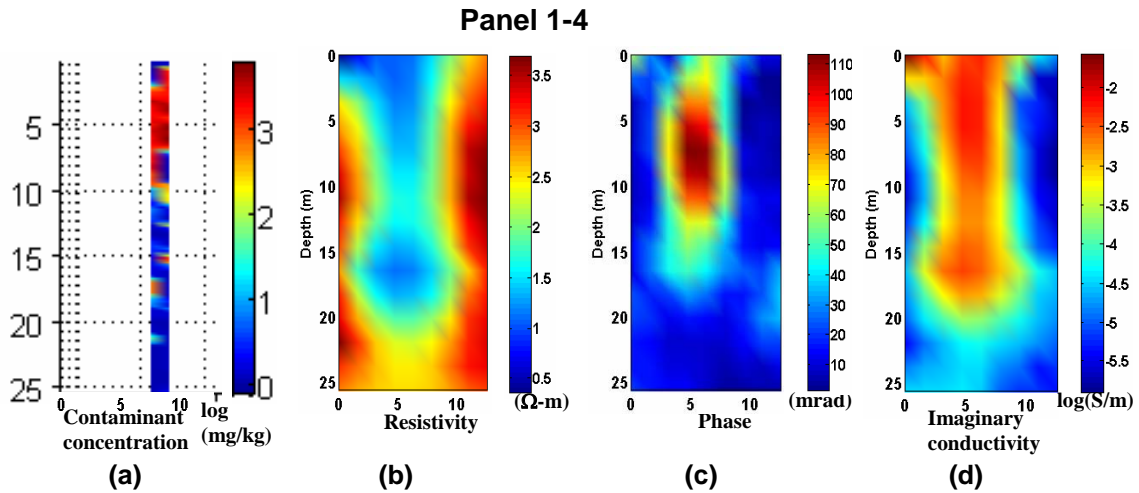


Figure 8: Comparison of the ground-truth PCE anomaly (a), the resistivity anomaly (b), the SIP phase anomaly (c), and the imaginary conductivity anomaly (d). Panel (a) has been generated by taking a slice along the MIT-14 panel from the volumetric PCE concentration (interpolated from the CR series of boreholes, taken during the FY03 ground-truth exercise). Panels b, c and d are the inversion results along the MIT-14 panel. MIT-4 is located on the right-hand side of all four panels.

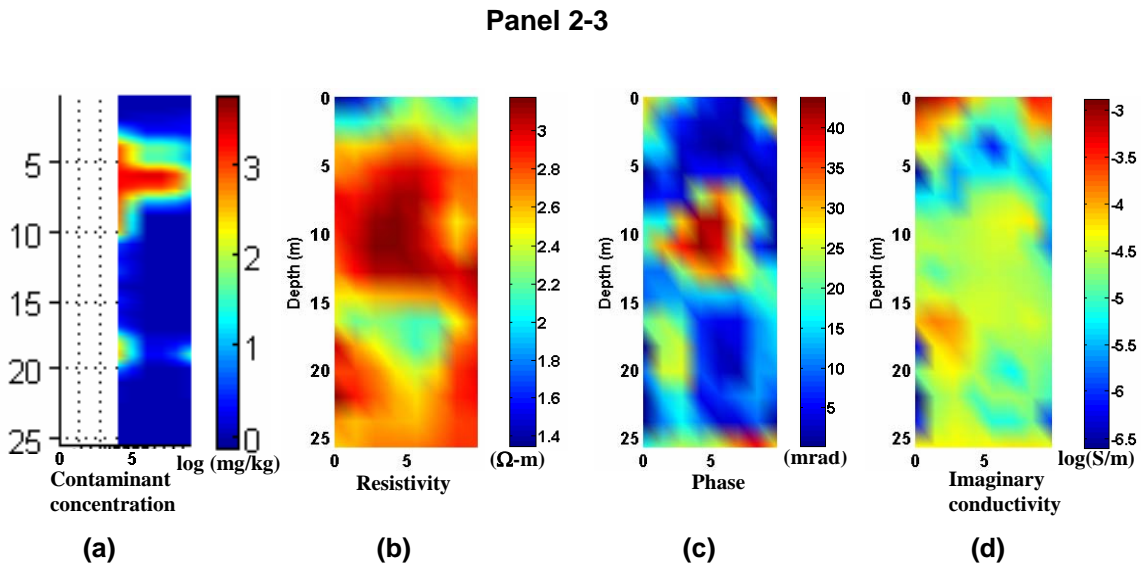


Figure 9: Comparison of the ground-truth PCE anomaly (a), the resistivity anomaly (b), the SIP phase anomaly (c), and the imaginary conductivity anomaly (d). Panel (a) has been generated by taking a slice along the MIT-23 panel from the volumetric PCE concentration (interpolated from the CR series of boreholes, taken during the FY03 ground-truth exercise). Panels b, c and d are the inversion results along the MIT-23 panel. MIT-3 is located on the right-hand side of all four panels.

Panel 2-4

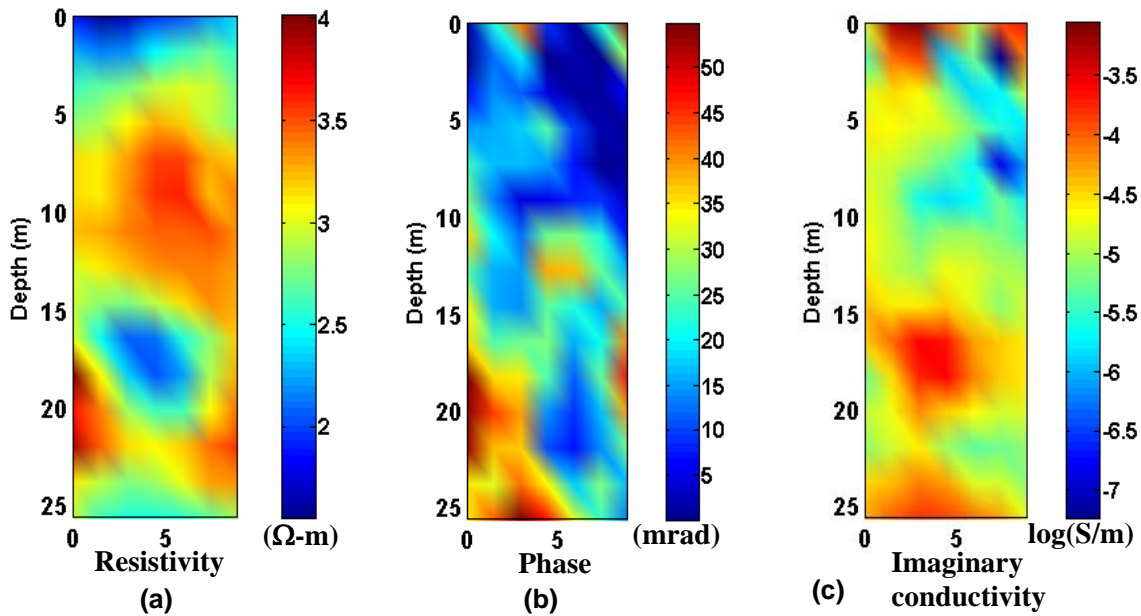


Figure 10: Inversion results for panel MIT-24 shown as the resistivity anomaly (a), the SIP phase anomaly (b), and the imaginary conductivity anomaly (c). MIT-4 is located on the right-hand side of all three panels.

Panel 3-4

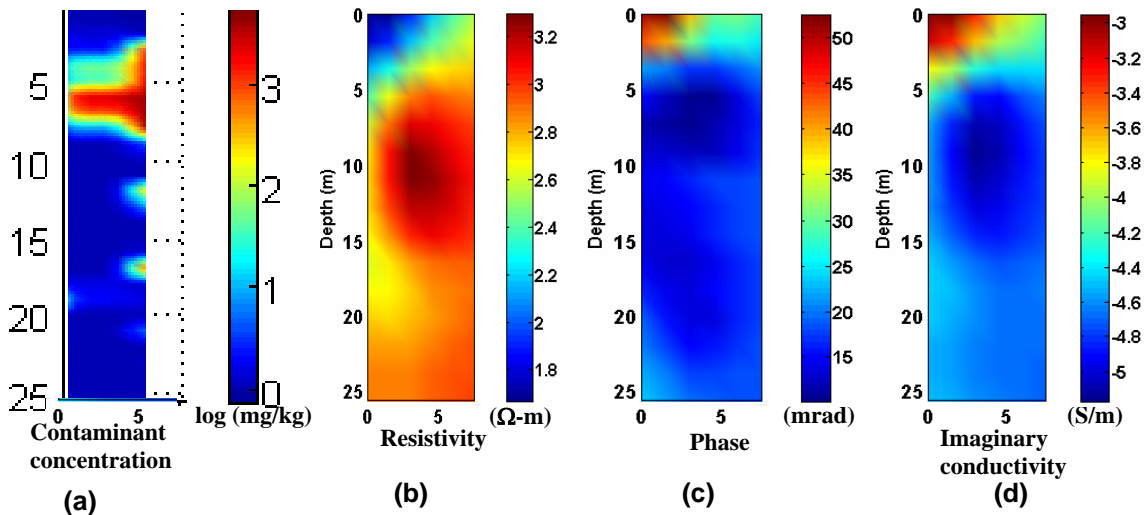


Figure 11: Comparison of the ground-truth PCE anomaly (a), the resistivity anomaly (b), the SIP phase anomaly (c), and the imaginary conductivity anomaly (d). Panel (a) has been generated by taking a slice along the MIT-34 panel from the volumetric PCE concentration (interpolated from the CR series of boreholes, taken during the FY03 ground-truth exercise). Panels b, c and d are the inversion results along the MIT-34 panel. MIT-4 is located on the right-hand side of all four panels.

6.0 Comparison of Panel results using 2D and 3D inversions

Because the geology of the A-14 outfall area is predominantly heterogeneous, it is suspected that a 2D model might not adequately describe the complexity or might generate considerable model errors. To address this concern, 2D SIP inversion results were compared to equivalent panels derived from transects of 3D inversion results.

Figures 12 and 13 show results of the comparison of the 2D inversion results of panel MIT-14 and MIT-23 with the equivalent transects of the 3D inversion of the same volume. Figure 16 shows that the resistivity, phase, and imaginary conductivity results for panels MIT-14 are equivalent for both 2D and 3D. However, the match is not that good for panel MIT-23 between 2D and 3D results. Noteworthy is the fact that the 2D polarization anomaly is resistive but in a zone the 3D predicted to be resistive.

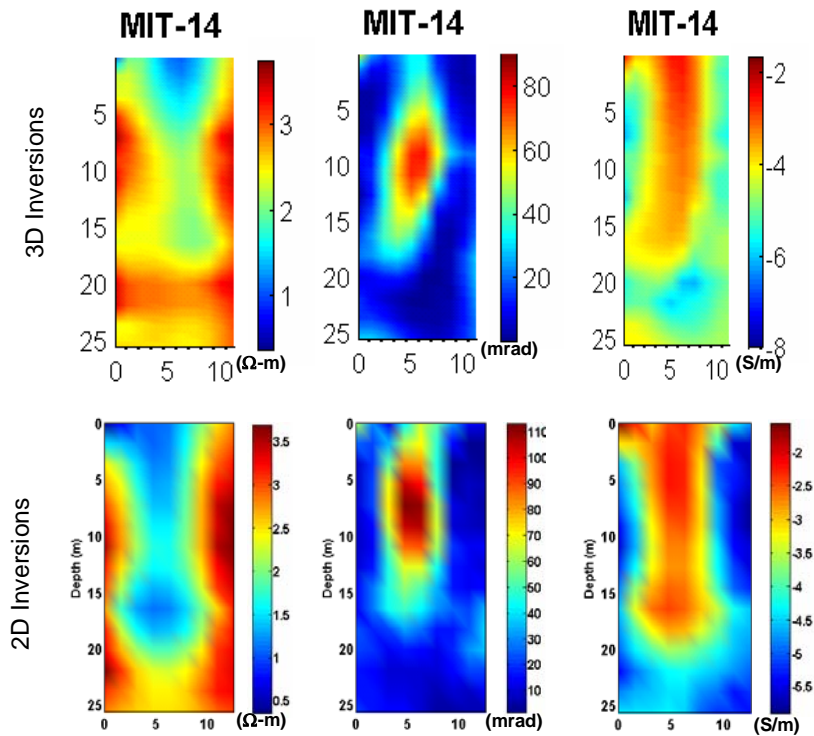


Figure 12: Comparison of the 2D results for MIT-14 bottom panels to equivalent transects of 3D results top panel. From left to right are resistivity magnitude, phase, and imaginary conductivity panels. Note the good correlation between 2D and 3D results.

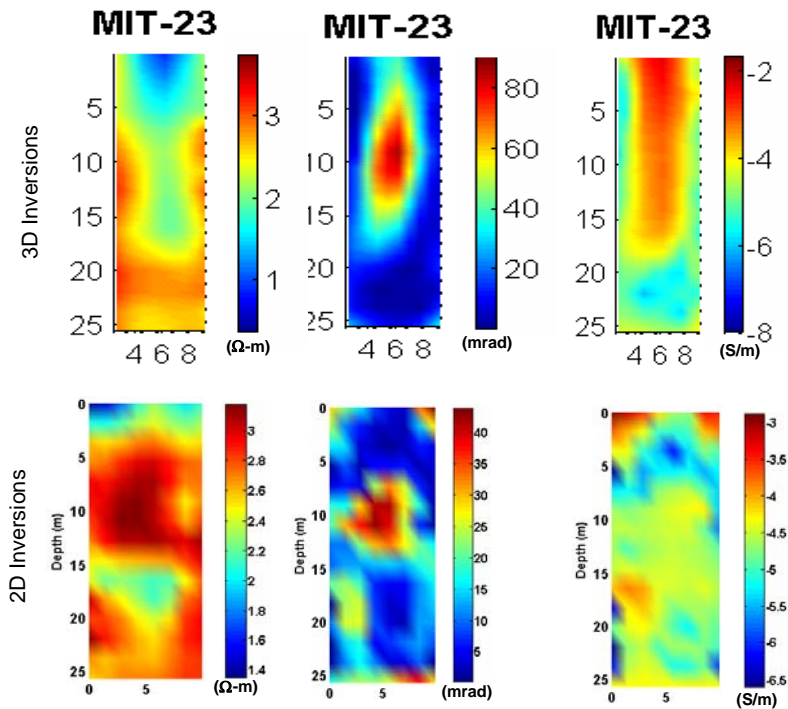


Figure 13: Comparison of the 2D results for MIT-24 bottom panels to equivalent transects of 3D results top panel. From left to right are resistivity magnitude, phase, and imaginary conductivity panels. Note the poor correlation between 2D and 3D resistivity magnitude results.

7.0 Discussion and Conclusion

The results displayed in Figure 5 for panel MES-24, show a very remarkable correlation between the location of the concentration anomaly and polarization anomaly given by phase for SIP and chargeability for TDIP. It should be noted that the TDIP dataset was not optimized for the given volume of investigation and this might explain the slight offset of the center of the chargeability anomaly from the concentration anomaly. The panel MES-14 result showed some correlation with the concentration anomaly located on the right of the panel at the 10m depth, but did not pick up the significant concentration anomaly at the 16m depth and showed an anomaly at 5m depth not recorded by the ground-truth borehole. It is not clear whether this is due to (1) absence of a polarization effect, (2) inversion errors (i.e. model errors), (3) inadequate interpolation of sparse borehole data leading to false or missed anomalies, (4) significant data distortion of the MES-14 panel data as shown earlier. What is clear with this experiment is that panel MES-24, which has the better data quality, showed evidence of a polarization effect due to PCE/TCE contamination at very low concentration levels (1-3 $\mu\text{g/g}$), and is mapped by both SIP and TDIP. Panel MES-14 maps this same anomaly but the deeper anomaly was missed. There appear to be another anomaly between 5 and 11m on the left of panel MES-14 that is not covered by ground-truth information.

For the FY03 results, only those for MIT-14 and MIT-23 will be discussed because these are the only panels that are located near at least two ground-truth boreholes. The FY03 polarization anomalies agree closely with ground-truth information in some cases and partially in others. For example the phase and imaginary concentration anomaly of panel MIT-14 result correlates very closely with the location of the concentration anomaly. The phase and imaginary conductivity anomaly of panel MIT-23, on the other hand agrees only partially with the concentration data. The phase anomaly on panel MIT-23 suggests a polarized zone slightly offset in depth from the concentration anomaly. While this might be due to any of the possible sources of problems or errors outlined earlier. It should be noted in addition that the volume seen by the SIP inversion is significantly larger than those of the borehole. For example the inversion block size is 5ft by 6ft, whereas the concentration data were acquired at 1 ft sampling interval in 3in boreholes, which are separated by as much as 20ft. A closer look at the resistivity result of MES-14 and MES-24 in figures 8 and 9, respectively, showed that the polarization anomaly on panel MIT-14 is located in a conductive zone, and the MIT-23 anomaly in a resistive zone. Therefore, there is significant heterogeneity at this site, and the effect on 2D inversions can be unpredictable. The results of the comparison of 2D and 3D inversion results shown in figures 12 and 13, support the idea that 2D inversions can sometimes provide very good and accurate depiction of the features along a panel but can also be significantly distorted by heterogeneity.

In conclusion, 2D SIP inversions can provide a fast reconnaissance tool for mapping and detection of PCE/TCE contamination in heterogeneous geology. It should be used however, with the clear understanding that false positives are possible and supplementary information should be used as much as possible. In addition, the possibility that the polarization effect produced by PCE/TCE contamination is dependent on soil lithology or mineralogy cannot be ruled out. This view is supported by laboratory and field experimentation at the A-14 outfall area by McKinley (2003) who showed that contaminated clay-rich soils could produce low or high polarization effects dependent on the presence or absence of smectite clay component.

Acknowledgements

The authors wish to express their gratitude to Mr. Paul Wang of Concurrent Technologies Corporation (CTC), and the Environmental Management Science Program (EMSP) of the US Department of Energy (DOE), for the funding of parts of this work via the projects CTC project 004846/DOE project DE-AM26-99FT40465DOE and EMSP project DE-FG07-96ER14714.

References:

Abdel Aal, G. Z., Atekwana, E. A., Slater, L. D., and Ulrich, C. (2003) Induced polarization (IP) measurements of soils from an aged hydrocarbon contaminated site, paper presented at Symposium on the Application of Geophysics to Engineering and Environmental Problems, Environ. and Eng. Geophys. Soc., San Antonio, Tex., April 6– 10, 190– 202.

- Abdel Aal, G. Z., Atekwana, E. A., Slater, L. D., and Atekwana, E. A. (2004) Effects of microbial processes on electrolytic and interfacial electrical properties of unconsolidated sediments, *Geophys. Res. Lett.*, **31**, L12505, doi:10.1029/2004GL020030
- Börner, F., Gruhne, M., and Schön, J. (1993). Contamination indications derived from electrical properties in the low frequency range. *Geophysical Prospecting*, 41:83–98.
- Chelidze, T.L., Gueguen, Y. (1999a) Electrical spectroscopy of porous rocks: a review – I. Theoretical models, *Geophys. J. Int.*, 137: 1-15.
- Chelidze, T.L., Gueguen, Y., and Ruffet, C. (1999b) Electrical spectroscopy of porous rocks: a review - II. Experimental results and interpretation, *Geophys. J. Int.*, 137: 16-34.
- Cohen, R., Mercer, J., Mathews, J. (EPA Project Officer). (1993) DNAPL Site Evaluation, C.K. Smoley
- deGroot-Hedlin, C. and Constable, S. (1990) Occam's inversion to generate smooth, two-dimensional models from magnetotelluric data, *Geophysics*, 56, 2102
- Lesmes, D.P., and Morgan, F.D. (2001) Dielectric spectroscopy of sedimentary rocks, *J. of Geophys. Research*, 106 (B7): 13329-13346.
- Levenberg, K. (1944) A method for the solution of certain problems in least squares, *Quart. Appl. Math.*, **2**, 164-168.
- Madden, T.R., 1972, Transmission systems and network analogies to geophysical forward and inverse problems, O.N.R. Tech. rep. no. 72-3, M.I.T.
- Marquardt, D. (1963) An algorithm for least-squares estimation of non linear parameters, *SIAM J. Appl. Math.*, **11**, 431–441
- McKinley, K. S. (2003). Nonlinear complex resistivity to investigate clay-organic reactions at the savannah river site, south carolina. Master's thesis, Colorado School of Mines.
- Morgan, F.D., Scira-Scappuzzo, F., Shi, W., Rodi, W., Sogade, J., Vichabian, Y., and Lesmes, D. (1999) Induced Polarization Imaging of a Jet Fuel Plume, proceedings of the Symposium on the Application of Geophysics to Engineering and Environmental Problems, Oakland, CA, Environmental and Engineering Geophysical Society, Expanded, Abstracts, 541–548.
- Olhoeft, G.R. (1979) Nonlinear electrical properties, in Neel, L., ed., in *Nonlinear Behavior of Molecules, Atoms and Ions in Electric, Magnetic or Electromagnetic fields*: Amsterdam, Elsevier Publishing Co., p. 395-410
- Olhoeft, G. R. (1984). Clay-organic reactions measured with complex resistivity. 54th Ann. Internat. Mtg., Soc. Explor. Geophys., Expanded Abstracts, pages 356–357.
- Olhoeft, G.R., and King, T.V.V. (1991) Mapping subsurface organic compounds noninvasively by their reactions with clays, U.S. Geological Survey Toxic Substance Hydrology Program, in Proceedings of technical meeting, Monterey, California, March 11–15, 1991, edited by G.E. Mallard and D.A. Aronson, USGS Water Resources Investigation #91-4034, 552-557.
- Pape, H, Riepe, L., and Schopper, J.R. (1987) Theory of self-similar network structures in sedimentary and igneous rocks and their investigations with microscopical and physical methods. *J. Microscopy*, 148, 121-147.
- Ramirez, A., Daily, W., and LaBrecque, D. (1996) Complex Electrical Resistance

- Tomography of a Subsurface PCE Plume, proceedings of the Symposium on the Application of Geophysics to Engineering and Environmental Problems, held at Keystone, CO, April 28-May 1.
- Sasaki, Y. (1989) Two-dimensional joint inversion of magnetotelluric and dipole-dipole resistivity data, *Geophysics*, 54, 254-262.
- Shi, W. (1998). Advanced modeling and inversion techniques for three dimensional geoelectric surveys. PhD thesis, MIT.
- Weller, A.; Frangos, W.; Seichter, M.: (1999) Three-dimensional inversion of induced polarization data from simulated waste. *Journal of Applied Geophysics*, 41, 31-47
- Zhang, J., Mackie, R.L., and Madden, T.R. (1995) 3-D Resistivity Forward Modeling and Inversion Using Conjugate Gradients, *Geophysics*, **60**, 1313-1325.

MAPPING TCE AND PCE VADOSE ZONE CONTAMINATION USING 3-D COMPLEX RESISTIVITY BOREHOLE SURVEY DATA

by

John Sogade, Victoria Briggs, Burke Minsley, Michael Lambert, Yervant Vichabian,
Phillip Reppert, Frank Dale Morgan¹,

and

Joseph Rossabi, Brian Riha²

Abstract

In-situ complex resistivity (CR) or Spectral Induced Polarization (SIP) data are collected using a 3D array of surface and borehole electrodes over an area known to be contaminated with DNAPLs (Dense Non-Aqueous Phase Liquids). The contaminants include Tetrachloroethylene (TCE) and Trichloroethylene (PCE), which, until the 1980s were disposed directly into the environment. Two sets of measurements were carried out; the first in March 2003 was to determine if SIP can map subsurface contamination, and the second in June 2004 was to determine if IP can monitor contaminant movement. The design of the surface and cross-borehole array allows for a 3D IP inversion. Data were measured at two base frequencies (1/4 and 1/16 Hz), and are inverted for resistivity magnitude and phase. The inversion results are compared with PCE and TCE contaminant concentrations measured from core samples taken from five ground truthing wells drilled within the region of interest shortly after the March 2003 measurements. The imaginary conductivity, calculated from the resistivity magnitude and phase, is well correlated with the concentration data from the three ground truthing boreholes where the TCE and PCE concentrations are above 1mg/kg. Based on the good correlation with the PCE/TCE concentration data, the imaginary conductivity volume distribution was used to develop a conceptual model of the contaminant distribution at this site.

Introduction

The Induced Polarization method was traditionally used in the search for metallic mineral ores (Bleil, 1953; Wait, 1958; McEuen et. al, 1959; Marshall and Madden, 1959; Fraser et. al, 1964; Zonge and Wynn, 1975; Pelton et. al, 1978) and for groundwater (Vacquier et. al, 1957; Bodmer et. al, 1968). In the 1970s IP was used for the first time for investigation of municipal waste (Angoran, et al., 1974).

In the 1980s there was increasing public concern that many of the ground water reserves in the US were contaminated and that remedial action was needed. IP research therefore headed in the new direction of delineation of certain key contaminants, namely organic chemicals such as TCE and PCE, which were known to have been released into

¹ Earth Resources Laboratory, Department of Earth, Atmospheric, and Planetary Sciences, Massachusetts Institute of Technology, Cambridge, MA, E-mail: sogade@erl.mit.edu

² Savannah River Technology Center, Westinghouse Savannah River Company, LLC, Savannah River Site, Aiken, SC

the environment during the previous decades. Olhoeft (1984, 1985) looked at the spectral IP response of clay samples contaminated with industrial solvents and pesticides. The focus was to monitor the performance of clay liners or natural clay horizons as impermeable barriers to contaminant movement in ground water systems. Vanhala et al. (1992) studied the IP response of contaminated glacial till deposits which contained little or no clay. The results showed a decrease in phase shifts for ethylene glycol and heptane contaminated samples, and an increase in phase for toluene contamination, compared to the uncontaminated samples.

The first systematic study of the polarization properties of organic and inorganic contaminated rocks/soils was carried out by Börner et al. (1993). He showed that contamination in certain cases produced a significant and measurable polarization response and affected both the level and shape of both the real and imaginary parts of the spectral response. Interest in the delineation of DNAPLs, particularly PCE and TCE, using IP increased in the 1990s. In this period a scaled model experiment was performed where intentional spill of contamination (PCE) were monitored by IP (Ramirez et al., 1996). McKinley (2003) performed complex resistivity experiments on soil samples taken from the Savannah River Site (SRS), a well documented contamination zone, and calibrated the results using x-ray diffraction and infrared spectroscopy. She concluded that IP was indeed able to delineate areas of contaminated smectite clays, but had no identifiable response in contaminated illite or kaolinite clays. This paper continues this more current trend in research and addresses the feasibility of using IP in a cross borehole configuration to make 3-D images of contaminated zones. The data were collected from the A14-outfall at the SRS in the same area used in McKinley's work.

Background

Site Description

The A-14 outfall at the Savannah River Site was a discharge point for chlorinated solvents between the 1950's and 1980's, including PCE (tetrachloroethene) and TCE (trichloroethene), both of which are DNAPLs. Migration of the contaminants is complicated by subsurface structure, which consists of several clay layers interbedded with sand and silt. The A-14 outfall leads to a tributary of Tims Branch, which eventually discharges into the Savannah River and into local water supply.

Mechanisms of Induced Polarization

There are two main processes believed to be responsible for the IP effect, electrode polarization, and electrolytic or membrane polarization, Madden and Cantwell (1967) and Sumner (1976). Both of these diffusion driven mechanisms allow the subsurface to temporarily store some electric energy by changing ion mobility and thus creating a potential difference. Electrode polarization occurs at the boundary of a metal placed in contact with an ionic solution: the charges with different polarities separate and a potential is established between the electrode and the solution.

For contaminant delineation, it is the second process, membrane polarization, which is of the most importance. This electrolytic polarization takes place in the absence of any current flow, and is due to the negatively charged surface area that rocks and clays generally exhibit (Pape et al., 1987). In this case, positive cations in solution are attracted to the negative surface and cause a build up of excess charge, the two zones of charge

accumulations usually called the electric double layer (EDL) of ions. When an external current is then applied, this cloud of excess positive charge can impede the flow of current by trapping the negative anions on one side while the cations flow freely. The depth of adsorbed charge, and thus the size of the blockage, depends on the valence of active ions, the concentration of active ions, and the relative dielectric permittivity of the electrolyte (Ward, 1990). Other factors include the width of the pore paths, the size and concentration of the ions in the pore fluid, and the amount of pore fluid present, all of which can vary greatly within the vadose zone. If a pore path is effectively blocked by this mechanism, an applied current causes a potential difference across the blocked zone, which again decays when the applied current is ceased. Figure 1 shows a cartoon of these two processes in a geologic setting.

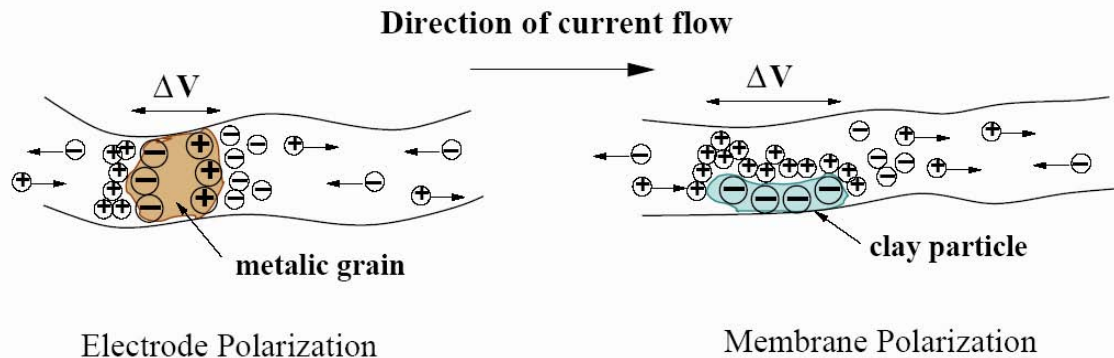


Figure 1: Mechanisms of IP

Polarization of the EDL layer can also lead to the IP effect (Chelidze et al. 1999a,b; Lesmes and Morgan, 2001), but we consider this to be insignificant compared to those of membrane polarization at the frequencies usually considered in IP (i.e. less than 100Hz).

In contaminated zones, there is mounting evidence that microbes bio-degrading the contaminant form as bio-films on mineral surfaces and can either (1) directly contribute to the membrane effect because of their effective large surface areas or (2) because of the complex redox reactions accompanying biodegradation, contribute to the electrochemical alterations of the mineral surface and pore fluids, therefore producing an enhanced IP effect (Abdel Aal et al, 2004).

Atekwana and her colleagues showed by laboratory and field experimentation that the electrochemical alterations due to biodegrading hydrocarbon contamination increased pore fluid salinity (i.e. increased mineral dissolution), and thereby in all cases caused an increase in the effective conductivity of the contaminated zone (Atekwana, et al., 2004).

Experimental Design

The IP array employed during the A-14 outfall experiment consists of four boreholes, each with a total depth of approximately 26 m (84 ft), and 5 surface electrodes as shown in figure 2. Each borehole has 7 current bearing electrodes and 7 potential electrodes placed intermittently at 1.83 m (6ft) intervals. Data collected using current electrodes between two boreholes is referred to as a panel, as labeled in figure 2. Figure 3 shows a cartoon of the panel between boreholes MIT-1 and MIT-2 as an example of the

potential measurements made for one current pair in that panel. The current bearing electrodes (Tx) are made of elemental copper pipes, and the potential electrodes (Rx) are Ag-AgCl non-polarizing porous pot electrodes, which were designed to be emplaced for 2 years. In addition to the borehole Tx electrodes, there are 5 surface Tx electrodes, four on the perimeter and one in the center of the borehole array.

An alternating current is injected through a pair of the copper Tx electrodes across two boreholes, or from a surface electrode to a borehole electrode. During each current injection, the potential field is measured between the reference Rx electrode in borehole MIT-1 and every other Rx electrode in each of the boreholes. The equipment used for the complex resistivity measurements was the Zonge GDP-32 II system, enhanced by the MX-30 multiplexing system, which allows programmable switching of the current and potential electrodes. This measurement system records the phase angle and the amplitude of both the injected current and measured potentials. For each current injecting pair, there are 27 measurements collected (6 in MIT-1 and 7 in the other three boreholes). In each panel there are a total of 63 current pair configurations and there are six panels giving a data set of $27 \times 63 \times 6 = 10206$ samples of the generated potential field for each measured frequency. For the purpose of this investigation, two sets of data were collected, one at $(1/4)$ 0.25 Hz and the other at $(1/16)$ 0.0625 Hz.

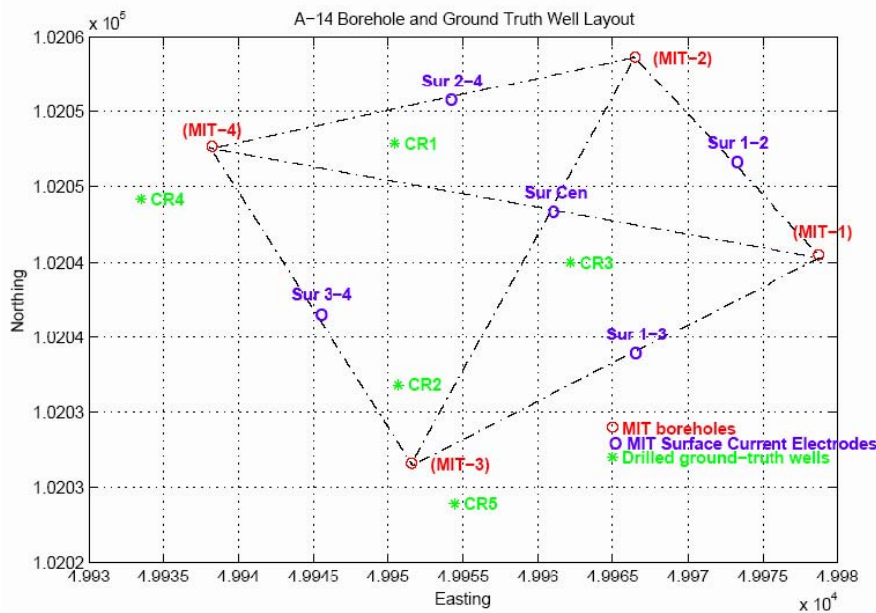


Figure 2: Map view of MIT surface electrodes and boreholes and the ground truthing boreholes.

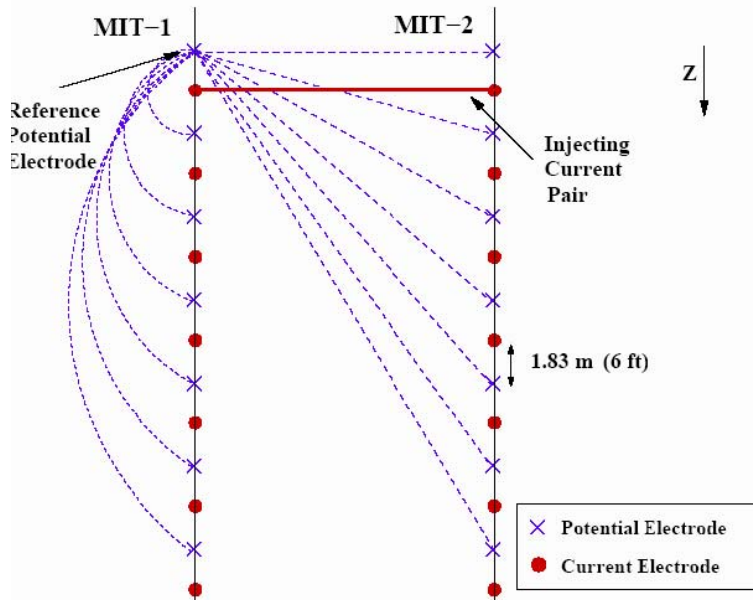


Figure 3: Example of potential measurements made for one current pair in one panel.

Raw Data and Preprocessing

Noise and Data Distortions

Before inverting the data set for the subsurface properties, it is important to filter out noisy data and account for any data distortion. Possible sources of noise include random or correlated errors in the equipment, and ambient current sources within the ground, such as telluric currents or self potentials. Electromagnetic inductive or capacitive coupling, both of which scale with frequency, can also give spurious results, but this is considered to be a distortion of the data rather than noise (Wait, 1959; Dey and Morrison, 1973; Madden and Cantwell, 1967). Because many of the measurements are made at the millivolt level, it is important to reduce noise levels at the site to a minimum and to filter out any spurious data points in the data set before performing an inversion.

Capacitive coupling is due to current leakage between proximate wires or between wires and ground, and can be reduced by careful wiring layout and some instrumentation enhancements (Appendix 16.1.4, this volume). Electromagnetic coupling is due to the injecting and receiving circuits behaving as an electrical transformer with the ground and free space being the intervening medium. The mutually inducted currents can be picked up by the electrodes and contaminate the real signal. While a rigorous analysis of the electromagnetic coupling is beyond the scope of this report, previous experiments carried out at the Earth Resource Laboratory (ERL) on SRS data suggest that electromagnetic coupling is prevalent in data collected at frequencies higher than 1 Hz, Morgan (2001). The data collected for this experiment were therefore below the 1Hz cut off.

Phase Editing

The data can be displayed in the complex plane showing real and imaginary impedance. A linear fit to this dataset gives an estimate of the average phase of the

subsurface. If the ground were homogeneous, the data would fall on a straight line through the origin and the gradient would give the phase. Because the phase difference between injected and recorded current is, by definition, a delay, the slope must be negative. For zero frequency (DC current) the data would all lie on the real axis. Phase measurements are more error prone because of small signal amplitudes that often occur. There are two types of data points which are edited out. First, any data that fall in the first or third quadrants on the real/imaginary plane are removed. These are data which have a positive phase (phase lead opposed to lag) and might suggest an inductive process.

The theory of IP in rocks is based on capacitive processes and thus any data suggesting an inductive phenomenon are either due to ambient noise, capacitive, electromagnetic, or geometric coupling distortion. Geometric coupling is accommodated in the model and several synthetic model runs, using SRS geometry, suggest it accounts for about 2.5% of the data at the maximum. The fraction of data with positive phases in FY03 data is about 18% therefore we suspect these may have arisen from sources apart from geometric coupling. Secondly any data with an absolute value of phase greater than 200 milliradians are also edited out before inversion. McKinley (2003) conducted IP measurements at the SRS site and in the laboratory using core from SRS and found no phase lags above 500 milliradians; the vast majority were below 200 milliradians. These high phase data could be the result of any of the sources of noise discussed earlier. Figure 4 shows the phase edited data as input to the inversion code. Approximately 20% of the data have been removed by editing.

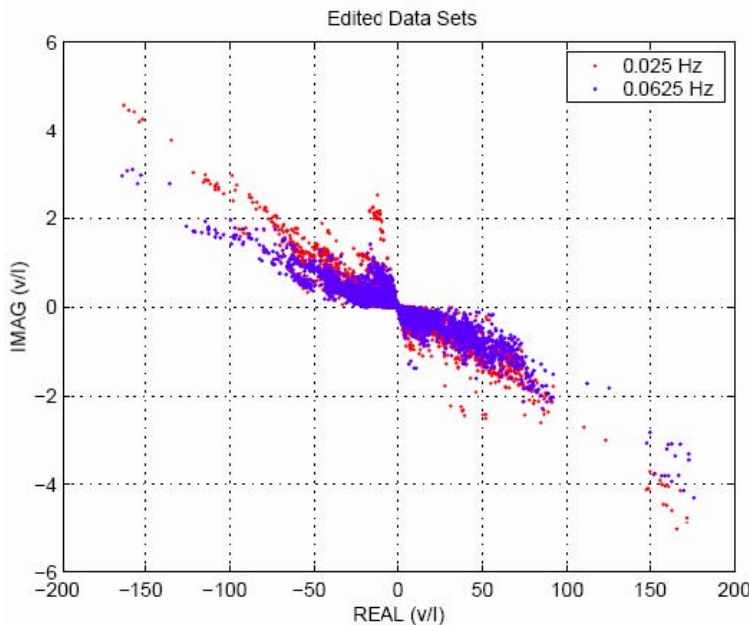


Figure 4: Phase Edited Data (1/16 and 1/4 Hz)

Inversion Algorithm

An inversion algorithm based on a 3D complex resistivity model of the earth was developed at the ERL (Shi, 1998). The forward problem can be written as

$$\nabla \left(\frac{1}{\rho(\mathbf{x})} \nabla V(\mathbf{x}) \right) = \sum_{\alpha} \mathbf{I}(\mathbf{x}) \delta(\mathbf{x} - \mathbf{x}_{\alpha}) \quad (1)$$

where $\rho(\mathbf{x})$ is the distribution of complex resistivities at spatial locations \mathbf{x} in the earth, and $V(\mathbf{x})$ are the distribution of complex potentials during the injection of the currents at locations \mathbf{x}_{α} (in our case, $\alpha = 1, 2$, and $\mathbf{I}(\mathbf{x}_1) = -\mathbf{I}(\mathbf{x}_2)$). Note that the above formulation assumes a DC formulation, and therefore does not account for electromagnetic coupling effects.

The 3D space of the forward problem can be discretized into network nodes and impedance branches and solved as a transmission network problem, a concept introduced into geophysics by Madden (1972). The discretized forward problem results in algebraic equations which is solved using a complex conjugate gradient algorithm. The solution to the 3D complex resistivity forward and inverse problem is already aptly described in Weiqun Shi's thesis (Shi, 1998) and will not be repeated here. The solution to the 3D forward and inverse problem for real resistivities using the transmission network model can also be found in Zhang et al., (1995). However, certain pertinent aspects of the inverse problem not described by Shi follow.

In order to solve the non-linear, ill-posed inverse problem in the complex domain, Thikonov regularization is needed as for the regularization (Thikonov and Arsenin, 1977) to help the ill-posed inversion to converge to a solution that has the minimum structure needed to fit the data to a prescribed RMS error. Therefore the inverse problem can be posed as an optimization problem for an objective functional $\Phi(\mathbf{d}, \mathbf{x}, \tau)$ given by

$$\Phi(\mathbf{d}, \mathbf{x}, \tau) = (\mathbf{W}(\mathbf{d} - \mathbf{g}(\mathbf{x})))^H (\mathbf{W}(\mathbf{d} - \mathbf{g}(\mathbf{x}))) + \tau (\mathbf{L}\mathbf{m})^H \mathbf{L}\mathbf{m} + \tau (\mathbf{m} - \mathbf{m}_0)^H (\mathbf{m} - \mathbf{m}_0) \quad (2)$$

where H stands for the Hermitian. The measured data is represented by a complex vector valued function \mathbf{d} ($d_i, i = 1 \cdots N$), and the inversion parameters \mathbf{m} ($m_i, i = 1 \cdots M$), is a complex vector valued function whose components are log-rescaled resistivities of the model blocks according to $m_i = \log(\rho_i)$. Data and model lengths of N and M have been assumed respectively. Note that for both \mathbf{m} and ρ the location \mathbf{x} in parentheses has been dropped for convenience.

The data weighting matrix, \mathbf{W} , is given by $\mathbf{W} = \text{diag} \left[\frac{1}{\sqrt{\sigma_{ii}}} \right]$, for $i = 1$ to N , where σ_{ii} is data variance at the i th measurement point. The Zonge GDP 32II system records only a standard error of the mean for the phase, which we call $\Delta\phi$. This can be converted to the data variance used in \mathbf{W} by $\sqrt{\sigma_{ii}} = i\Delta\phi$.

\mathbf{L} is a first or second order difference operator; $\mathbf{m}_0 = \log(\rho_0)$ represents an a priori model, and τ acts as a Lagrange multiplier or a regularization parameter. The optimization problem defined in (2) attempts to minimize the data misfit with the first term, enforce smoothness between close neighbor cells with the second term, and ensures the closeness of the constructed model to a priori specification with the third term.

The inversion is iterative; it starts with an initial guess for $\mathbf{m}_{\text{orig}} = \log(\rho_{\text{orig}})$, calculates updates $\Delta\mathbf{m}$, and then constructs a new model $\mathbf{m}_{\text{new}} = \mathbf{m}_{\text{orig}} + \Delta\mathbf{m}$ that moves in

the direction of decreasing $\Phi(\mathbf{d}, \mathbf{x}, \tau)$. Subsequent iterations replace \mathbf{m}_{orig} with \mathbf{m}_{new} , and repeat the update process. Note that the updates use a complex biconjugate gradient algorithm to solve the complex linear algebraic problem resulting from the minimization of the complex residual between data and model in a least squares sense.

The parameter τ starts with an initial guess value and is updated based on considerations similar to those introduced in the Levenberg-Marquadt algorithm (Levenberg, 1944; Marquardt, 1963). The parameter τ is decreased (division by a factor) along with a decrease of the data misfit from the previous iteration and increased (multiplication by a factor) otherwise. A cursory explanation for this choice of the τ update algorithm can be seen by noting that τ moves the inversion in $\Phi(\mathbf{d}, \mathbf{x}, \tau)$ space. The larger τ gets, the inversion biases the constructed solution towards smoother character and the a priori specification. Contrarily, the smaller τ gets, the inversion is biased to construct models, which preferentially reduce data misfit. Thus, increasing or decreasing τ at a given iteration based on feedback from the inversion, adjusts to the competing demands of the optimization problem. Without going into numerical evaluations, it can be noted that in terms of execution time, this algorithm should always do better than the (OCCAM) linear search algorithm for τ introduced by DeGroot-Hedlin and Constable (1990), and in many cases better than the constant τ algorithm of Sasaki (1989).

The accuracy of the inverted result depends on several different factors; the contrast of the anomalies, the background both in phase and resistivity magnitude, the size and shape of the anomaly, the location within the electrode geometry, and the electrode geometry itself. All of these factors can influence the results of a complex resistivity IP inversion. Before using the code on the field data, a series of synthetic examples were inverted to help the understanding of the final result.

Inversion of Field Data and Core DNAPL Concentrations

Here inversion results from the field data are presented and a comparison is made between the inverted result and the DNAPL concentrations taken from core samples in the ground truthing boreholes. The inverted data provide values of phase and resistivity magnitude for each block in the model space (5x5x6ft); from this information it is possible to calculate the real and imaginary conductivity.

Interpreting the IP inversion result in terms of contaminants is complicated by the presence of clays. It is well established that clay gives a strong IP response, Vaquier et al. (1957), Ogilvy and Kuzmina (1972) and Bodmer et al. (1968), and when mixed with contaminated zones the measured response is some combination of the two effects. According to Archie's law, the resistivity of a clay mineral should increase when contaminated with an organic solvent that displaces the less resistive pore fluids. However, this also depends on the length of time the clay has been exposed to the contaminants and the effect of microbial degradation activities. For example, Atekwana et al. (2004) showed based on laboratory and field experimentation that due to the effect of microbial degradation, LNAPL hydrocarbon contamination results in an increase of the conductivity of the affected zones. This probably reflects the difficulty of interpreting contamination induced polarization data based on only the physical theories. Horton (2001) also noted that physical adsorption of contamination by clays is a very fast process and can occur within the time frame of laboratory measurements. However, chemical

adsorption is usually much slower and would probably occur when the mineral surfaces have been exposed to the contamination for decades, a surface reaction probably not witnessed in laboratory time frames. In addition, the type of clay will also play a role. The cation exchange capacity, which is a measure of the clay's ability to retain cations, varies between clays, and is an indicator as to how much adsorption will take place on the surface and therefore affect the IP response. This paper does not discriminate between types of clay, as there is typically a mix of several clay types found in one area. Based on laboratory results using contaminated samples of sandstones and clays (Börner et al., 1993; McKinley, 2003), one generally expects to see an increase in real resistivity coupled with an increase in phase. Thus, a basic interpretation of the inversion results can be constructed as shown in figure 5.

In addition to the basic interpretation chart we have found that in conductive polarizable areas, the imaginary conductivity correlates linearly with the contaminant concentration data.

	low phase	medium phase	high phase
high resistivity	Clean sands with low water saturation	Possible Contaminant	Very likely Contaminant
low resistivity	Clean sands with high water saturation	Clay or Clay-disseminated sand. Possible contaminant	Likely Contaminant

Figure 5: Basic interpretation of inversion results

Results

SIP for Mapping PCE/TCE contamination

For mapping contamination, the interpretation chart that was shown in figure 5 can be used for the interpretation of the polarization distribution of the subsurface at a given frequency. Different polarized regions of the subsurface can reach spectral peaks at different frequencies. This is because the grain size distribution mostly controls polarization spectral peaks (Lesmes and Morgan, 2001) and can be different for polarized regions thereby leading to different spectral responses. In addition, the chemical interactions in certain regions might be frequency dependent in certain cases of clay-organic reactions (Olhoeft, 1985). Thus, a look at the imaged sections at different frequencies is warranted. SIP results presented here for mapping of PCE/TCE contamination are at base frequencies of 1/16 and 1/4 Hz. These two frequencies were chosen based on carefully performed initial tests at this site (Morgan, 2001).

The plot in Figure 6 shows the strong correlation between the contaminant concentrations of PCE and the inverted FY03 imaginary conductivity for the 1/16 Hz. The plot also shows a partial correlation for the 1/4 Hz SIP data. The imaginary conductivity is derived by extracting the inversion results along each borehole location then scaling by a constant factor of 20,000 to bring it to the same range as the concentration data, allowing for easy visual comparison. The imaginary conductivity data of the five boreholes can be cross-compared in the figure, because they are all scaled by the same constant, making it clear where the high and low contaminant zones are within the five boreholes. It appears that there is a linear relationship between $\log_{10}(\text{PCE})$ concentration and imaginary conductivity, and the fact that the constant scaling factor brought the lowest polarization data to about 1mg/kg suggests that the background polarization in this area is equivalent to 1 mg/kg of PCE and therefore sets the resolution limit using IP to 1mg/kg. The TCE concentration at the same sampled point is known to be consistently lower than those of PCE at this site therefore it is not shown in the correlation plots.

Note that only boreholes CR-1, CR-2, and CR-3 are within the volume designed to be imaged by the four MIT boreholes (figure 2). Additionally, the MIT boreholes extended to about 25m depth while the CR boreholes sometimes extend to 35m. Thus, only the imaginary conductivity data in the first 25m of CR-1, CR-2, and CR-3 are to be trusted, though all the results for all the CR boreholes are shown.

Also, the correlation in CR-3 was not very good for the 1/4 Hz data and could be due to data distortion by noise, electromagnetic or capacitive couplings. However, the most contaminated part of CR-3 also presents the strongest change in frequency between 1/16 and 1/4 Hz suggesting that this part might contain reactive materials undergoing strong frequency dispersions in this bandwidth. McKinley (2003) reported that such regions which show strong dispersion and high phase values contain smectites.

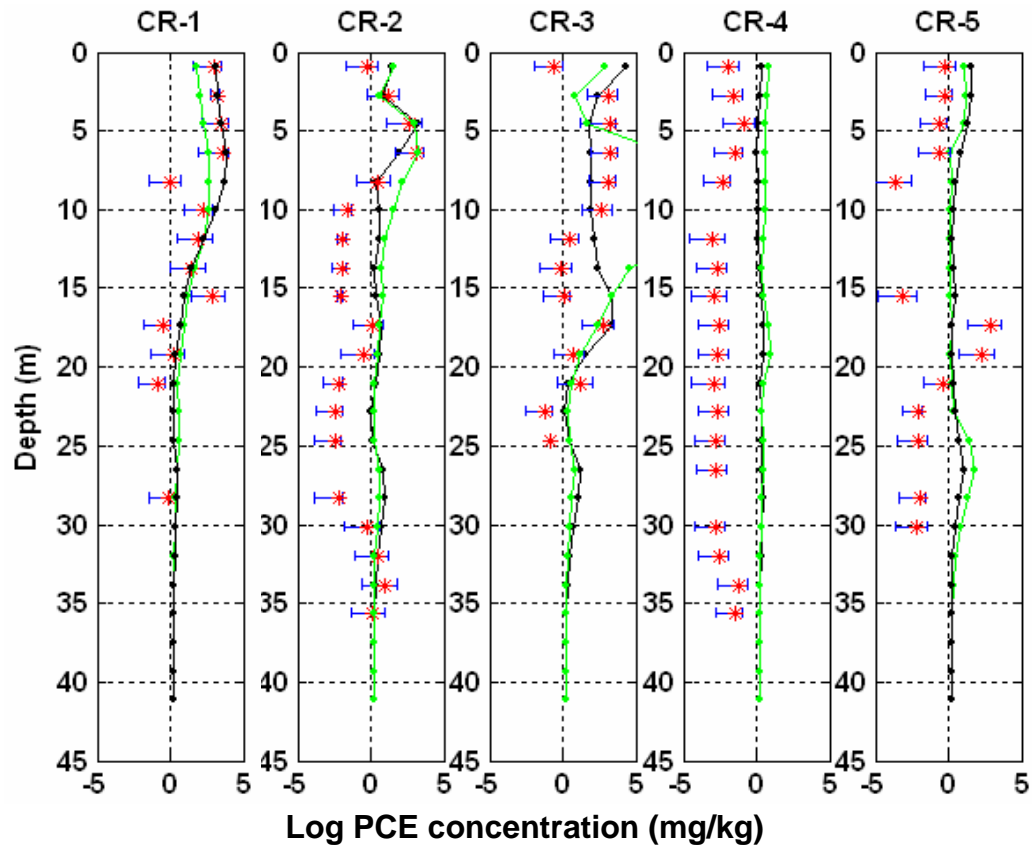
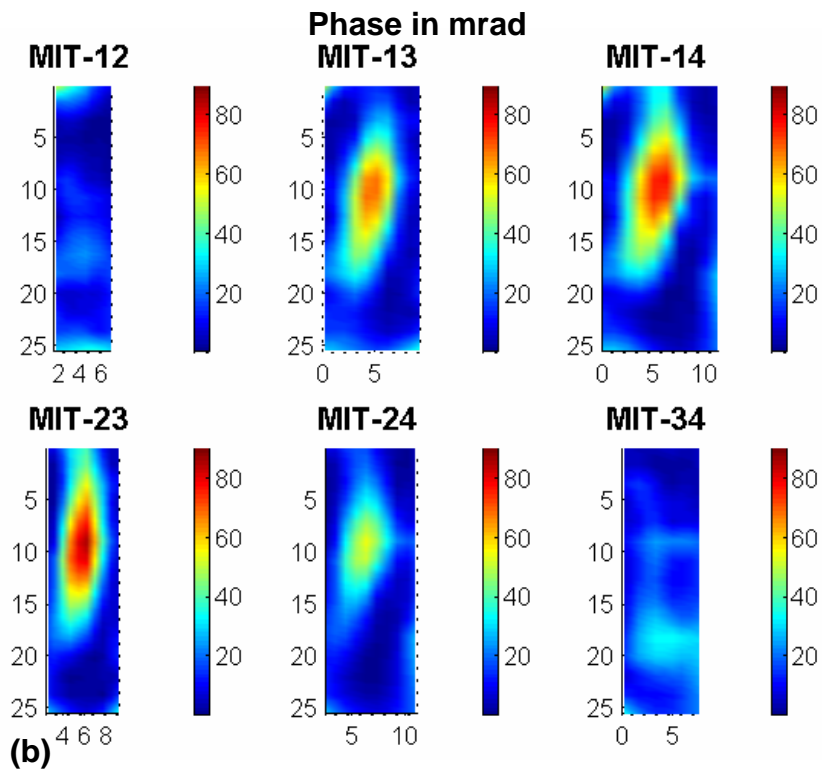
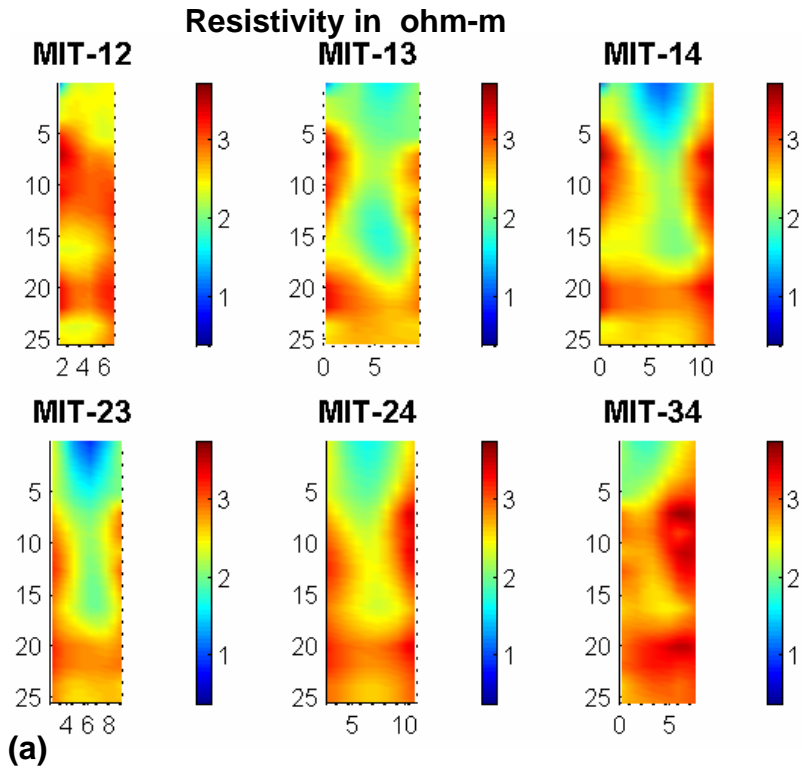


Figure 6: Comparison of ground-truth PCE concentration data (red star) in the five CR ground-truth wells and scaled imaginary conductivity derived from inversion of the FY03 1/16Hz (black lines) and 1/4Hz (green lines) data. The blue bars indicate the error bar attached to each concentration data

Figure 7 shows the resistivity, phase, and imaginary conductivity distribution in the contaminated zone along the six panels MIT-12, MIT-13, MIT-14, MIT-23, MIT-24, and MIT-34. It shows that the contaminated zones, as revealed by the imaginary conductivity, are relatively more conductive zones supporting the results of Atekwana, et al. (2004). The phase anomaly visually reveals the polarized volume although it does not correlate well with borehole concentration data. Our experience has shown that phase anomalies correlate very well with concentration data for resistive polarized targets and imaginary conductivity for conductive polarized targets.



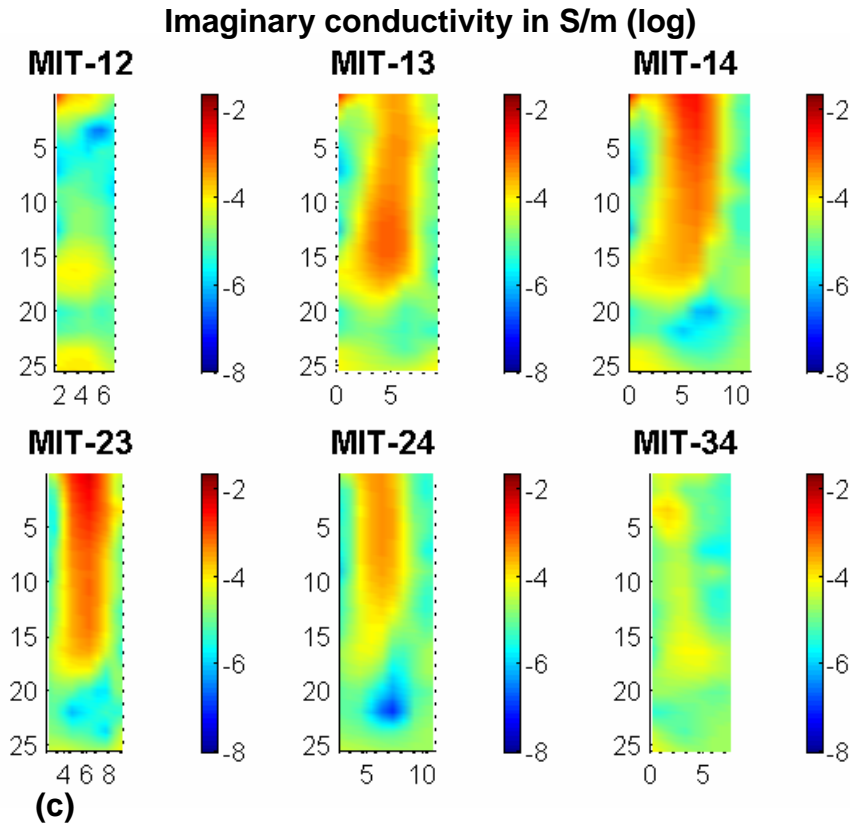


Figure 7: The inversion results of the 1/16Hz data of 2003 shown as 2D panels taken from transects of the 3D volume. (a) Magnitude resistivity (Ω -m), (b) phase (mrad), and (c) imaginary conductivity (S/m)

SIP for monitoring PCE/TCE contaminant fate and transport

We had hoped that since SIP provided such good correlation with contaminant concentration data at the 1mg/kg level during the FY03 study, it might also provide some monitoring capabilities. The experiment in FY04 hoped to detect whatever alterations there might be to the distribution of PCE/TCE after the FY03 measurements. The FY04 measurements were supposed to be acquired during the same season as the FY03 so that some of the site conditions might remain the same i.e. soil moisture distribution, temperature etc., but logistic difficulties delayed acquisition till June 2004, when it is warmer, and possibly drier and the soil might have lost more moisture.

Figure 8 shows a similar plot for the FY04 data where the imaginary conductivity showed up only in small regions in boreholes CR-1 and CR-2 equivalent to 100mg/kg. This was not detected earlier in FY03. The remarkable similarity of the 1/16 and 1/4 Hz imaginary conductivity response in the five CR plots suggests that there is little spectral difference between the 1/16 and 1/4 Hz response. The similarity of the result of the two independent measurements at 1/16 and 1/4 Hz also affirms the validity of the result. If we are to assume based on the FY03 result that imaginary conductivity predicts PCE concentration then definitely a major movement of the contaminant in this area has occurred. In addition there are large imaginary conductivity values within the first 5

meters of all the boreholes except CR-2, which suggest a surface activity in this area between March 2003 and June 2004 might have affected polarization response. However, the disappearance of the contaminated regions is probably due to movements of the contaminant mass during ground-truthing and nearby remediation activities using Soil Vapor Extraction.

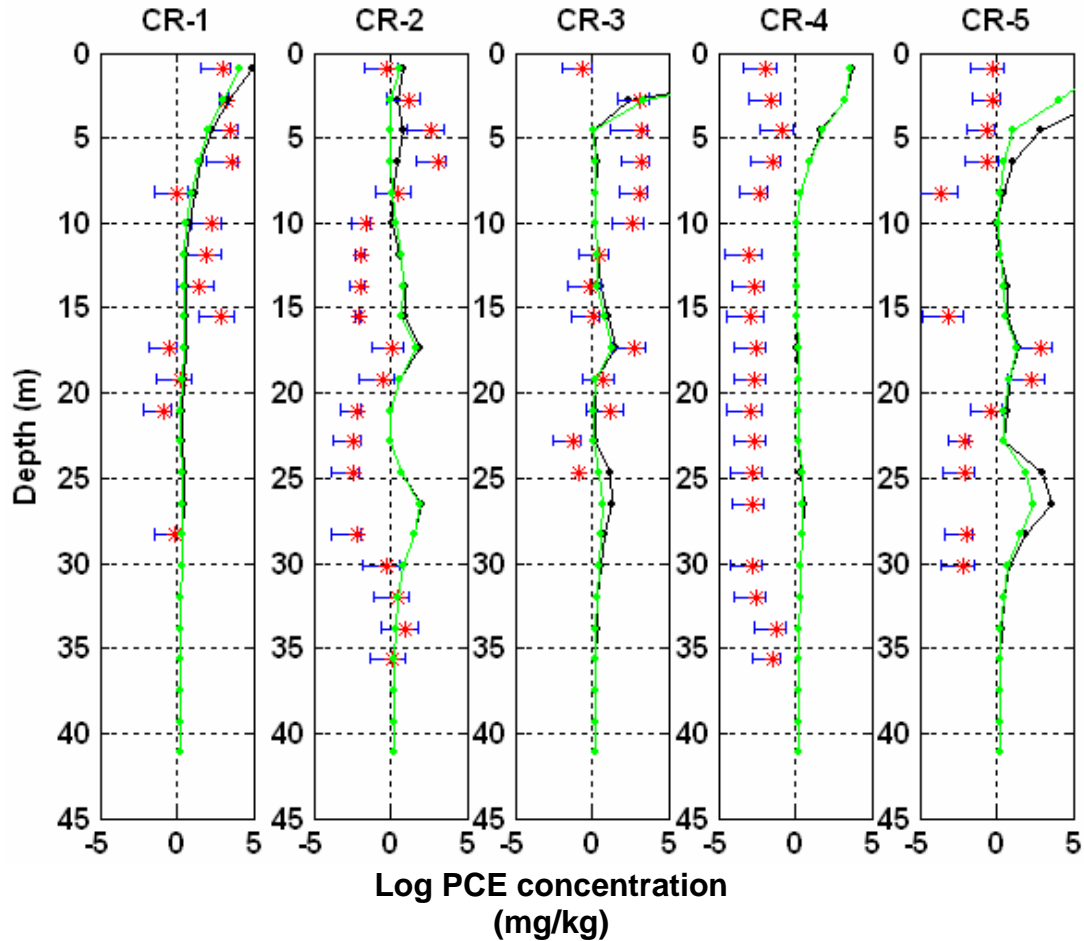
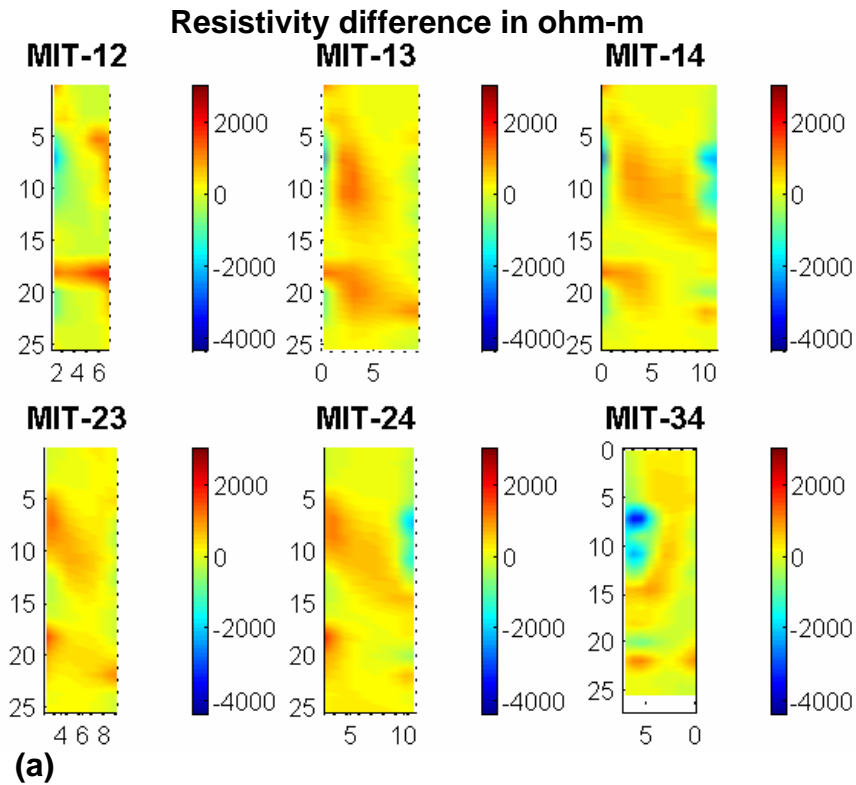
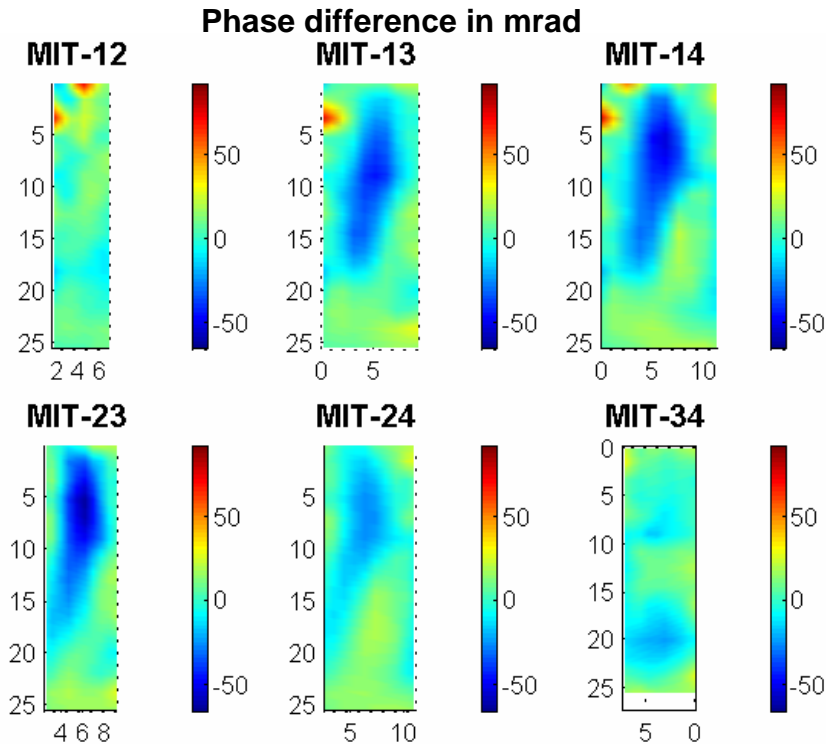


Figure 8: Comparison of ground-truth PCE concentration data (red star) in the five CR ground-truth wells and scaled imaginary conductivity derived from inversion of the FY04 1/16Hz (black lines) and 1/4Hz (green lines) data. The blue bars indicate the error bar attached to each concentration data.

To get a sense for the resistivity changes in the area during the period of the time-lapse study, figure 9 shows the resistivity and phase difference between March 2003 and June 2004. Positive values indicate increased resistivity or phase between June 2004 and March 2003, and vice versa for negative values. It is seen that significant resistivity increases had occurred only in some isolated zones of the ground where there had been polarization i.e. between 5 and 15m on panels MIT-13, MIT-14, MIT-23, and MIT-24. There is an isolated resistivity decrease between 5 and 10m near MIT-3 on panel MIT-34.

We can associate the resistivity changes to loss of moisture especially in sandy areas and might be due to the slightly off season repeat measurements in 2004, or any of the activities mentioned earlier. In addition, because the resistivity increases also correlate with zones that were previously polarized, it is likely that the changes are related to processes that can decrease polarization such as loss of material or stoppage of biodegradation, both somehow also related to loss of moisture.





(b)

Figure 9: The difference of the inversion results of both the FY03 and FY04 1/16Hz data shown as 2D panels taken from transects of the 3D volume. (a) Magnitude resistivity difference ($\Omega\text{-m}$), (b) phase difference (mrad), and (c) imaginary conductivity difference (S/m)

SIP for Development of conceptual models

Figure 10 shows a 3D volume distribution of the contaminant mass in this area based on the interpolation of the 5 CR ground-truth wells (Rossabi et al., 2004). It should be noted that sampling in each of the 5 CR wells started at 1ft depth and there is no concentration data within the first 1 foot of the surface. Based on the linear connection between imaginary conductivity and $\log_{10}(\text{concentration})$ data for this area it is interesting to consider the possibility of producing a 3D volume distribution of the contaminant mass for this site. Figure 11 and 12 shows a 3D distribution of the contaminant mass derived based on the FY03 imaginary conductivity data at 1/16 Hz. Figure 11 shows the predicted contaminant distribution at the level of 1mg/kg and above, and uses the same view as that in figure 10. There is a general agreement in the distribution of the contaminant mass though the SIP derived mass showed more details, in terms of exit points outside the bounded volume. Note also that figure 10 is produced for the volume encompassed by the five CR wells which is larger than the volume spanned by the four MIT wells (see figure 1 for distribution of wells). Figure 12 shows the distribution at the 10mg/kg level and above from a different view. From the result in figure 12, it is possible to develop a conceptual model of contaminant distribution at this site, which is not offered by figure 10. It appears that the contaminant mass entered from

the surface between MIT-24 and MIT-13, and subsequently exited somewhere between 7.5 and 15m from the MIT-13 interface in a SE direction.

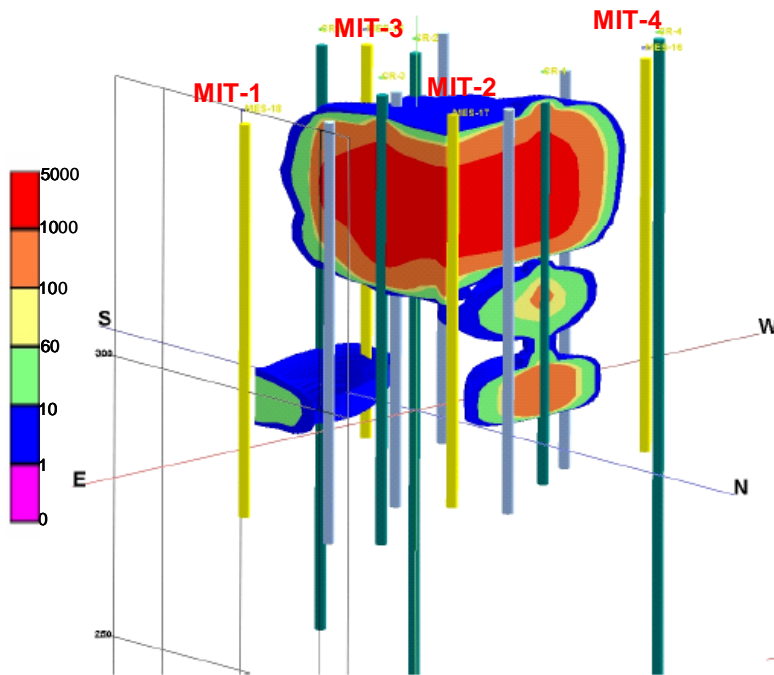


Figure 10: The conceptual model for contaminant mass developed based on the concentration data from five ground-truth wells (after Rossabi et al., 2004)

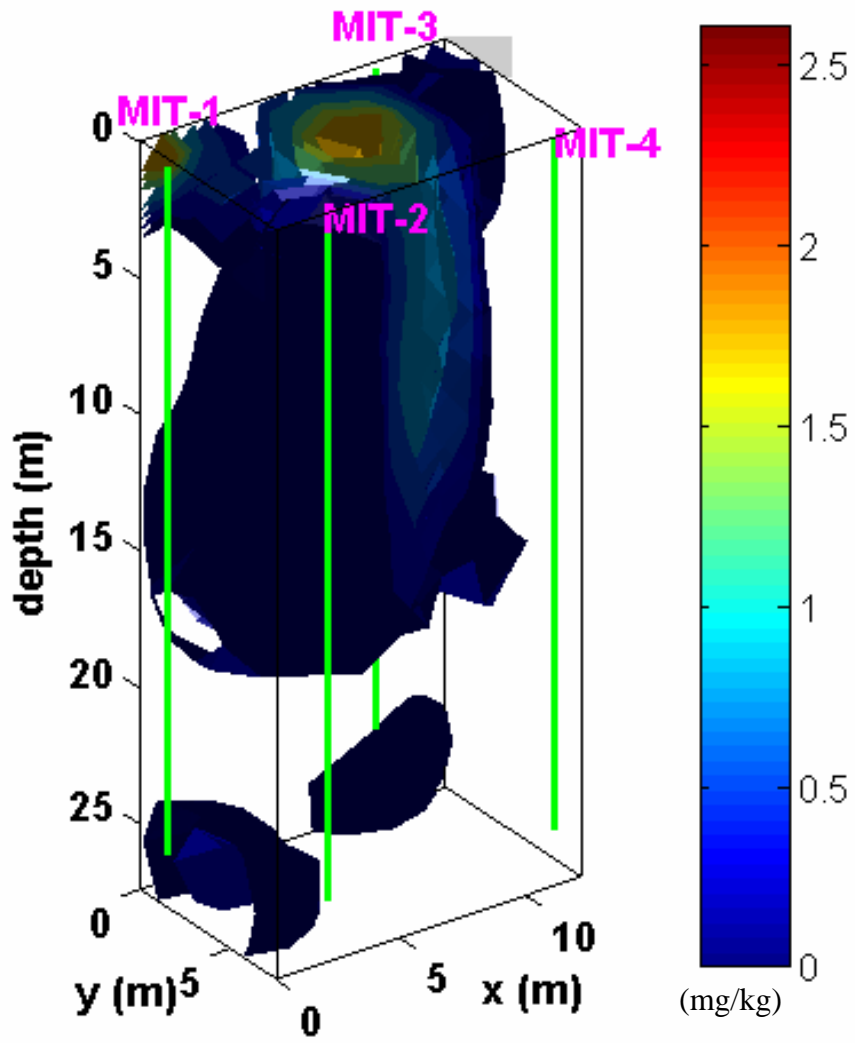


Figure 11: The conceptual model for contaminant mass at the level of 1mg/kg and above, developed from prediction of the inverted imaginary conductivity

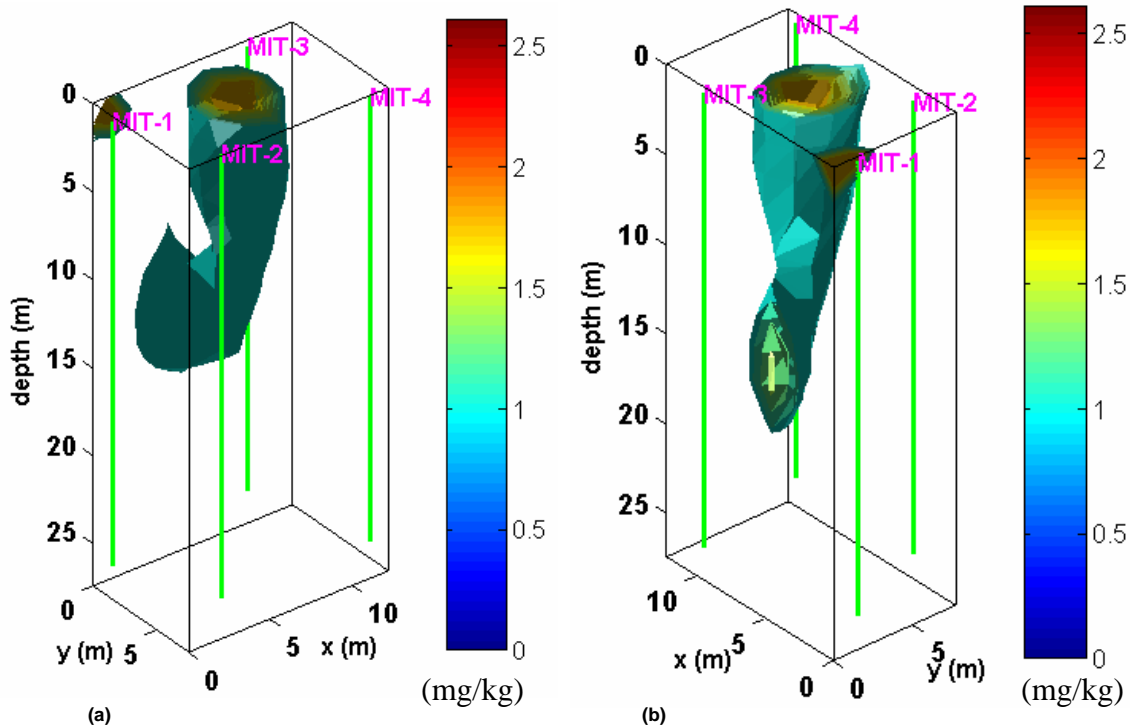


Figure 12: Two views of the conceptual model for contaminant mass at the level of 10mg/kg and above, developed from prediction of the inverted imaginary conductivity

Discussions

The good correlation between the FY03 imaginary conductivity inversion result and the contaminant concentration data was very encouraging and has been used to judge significant contaminant movements based on the FY04 inversion results. Based on results of 2D inversions of SIP data in some other part of the A-14 Outfall area (Morgan, 2001), good correlation has been recorded for the location of a phase anomaly with concentration data for a resistive polarizable target. We are beginning to suspect that phase is better correlated with resistive targets and imaginary conductivity for conductive targets as in the current study, though this aspect needs more careful investigation. However, if the findings that degrading LNAPL hydrocarbon contamination produces conductivity increase of the contaminated zone (Atekwana et al., 2004) can be extended to chlorinated solvents (i.e. PCE/TCE DNAPL). Then it appears that the correlation of imaginary conductivity with concentration data observed in the present study will be applicable at other PCE/TCE contaminated sites.

It is also pertinent to point out that the loss of correlation between imaginary conductivity and concentration data near the surface, especially in borehole CR-3, might be related to the fact that the two measurements might not be quantifying exactly the same property in the rock. This is because there was a lapse of three months between the

IP measurements and the core sampling and groundwater processes may have affected the spatial concentration of TCE and PCE in that time. Additionally, the discharge outlet is located somewhere in the vicinity of the CR-1, CR-2 and CR-3 boreholes with constant discharge of water throughout the measurement period. The moving water could create self-potential anomalies which then produce anomalous IP effects by a process of cross coupling of flows (i.e. see, Marshall and Madden, 1959). However, in regard to the whole experiment these are considered as second order effects, the more important issue being that of scaling. The scaling issue arises because the concentrations of TCE and PCE were measured at 1ft intervals from a small cored sample (< 3 inches), as opposed to the inversion block size of 5x5x6 ft. Thus, to compare the two data sets the concentrations must be averaged over 6ft intervals. The errors bars in figures 6 and 8 show the standard error of the mean associated with repeat measurements and averaging the concentrations over a 6ft interval. It is likely these error bars could be substantially larger because the contaminant content in the soil varies laterally as well as in depth. Therefore comparing a block from the inversion, which represents some average concentration, and 6 samples taken from a small core can be a source of error. This is more so because in unsaturated soils, i.e. the vadose zone, DNAPL's have a tendency to finger down into sandy areas giving high concentrations in localized areas and then spread over less permeable clayey zones. Experiments performed using TCE in unsaturated sands showed that contaminants behave similarly to petroleum organic liquids, Pankow and Cherry (1996).

Note also from the plots in figures 6 and 8 that where the concentration data changed sharply the imaginary conductivity took a more gradual path suggestive of an averaging effect. Making sharp conductivity changes is a major limitation of the resistivity method. In addition, regularization enforces a smoothness constraint with the consequence that nearest neighbor parameter values hardly makes sharp changes.

Conclusions

From the inversion results and subsequent comparison with concentration data, there is good correlation for imaginary conductivity in the three ground truth boreholes within the survey area. The concentrations predicted by imaginary conductivity have a threshold of 1mg/kg, which is related to the background imaginary conductivity at this site, probably due to clean clay-sand mixtures. Of the two measured frequencies, there is a better correlation in the 1/16 Hz data. It is natural to assume that for lower frequencies there is less noise and distortion from EM-coupling, and the improved correlation with the concentrations may be a consequence of this.

The primary objective of this work was to show that a borehole electrode array could detect an IP signal that is correlated with concentration data, and we believe these results are promising. The secondary objective was to show that IP could provide a monitoring capability for contaminant fate and transport. Our results indicate that this is the case.

The main area that needs further attention is EM-coupling and instrumentation improvements. In order to look at the full spectral signature of attributes such as phase or imaginary conductivity, an analysis of EM-coupling in a borehole environment is necessary to account for the distortion at higher frequencies. Laboratory experiments (McKinley, 2003) have shown that the TCE and PCE show certain spectral signatures over a broad range of frequencies, which differentiates them from uncontaminated soil. If

the distortion from EM-coupling is accounted for, data can be collected over a wider frequency band and these signatures can be used as diagnostics in interpretation.

Acquiring broadband SIP data is a very time-consuming process, and data acquisition speed is an area that needs more attention. Instrumentation improvements offering an order of magnitude increase in acquisition speed will make SIP a very appealing technology for site characterization applications.

Acknowledgement

The authors wish to express their gratitude to Mr. Paul Wang of Concurrent Technologies Corporation (CTC), and the Environmental Management Science Program (EMSP) of the US Department of Energy (DOE), for the funding of parts of this work via the projects CTC project 004846/DOE project DE-AM26-99FT40465DOE and EMSP project DE-FG07-96ER14714.

References

- Abdel Aal, G. Z., Atekwana, E. A., Slater, L. D., and Atekwana, E. A. (2004) Effects of microbial processes on electrolytic and interfacial electrical properties of unconsolidated sediments, *Geophys. Res. Lett.*, 31, L12505, doi:10.1029/2004GL020030
- Angoran, Y.E., Fitterman, D.V., and Marshall, D.J. (1974) Induced polarization: A geophysical method for locating cultural metallic refuse, *Science*, 184, 1287–1288.
- Atekwana, E. A., Werkema, D. D. , Duris, J. W. , Rossbach, S., Atekwana, E. A., Sauck, W. A., Cassidy, D. P., Means, J., and Legall, F. D. (2004) In-situ apparent conductivity measurements and microbial population distribution at a hydrocarbon contaminated site, *Geophysics*, 69, 56– 63.
- Bleil, D. F. (1953). Induced polarization: A method of geophysical prospecting. *Geophysics*, 18:636– 661.
- Bodmer, R., Ward, S. H., and Morrison, H. F. (1968). On induced electrical polarization and groundwater. *Geophysics*, 33:805–821.
- Börner, F., Gruhne, M., and Schön, J. (1993). Contamination indications derived from electrical properties in the low frequency range. *Geophysical Prospecting*, 41:83–98.
- Chelidze, T.L., Gueguen, Y. (1999a) Electrical spectroscopy of porous rocks: a review – I. Theoretical models, *Geophys. J. Int.*, 137: 1-15.
- Chelidze, T.L., Gueguen, Y., and Ruffet, C. (1999b) Electrical spectroscopy of porous rocks: a review - II. Experimental results and interpretation, *Geophys. J. Int.*, 137: 16-34.
- deGroot-Hedlin, C. and Constable, S. (1990) Occam's inversion to generate smooth, two-dimensional models from magnetotelluric data, *Geophysics*, 56, 2102
- Dey, A. and Morrison, H. F. (1973). Electromagnetic coupling in frequency and time domain induced polarization surveys over a multilayered earth. *Geophysics*, 38(2):380–405.
- Fraser, D. C., Keevil, N. B., and Ward, S. H. (1964). Conductivity spectra of rocks from the craigmont ore environment. *Geophysics*, 29(5).
- Horton, R.J., 2001, Adsorption of Chlorinated Non-Polar Organic Solvent on

- Montmorillonite, Colorado School of Mines, Department of Geology and Geologic Engineering, Ph.D Thesis, Golden, CO., 127p.
- Jackson, D. G., Rossabi, W. K., and Riha, J. (2000). Characterization activities to determine the extent of dnapl in the vadose zone at the a-014 outfall of a/m area. Technical report, D.O.E. WSRC- RP-99 00569.
- Lesmes, D.P., and Morgan, F.D. (2001) Dielectric spectroscopy of sedimentary rocks, *J. of Geophys. Research*, 106 (B7): 13329-13346.
- Levenberg, K. (1944) A method for the solution of certain problems in least squares, *Quart. Appl. Math.*, **2**, 164-168.
- Madden, T.R., 1972, Transmission systems and network analogies to geophysical forward and inverse problems, O.N.R. Tech. rep. no. 72-3, M.I.T.
- Madden, T. R. and Cantwell, T. (1967). Induced polarization a review. *Mining Geophysics, Society of exploration geophysics*, 2:373–400.
- Marine, I. W. and Bledsoe, H. W. (2000). Supplemental technical summary m-area groundwater investigation. Technical report, E. I duPont de Nemours & Co. DPSTD-84-112.
- Marquardt, D. (1963) An algorithm for least-squares estimation of non linear parameters, *SIAM J. Appl. Math.*, **11**, 431–441
- Marshall, D. J. and Madden, T. R. (1959). Induced polarization, a study of it's causes. *Geophysics*, **24**(5): 780–816.
- McEuen, R. B., Berg, J. W., and Cook, K. (1959). Electrical properties of synthetic metalliferous ore. *Geophysics*, 24:510–530.
- McKinley, K. S. (2003). Nonlinear complex resistivity to investigate clay-organic reactions at the savannah river site, south carolina. Master's thesis, Colorado School of Mines.
- Morgan, F. D. (2001). A spectral induced polarization survey to delineate subsurface contamination for the U.S. Department of Energy : A-14 outfall, savannah river site. Technical report, DOE.
- Ogilvy, A. and Kuzmina, E. (1972). Hydrogeologic and engineering-geologic possibilities for employing the method of induced potentials. *Geophysics*, 37(5):839–861.
- Olhoeft, G. R. (1984). Clay-organic reactions measured with complex resistivity. 54th Ann. Internat. Mtg., Soc. Explor. Geophys., Expanded Abstracts, pages 356–357.
- Olhoeft, G. R. (1985). Low frequency electrical properties. *Geophysics*, 50(12):2492–2503.
- Pankow, J. F. and Cherry, J. A. (1996). Dense chlorinated solvents and other DNAPL in groundwater Waterloo Press.
- Pape, H, Riepe, L., and Schopper, J.R. (1987) Theory of self-similar network structures in sedimentary and igneous rocks and their investigations with microscopical and physical methods. *J. Microscopy*, 148, 121-147.
- Pelton, W. H., Ward, S. H., Hallof, P. G., Sill, W. R., and Nelson, P. H. (1978). Mineral discrimination and removal of inductive coupling with multi frequency ip. *Geophysics*, 43(3):588–609.
- Ramirez, A., Daily, W., and LaBrecque, D. (1996) Complex Electrical Resistance Tomography of a Subsurface PCE Plume, proceedings of the Symposium on the Application of Geophysics to Engineering and Environmental Problems, held at Keystone, CO, April 28-May 1.

- Rossabi, J, Riha, B., and Jackson, D. (2004) Sediment Sampling at the A-014 Outfall for Comparison with Complex Resistivity Measurements, proceedings of the Symposium on the Application of Geophysics to Engineering and Environmental Problems, 22-26 February 2004, Colorado Springs, Colorado, Environmental and Engineering Geophysical Society, Denver, CO. p 484-495
- Sasaki, Y. (1989) Two-dimensional joint inversion of magnetotelluric and dipole-dipole resistivity data, *Geophysics*, 54, 254-262.
- Shi, W. (1998). Advanced modeling and inversion techniques for three dimensional geoelectric surveys. PhD thesis, MIT.
- Sumner, J. S. (1976). Principles of induced polarization for geophysical exploration. Elsevier Scientific Publishing Company.
- Tikhonov, A.N., and Arsenin, V.Y. (1977) Solution of ill-posed problems, V.H Winston and Sons, 258pp
- Vangelas, K. M. (2000). Summary and status of dnapl characterization and remediation activities in the a/m-area, savannah river site. Technical report, D.O.E. WSRC-RP-2001-00171.
- Vanhala, H., Soininen, H., and Kukkonen, I. (1992). Detecting organic chemical contaminants by spectral induced polarization method in glacial till environment. *Geophysics*, **57**(8):1014–1017.
- Vaquier, V., Holmes, C. R., Kintzinger, P. R., and Lavergne, M. (1957). Prospecting for ground water by induced polarization. *Geophysics*, **22**:660–687.
- Wait, J. (1959). Overvoltage research and geophysical applications. Pergamon Press. Chapter 4.
- Ward, S.H. (1990) Resistivity and induced polarization methods, in S. Ward (Ed.) Geotechnical and environmental geophysics – Investigations in Geophysics No. 5, SEG, 169-180.
- Zhang, J., Mackie, R.L., and Madden, T.R. (1995) 3-D Resistivity Forward Modeling and Inversion Using Conjugate Gradients, *Geophysics*, **60**, 1313-1325.
- Zonge, K. L. and Wynn, J. C. (1975). Recent advances and applications in complex resistivity measurements. *Geophysics*, 40(5):851–864.

Instrumentation and coupling problems in spectral induced polarization field applications

by

John Sogade¹, Frank Dale Morgan¹

Abstract

Acquisition of broadband spectral induced polarization (SIP) data is still limited mostly by the acquisition time. To solve this problem, currently available instrumentation needs to be made an order of magnitude faster. Ideas about how this can be realized are presented in this work. In addition, the limitations imposed by inductive and capacitive couplings are investigated, with the conclusion that inductive coupling presents no problem for surface array deployments below about 100Hz. This is likely to be much lower for cross-borehole acquisitions. Some aspect of the capacitive coupling problem was shown to be reduced by use of a receiver with adequately high input impedance.

1.0 Introduction

The realization that contamination affected the polarization properties of wet rocks/soils (Olhoeft, 1979, 1984) led researchers to propose the induced polarization (IP) method for mapping the subsurface distribution of contaminants. Since then a number of laboratory and field studies have been directed to further understand the influence of contamination on the polarization properties of rocks/soils and to develop IP for field application at contaminated sites. We have been involved in deployment of IP based methodologies at contaminated sites using both spectral IP (SIP) and time-domain IP (TDIP). The major problems faced in the field application of TDIP and more so SIP include (1) acquisition speed (2) inductive coupling problems (3) capacitive couplings from electrode impedance, ground-to-wire, and wire-to-wire.

SIP requires measurements at a number of frequencies to capture the polarization response of the ground, and TDIP measures the polarization response within a given time window, long enough to record the longest measurable contamination related relaxation processes in the earth. TDIP is relatively faster to deploy than SIP, and because the response is measured during the off period of the exciting source, it is less prone to inductive coupling. However, SIP data is more amenable to accurate modeling than TDIP data, and this probably explains why SIP has seen more preferential development than TDIP. To capture useful SIP data the time-budget is related to instrumentation issues

¹ Earth Resources Laboratory, Department of Earth, Atmospheric and Planetary Sciences, Massachusetts Institute of Technology. e-mail: sogade@erl.mit.edu

such as acquisition speed, and number of stacking to improve signal-to-noise ratio. Our own estimate is that SIP instrumentation needs to be an order of magnitude faster than what is currently available. Ideas about changes that can be made to improve instrumentation designs are presented.

For time varying systems such as SIP and TDIP, the transmitter and receiver circuits are coupled inductively like transformers with the free space and/or the conductive earth being the intervening medium between them. Thus, the accurate model of the transmitter-earth-receiver system should be based on the ac transformer model. At DC, the inductive coupling action breaks down, and only galvanic coupling occurs through the direct distribution of currents in a conductive medium. Most processing algorithms are based on the DC model, warranting that contributions from induction to the data be treated as a distortion to be corrected for or removed. As we show here, the DC model is adequate below about 100 Hz for most environmental applications using surface array deployment and is likely to be more limiting for cross-borehole geometries.

The proximity of transmitter and receiver wires to each other and to the conductive earth especially in cross-borehole geometries enable wire-to-ground, and wire-to-wire capacitive couplings, leading to data distortion. In addition the response of the electrode impedance, made up of resistive and capacitive components, couples with the response of the earth leading to data distortion. A model is offered to explain capacitive coupling contributions and a practical way to limit capacitive coupling is presented.

2.0 Instrumentation Design Considerations

We believe the issues that should go into SIP instrumentation design considerations includes operating frequency bandwidth, acquisition speed, input impedance, scalability of the transmitter power, the receiver dynamic range, digitization sampling rate, number of acquisition channels, and the equipment layout.

Based on laboratory and field data on contaminated soil/rock media (Borner, 1993; McKinley, 2003), the frequency bandwidth of interest for SIP is between 0.01 Hz and 1 kHz, and sets the limits for instrumentations designed for field studies of spectral polarization properties of subsurface contamination. Because of the slow rate of change of spectral polarization response, 3 measurements per decade may be sufficient to adequately capture the range of variations. For example 3 points is enough to adequately sample a quadratic variation and is judged to be enough for the range of variations recorded within a decade of most spectral responses. We take a typical measurement point to be defined by an electrode i.e. a transmitter/receiver dipole. Based on the foregoing, 5 orders of magnitude in frequency are required for spectral characterization and at 3 measurements per decade give 15 spectral measurements per sample point or quadripole. Typical measurement suites we have deployed have used 600 quadripoles or $15 \times 600 = 9000$ data points for the surface 2D array, 1200 quadripoles $15 \times 1200 = 18000$ data points for the 2D cross-borehole array, and 3960 quadripoles or $15 \times 3960 = 59400$ data points for the 3D cross-borehole array.

The actual measurement at a given frequency, f , requires sampling at a frequency f_s greater than that imposed by the Nyquist criterion i.e. $f_s \geq 2 \cdot f$ (but we use $f_s = 4 \cdot f$ in our analysis) and for a maximum frequency $f = 1\text{kHz}$ leads to 4000 sample points per

cycle or 4kHz sampling rate. We expect that with the expected large number of data points a 128 channel system is preferable, and if all the signals are multiplexed to a single A/D, then it has to be able to sample at $128 \times 4 \text{ kHz} = 512 \text{ kHz}$. To avoid signal cross-talk, and multiplexer noise problems with subsequent loss of bandwidth, that attend multiplexing signals as described above, most SIP equipments are designed with each channel path having its own signal conditioning, sampling and gain stages (see for example Zonge Engineering and Geophysics Incorporation Manual, chapter 16, 2003). However, for the purpose of this discussion we continue to consider the single multiplexer model since it simplifies the analysis and provides a convenient framework without jeopardizing the conclusions. Based on the single multiplexer model, it is seen that the time budget for signal digitization still at a single data point is still under few seconds at most. Other instrumentation issues include signal conditioning, self potential buckout, passband and anti-alias filters, dynamic range and other such details that will not impact significantly on field acquisition time.

To ensure good signal to noise ratio most equipments are designed to sample a full cycle and in many cases a number of cycles, n_{cycles} of the measured signal. The field acquisition time per data point, t_{field} is then approximated by

$$t_{\text{field}} = n_{\text{cycles}} \cdot \frac{1}{f}$$

For a typical SIP survey at 1/32 Hz using our surface, 2D cross-borehole array, or 3D cross-borehole the estimated acquisition time for characterization at 1 cycle of signal would be $32 \times 9000\text{s} = 80 \text{ hrs}$, $32 \times 18000\text{s} = 160 \text{ hrs}$, $32 \times 59400\text{s} = 528 \text{ hr}$, respectively. If 8 hours of acquisition time are allotted to each day the acquisition times in 8-hour days are respectively 10, 20, and 66 days for the surface, 2D cross-borehole, and 3D cross-borehole arrays. These are prohibitive times for environmental applications.

Though optimizations that reduce the number of data points deployed per survey are possible and desirable, the major limitation is the fact that at least a full cycle is sampled at the required low frequencies. Therefore, an effective optimization is necessarily tied to an optimized sampling of a cycle at low frequencies. In a bid to optimize the cycle sampling time one of the two major SIP equipment suppliers, Zonge Engineering and Research Incorporation provide simultaneous sampling of a signal at a base frequency and the first four odd harmonics, theoretically reducing the acquisition time by about five (see Zonge Engineering and Research Incorporation manual, chapter 10). However, signal level and integrity falls significantly after the first odd harmonic and in many cases only the first odd harmonic but sometimes the second is usable at very low frequencies (less than 1 Hz). An alternative worthy of consideration is based on the idea that it is possible to sample fractions of the cycle, and maintain signal fidelity provided the input frequency is precisely known (Morgan et al., 1986). In addition, the transmitter can be designed to output a multifrequency source signal which is after being analyzed at the receiver reduces the acquisition time by number of frequencies introduced. In the investigations of Morgan et al. (1986) a 3-frequency transmitter was used the minimum smallest fraction of a cycle used was a 1/2 cycle. These numbers can be changed by more careful investigation.

3.0 Investigation of EM Coupling

3.1 Correction for Inductive EM Coupling

As a simple illustration, let us assume a homogenous half-space excited by a frequency dependent current. The response is the potential measured at two receiving electrodes. For a polarizable earth, the measured spectral response is complex and can be modeled by a frequency dependent complex resistivity of the earth. The complex component of the response arises from the polarization properties of the earth. The response in addition always has a complex component due to electromagnetic induction (emi) regardless of the polarization of the earth. The influence of emi increases with the induction number, $|kr| \approx 2.8 \times 10^{-3} r \sqrt{f/\rho}$, where k is the wave number for the em field with magnitude, $|k| = (\omega\mu/\rho)^{1/2}$, r the separation distance between transmitter and receiver, and μ is the magnetic permeability of the material. Madden and Cantwell (1967) showed that a good rule of thumb for determining the upper frequency limit set by emi in IP field surveys is $r\sqrt{f/\rho} < 200$. Using this rule of thumb the upper frequency limit for a field survey in which $r=600\text{m}$ and $\rho = 100 \text{ Ohm-m}$ is about 11 Hz.

Measured field SIP data have two components; the desired pure SIP signal and the emi contribution. Proper interpretation of field data requires a correction to separate emi noise from the desired data. An intuitive correction method is to predict the emi components and subtract them from the measurements (Pelton et. al., 1978). However, this method necessitates a prior knowledge of the pure resistivity of the earth, which is not directly attainable from SIP measurements and it assumes that SIP measurements are a simple superposition of pure SIP and emi. Another technique based on the assumption of simple superposition was introduced by Hallof (1974).

The full expression for the measured potential at the receiving electrodes over a layered half-space excited by an electric dipole source is well known and given in Dey and Morrison (1973), and Ward and Hohmann (1988). For our illustration we only show the expressions for the homogenous half-space model.

$$V(\omega) = I(\omega)Z(\omega) \quad (2)$$

where $Z(\omega)$ is the mutual impedance of the transmitting wire, S , and receiving wire, s , and is given by

$$Z = Q(Aa) - Q(As) + Q(Bb) - Q(Bs) + L \quad (3)$$

Q is the grounding function which relates to galvanic current injection/extraction from the earth and L is the inductive function. (A, B) and (a, b) are the co-ordinates of the transmitter and receiver electrodes respectively.

$$Q(r) = \frac{-i\omega\mu_0}{2\pi k_1^2 r} \quad \text{and} \quad L = \int_A^B \int_a^b P(r) dS ds$$

where

$$P(\rho) = \frac{-i\omega\mu_0}{2\pi} \left\{ \frac{1 - (1 + i k_1 r) e^{-i k_1 \rho}}{k_1^2 r^2} \right\}. \quad (4)$$

$$k_1^2 = \omega^2 \mu_1 \varepsilon_1 - i \mu_1 \omega / \rho$$

At the low frequencies considered the quasi-static approximation is valid and

$$k_1^2 \approx -i \mu_1 \omega / \rho \quad \text{while the grounding function becomes} \quad Q(r) = \frac{\rho}{2\pi r}.$$

Also at zero frequency the inductive term vanishes and the impedance becomes only that of resistive coupling where

$$Q(r) = \frac{\rho}{2\pi r} \quad (5)$$

We assume that the IP effect arises from the Cole-Cole complex resistivity model (Pelton et. al., 1978, 1983 a, b) given by

$$\rho = \rho_0 \left[1 - m \left(1 - \frac{1}{1 + (i\omega\tau)^c} \right) \right] \quad (6)$$

where m = intrinsic chargeability as defined in Seigel (1959)

τ = time constant that characterizes the decay and

c = constant that controls the frequency dependence and bounded between 0.0 and 1.0 with typical values between 0.25 to 0.5.

Synthetic data made up of pure SIP, pure SIP and emi, and pure emi were generated for the dipole-dipole configuration using the Cole-Cole model with the following parameters: $m=0.2$, $c=0.25$, $\tau=0.1$, $N=2$, $\rho_0=100\Omega m$, where the dipole length is 200m and the transmitter-receiver separation is 600m.

The pure SIP is calculated using the resistivity in (6) with $L=0$ in (3), the pure SIP plus emi is given by using (6) with (4) and (3), em induction alone by L in (4). It is clearly seen from Figure 1 that *it is essential to solve the emi problem for field measured data to be useful. EM induction absolutely overwhelms the desired pure SIP signal.*

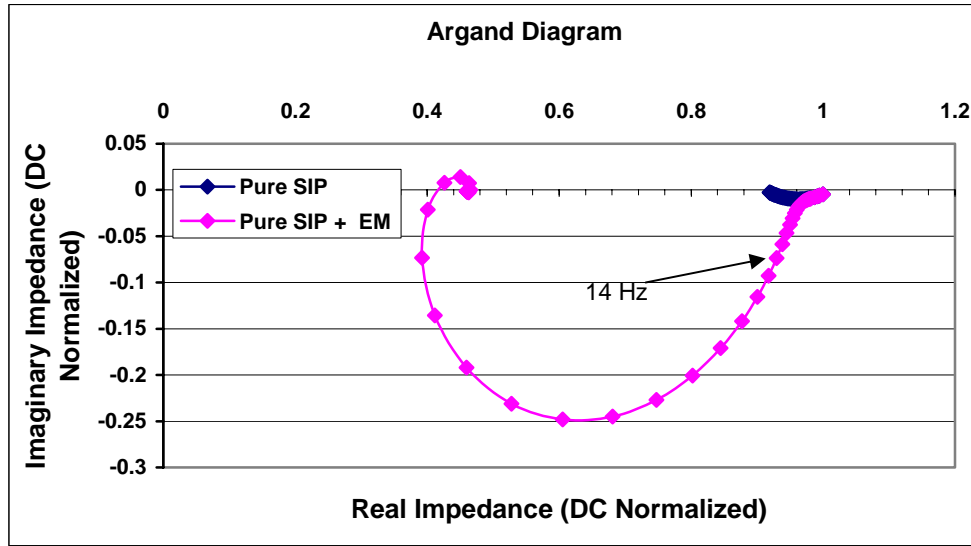


Figure 1: Calculated synthetic signals.

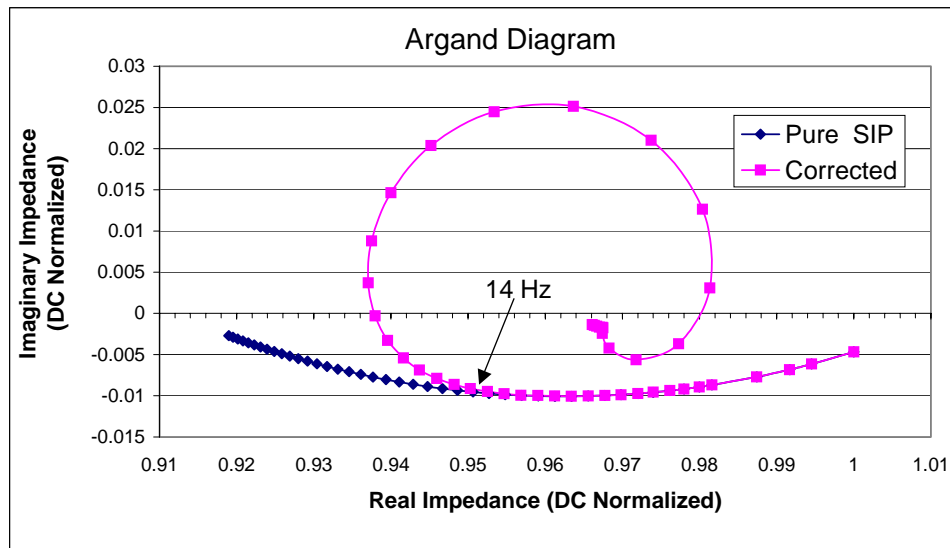


Figure 2: Disparity between corrected and pure SIP past 14Hz.

Figure 2 shows a comparison of the pure SIP signal and a corrected SIP signal. The standard correction practice of subtracting the emi component from the measured signal (SIP + emi) was used. The correction is accurate up to a certain frequency limit, for the particular parameters in this example the limit is 14Hz. The frequency limit is a function of transmitter-receiver separation, and resistivity of the earth.

Figure 2 shows that the pure IP response cannot be recovered from measured data (sum of SIP and emc) by any simple processing scheme beyond a certain frequency limit. This example is the simplest situation possible and correction becomes even more difficult for layered or heterogeneous earth models and for cross-borehole acquisitions. Therefore any correction approach is inadequate in separating emi component from

measured data beyond a usually unknown frequency limit. The approach we favor is to model the coupled IP and em directly from Maxwell's equations.

3.2 Summary of EM Coupling Components

Figure 3 is a schematic of the different sources of electrical coupling that can cause signal distortion in performing a surface IP survey in the field. The model is limited to only capacitive and inductive mechanisms, other natural and man made noise sources are discussed in Madden and Cantwell (1967) and Sumner (1976).

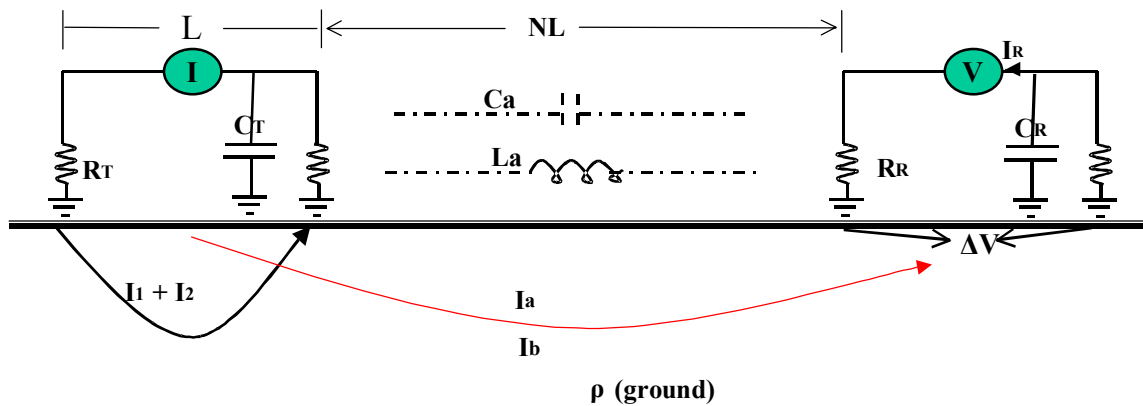


Figure 3: Schematic of conceptual model showing sources of measurable response.

Tx: Transmitter, **Rx:** Receiver

I: Tx-Current

I1: Tx-electrode current

I2: Tx-to-ground Capacitive leakage current

Ia: eddy currents from secondary magnetic field of Tx-electric field (Inductive em)

Ib: eddy currents from Tx-magnetic field (Inductive em)

IR: Rx-to-ground Capacitive leakage current

CT: Tx-to-ground leakage capacitance

CR: ground-Rx leakage capacitance

La: Tx-Rx or wire-to-wire Induction (air)

Ca: wire-to-wire leakage capacitance

RT: Transmitter electrode-ground resistance

RR: Receiver electrode-ground resistance

L: Tx and Rx dipole length

The schematic in figure 3 shows the various currents that flow in the ground and wires by inductive and capacitive mechanisms. These currents eventually establish measurable potentials at the receiver electrodes. The following is a list of potentials at the receiver, approximately from the greatest to smallest in magnitude, and the system variables they depend on are shown in parentheses.

ΔV : Potential difference between the receiver electrodes

ΔV^{I_1} : pd due to current I_1 (ρ, L, N),

ΔV^{I_2} : pd due to current I_2 ($C_T(L), R_T, N, \omega$),

ΔV^{I_a} : pd due to current I_a (ρ, ω, N),

ΔV^{I_b} : pd due to current I_b (ρ, ω, N),

ΔV^{I_R} : pd due to current I_R ($C_R(L), R_R, N, \omega$),

$\Delta V^{I_{C_a}}$: pd due to current I_{C_a} (ω, L, N),

$\Delta V^{I_{L_a}}$: pd due to current I_{L_a} (ω, L, N)

The magnitude of each component of capacitive and emi coupling were calculated for two dipole orientations, the dipole-dipole shown in figure 4, and the parallel dipole shown in figure 5. Figures 6 and 7 show the three most significant coupling components, which are inductive, transmitter-to-ground and receiver-to-ground capacitive, respectively in that order, plotted as frequency effect vs. frequency for the dipole-dipole orientation. Figures 8 and 9 shows equivalent plots for the parallel dipole orientation. The frequency effect is the ratio of the magnitude of coupling (noise), to the desired signal. A frequency effect greater than 1.0% is significant noise and the corresponding frequencies should not be used in interpretation.



Figure 4: Schematic for Dipole-Dipole

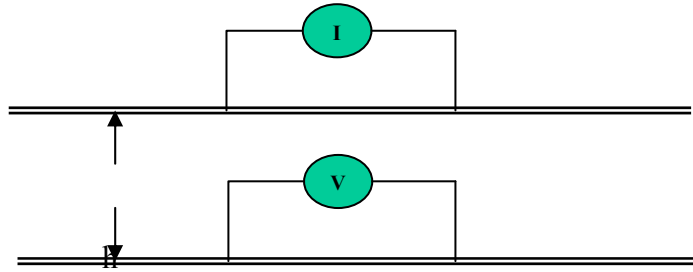


Figure 5: Schematic for Parallel Dipole

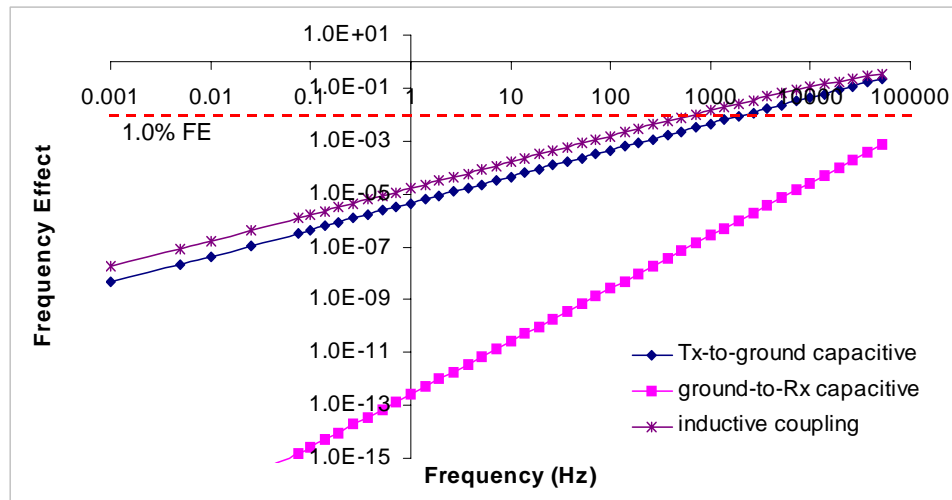


Figure 6: Dipole-Dipole, N=2

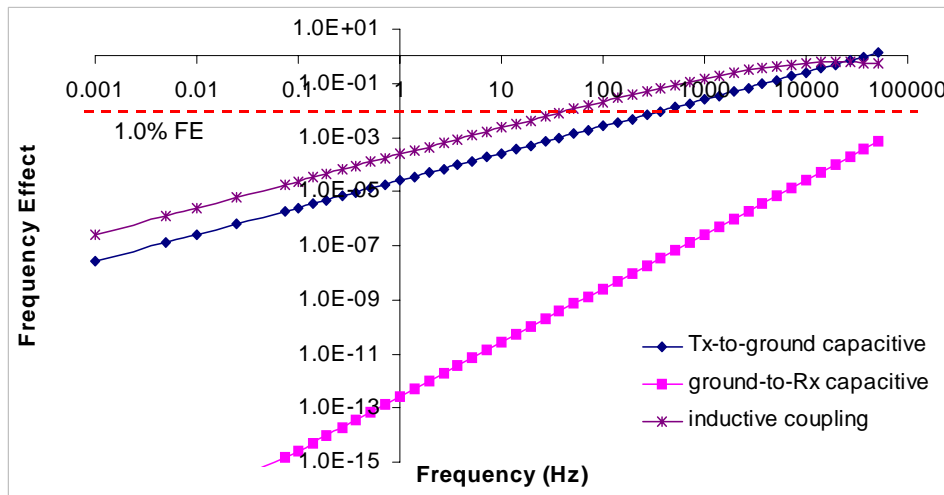


Figure 7: Dipole-Dipole, N=10

The parameters used in the calculations are $C_T=C_R = 16.2$ pF, dipole length = 10m, $R_T=R_R = 500$ ohms, half-space resistivity = 100 ohm-m, and $N=2$ or 10. For the parallel dipole orientation, the increase in dipole spacing, N , enlarges the current source dipole length by NL while maintaining the Tx-Rx separation, h , constant. These results suggest that at $N=2$ emi is not a factor up to several hundred hertz i.e. 850 Hz in figure (6). However, typical spacings in the field are greater than 2 and especially for 3D acquisitions they could be very large. For a dipole spacing of 10, which is typical, the upper limit drops to approximately 55Hz.

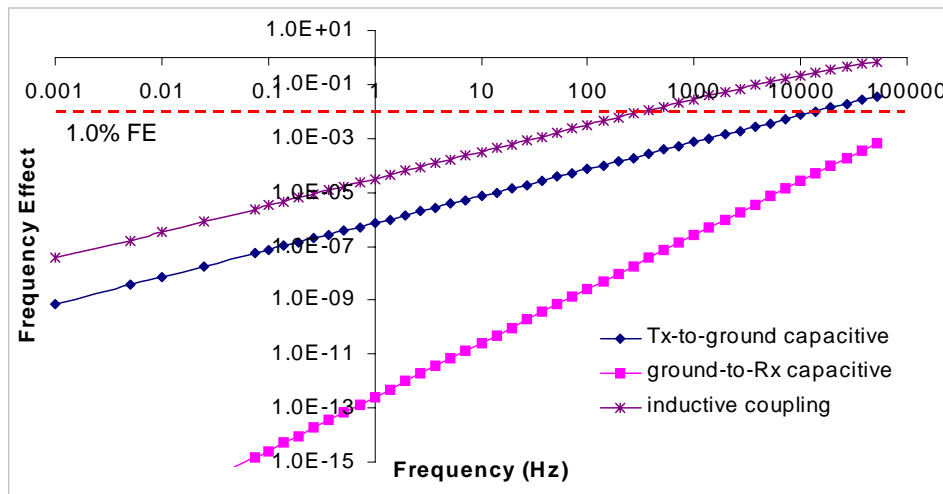


Figure 8: Parallel Dipole, $N=2$, $h=10$ m

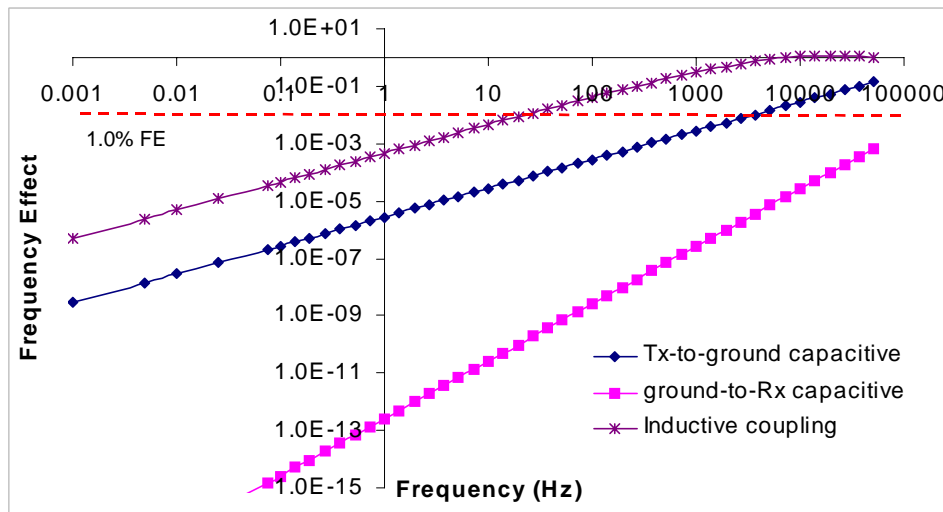


Figure 9: Parallel Dipole, $N=10$, $h=10$ m

Figures 8 and 9 show that the emi becomes is worse for the parallel dipole orientation than the dipole-dipole. The two dipole orientations studied are the two

extremes of the possible layouts. A 3D acquisition might include combinations of dipole-dipole, parallel dipole, and orientations in between the two. In all cases inductive coupling is the greatest component of electrical distortion, and hence it must be properly separated from field measurements. Therefore, emi will limit the usable frequency of SIP to below 100Hz for field surveys employing surface array configurations especially in the case of 3D where dipole spacings are inherently large.

4.0 Investigation of Capacitive Coupling

Parasitic capacitances arise because of proximate wires placed near each other and/or near the conductive earth. Under certain conditions leakage currents can flow to the receiving circuit via paths created by parasitic capacitive coupling, causing data distortion. A general condition is that the impedance of the current path via electrodes becomes as resistive as those created by parasitic capacitances. This usually happens as frequency increases, electrode contact resistance grows, or wires are placed too close. As identified in figure 3 above, the sources of capacitive couplings are wire-to-wire and wire-to-ground where the wire could be the transmitter's (Tx) or the receiver's (Rx). If the electrode impedance is modeled by a simple resistor and capacitor, then the electrode response could directly capacitively couple with the receiver circuit introducing data distortion. In addition, as identified in the previous section, the inductive component for surface electrode deployment appears to be the major distortion at the low frequencies engaged by SIP. However, for cross-borehole geometries, where both the transmitter and receiver wires have to be placed close together inside boreholes, capacitive coupling problems exacerbate.

The simple model shown in figure 10 is offered here to evaluate the effects of capacitive couplings from both wires and electrodes in a more general way. The earth is modeled as a distributed network of complex impedance elements (Z_{E1} , Z_{E2} , Z_{R-TX} , Z_{R-RX}), the transmitter electrodes are modeled as resistor-capacitor (RC) elements (R_{TX1} , C_{TX1} , R_{TX2} , C_{TX2}) injecting currents into the earth and the receiver electrodes are modeled as RC elements (R_{RX1} , C_{RX1} , R_{RX2} , C_{RX2}) retrieving currents from the earth. The transmitter injecting current, I , is modeled as a current source using a very high output impedance (a high value resistor T , and a small value capacitor, CW_{TX}) connected to the transmitting electrodes and the receiver measuring potential, V , is modeled by a very high input impedance (a high value resistor R , and a small value capacitance, CW_{RX}) connected to the receiving electrodes. Note that transmitter wire-to-wire capacitance is parallel to the transmitter's output capacitance thus both sum together and represented by CW_{TX} . Similarly, both the receiver input capacitance and the receiver wire-to-wire capacitance sum together and represented by CW_{RX} . The transmitter-to-receiver capacitances represent the capacitance between proximate transmitter and receiver wires and are represented by CW_{RX} , and CW_{RX} for wires connected to both the positive and negative poles of the transmitter and receiver respectively. Note that at the cost of additional complexity and without significant gain in insight it is possible to also arrange for the cross-pole (i.e. between wires connected to different polarities of the transmitter and receiver) transmitter-to-receiver capacitances.

The impedance elements for the earth are left to be more general in figure 10, and can be modeled as simple RC elements or by a more general Cole-Cole model (Pelton et al., 1978) given earlier in (6) as a complex resistivity and repeated here as a complex impedance

$$Z = Z_0 \left[1 - m \left(1 - \frac{1}{1 - (i\omega\tau)^c} \right) \right] \quad (7)$$

and depends on the following four parameters:

Z_0 = DC or low frequency impedance,

m = intrinsic chargeability as defined in Siegel (1959),

τ = time constant that characterizes the IP relaxation decay and,

c = constant that controls the frequency dependence and bounded between 0.0 and 1.0 with typical values ranging from 0.25 to 0.5.

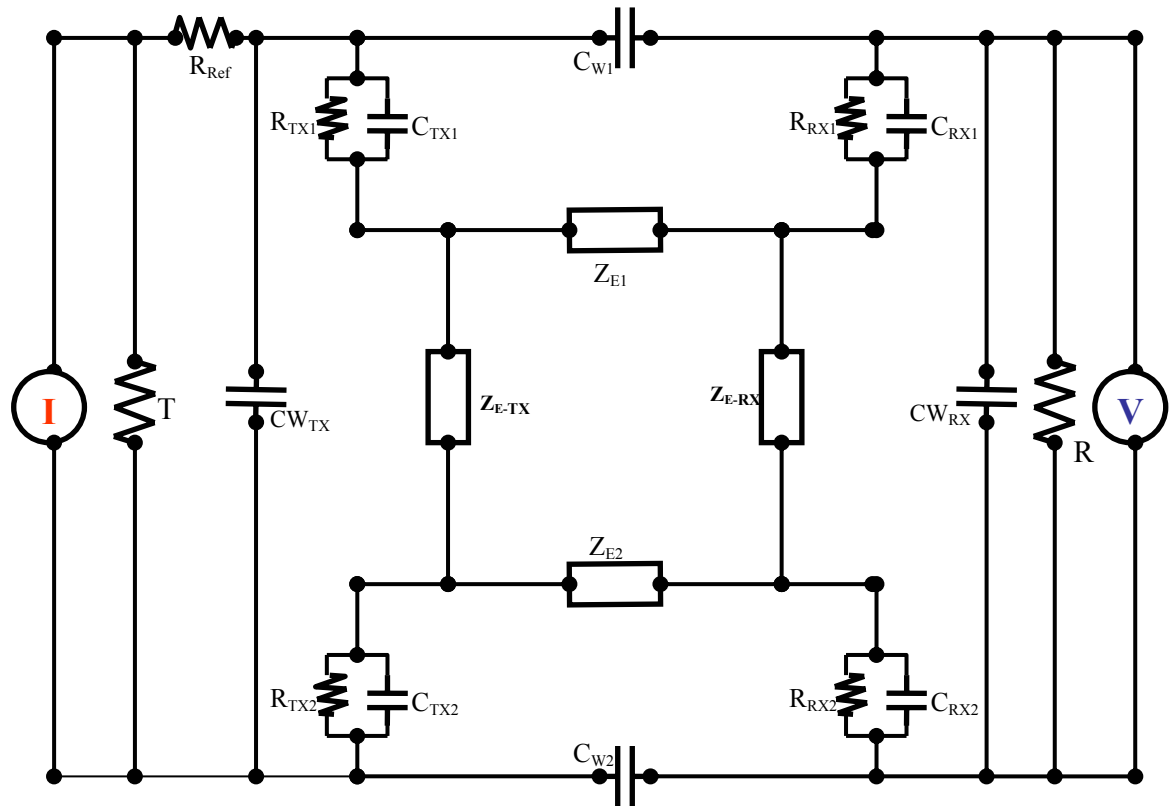


Figure 10: Capacitively Coupled Transmitter-Earth-Receiver-Measurement System Equivalent Circuit

The system equations were developed as a complex set of simultaneous equations and solved using Matlab's matrix inverse algorithm, using $I=1$ for current. The actual complex current used (magnitude and phase) were determined from the potential across

the reference resistance, R_{Ref} , using $I_{input} = V_{Ref}/R_{Ref}$ thus simulated the output response in terms of impedance and phase is given by

$$Z = \text{abs}(V/I_{input}) \quad (8)$$

$$\phi = \tan^{-1}(\text{imag}(V)/\text{real}(V)) \quad (9)$$

Using simple variations of RC elements for the earth impedances the predictions of this circuit was satisfactorily checked against pSpice's output. Also, the predictions were checked by actual measurements on constructed circuits. Figure 11 shows the undistorted amplitude and phase response using ideal transmitter and receiver electrodes ($T = 10 \text{ M}\Omega$, $R_{TX1}=R_{TX2} = 0$, $C_{TX1}=C_{TX2} = 0$, $R_{RX1} = R_{RX2} = 0$, $C_{RX1} = C_{RX2} = 0$, $R=10 \text{ M}\Omega$), and an earth model with impedance elements given by the following Cole-Cole model parameters:

$$Z_{E1}: Z_0 = 2000 \text{ }\Omega\text{-m}, m = 0.05, \tau = 0.01, c = 0.25.$$

$$Z_{E2}: Z_0 = 2000 \text{ }\Omega\text{-m}, m = 0.1, \tau = 0.001, c = 0.5.$$

$$Z_{R-TX}: Z_0 = 250 \text{ }\Omega\text{-m}, m = 0.05, \tau = 0.005, c = 0.5.$$

$$Z_{R-RX}: Z_0 = 250 \text{ }\Omega\text{-m}, m = 0.05, \tau = 0.001, c = 0.25.$$

The parameters were chosen so that the response shown in figure 11 is arranged to be very near that of the Cole-Cole response of Z_{R-RX} . This circuit configuration passed reciprocity test performed by interchanging the roles of transmitter and receiver electrodes but the resulting response remain unchanged.

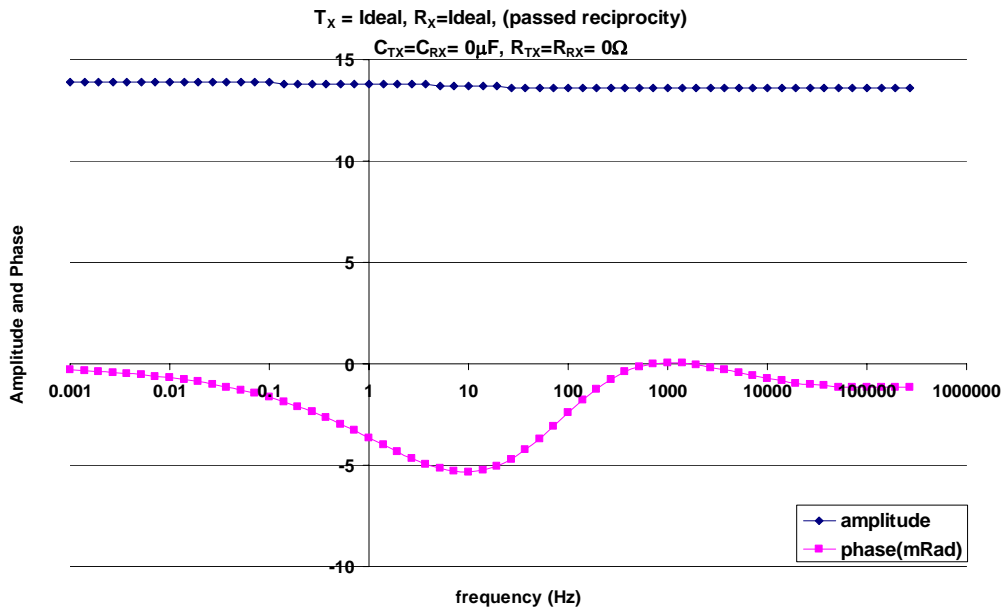


Figure 11: Spectral response of an earth modeled with Cole-Cole impedance, and using ideal transmitter and receiver electrodes.

There was no noticeable distortion for variations of the transmitter and receiver wire capacitances, CW_{TX} and CW_{RX} . Figure 12 shows the distortion that occurs by using an ideal transmitter electrode and a set of poor receiver electrodes ($R_{RX1} = R_{RX2} = 0.5k\Omega$, $20k\Omega$, $100k\Omega$, $C_{RX1} = C_{RX2} = 0.01\mu F$, $10\mu F$, $1000\mu F$) are used with a receiver input impedance of $10M\Omega$. Only the results for the ideal amplitude response is shown since the amplitude changes for the set of resistance/capacitances are marginal. Also, the phase response was not affected for all variations of capacitances when the electrode resistance is 500Ω . However, we can see that for both electrode resistances of $20k\Omega$ and $100k\Omega$ respectively, severe phase distortions occur, with a spectral peak determined by the electrode capacitance, but whose amplitude is determined by the electrode resistance. In general, the distortion amplitude increases with resistance, moving slightly down in frequency as resistance increases, but increasing capacitance greatly moves the distortion peak down in frequency.

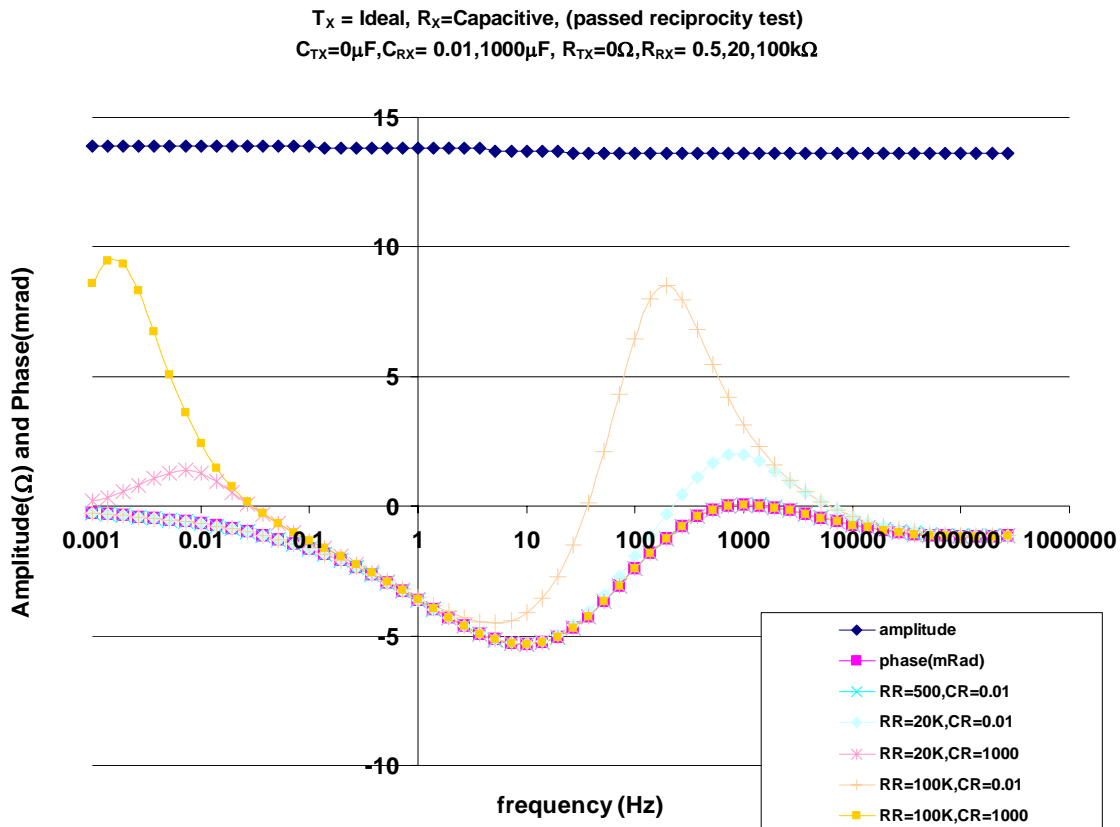


Figure 12: Spectral response of an earth modeled with Cole-Cole impedance elements, and using ideal transmitter but capacitive receiver electrodes. The receiver input impedance is $10M\Omega$. Since the amplitude changes are marginal only a single amplitude spectrum is shown. Receiver electrode resistance and capacitance introduce a phase distortion with a spectral peak which grows with increasing resistance and is moved higher in frequency by a decreasing electrode capacitance.

As seen in figure 13, increasing the receiver input impedance from 10M to 100M appears to have significantly suppressed the phase distortions, therefore establishing that the ratio of receiver electrode resistance to receiver input impedance is the important parameter.

Thus in designing electrodes the idea is to keep the electrode resistance to the barest minimum. However, the electrode resistance is not the only culprit because electrode contact resistance will also appear as the electrode resistance and cause the same effect. Thus, field deployments should strive to minimize electrode contact resistance. However, for cross-borehole deployments, especially those planned for time lapse studies, where electrodes might reside in boreholes for an extended period, the control of contract resistance becomes more difficult. Under these circumstances, it might be desirable to have front end electronics that can increase the input impedance of receivers.

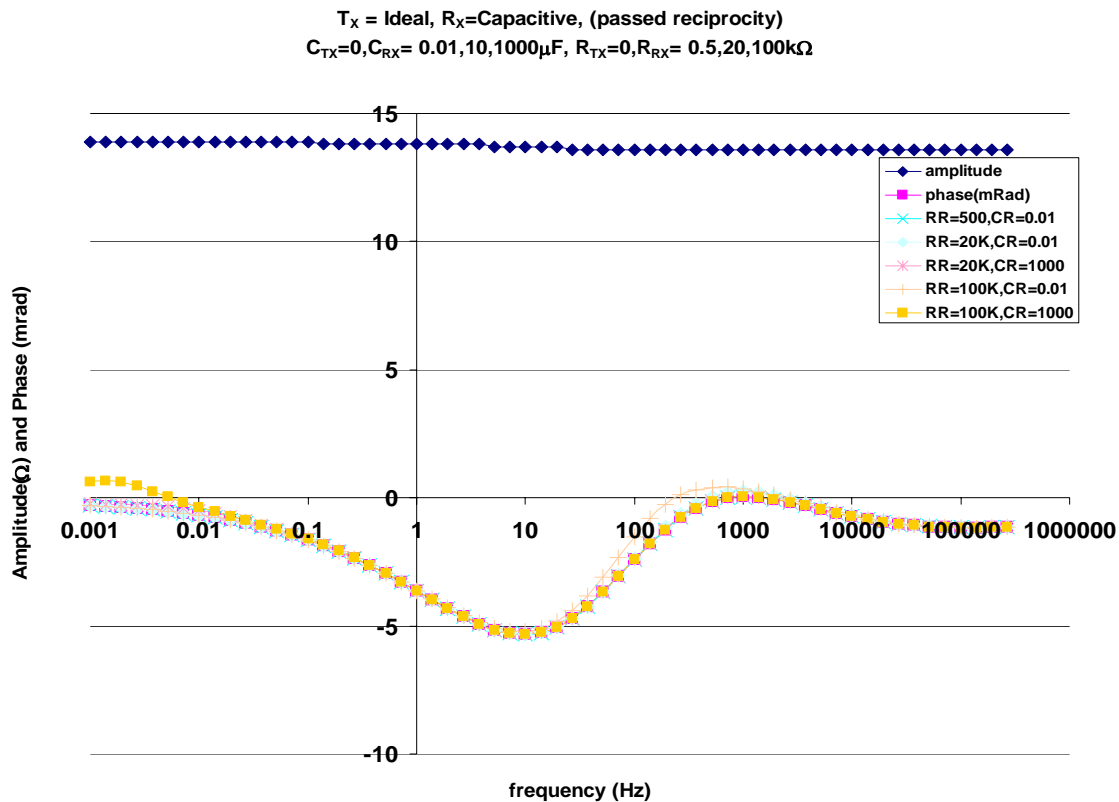


Figure 13: Spectral response of an earth modeled with Cole-Cole impedance elements, and using ideal transmitter but capacitive receiver electrodes. The receiver input impedance is 100MΩ. Note that compared to the response for the 10M receiver shown in figure 12, all the 20K distortions have disappeared and the 100k distortions are greatly reduced.

Figure 14 shows the distortion effect of the transmitter-receiver wire capacitances CW_1 and CW_2 . Ideal transmitter and receiver electrodes were used. Notice that the distortion sets in early at about 10Hz despite the fact that only a modest 1nF was used for CW_1 and CW_2 . Also, the input impedance of the receiver has no effect on this distortion. Other simulations carried out show that increasing the values of CW_1 and CW_2 , causes earlier onset of the distortion in frequency. Therefore, even in borehole geometries, careful wiring layout separating transmitter and receiver wires is desirable, and in addition efforts can be made to arrange acquisitions so that transmitter and receiver wires avoid using the same borehole as much as possible.

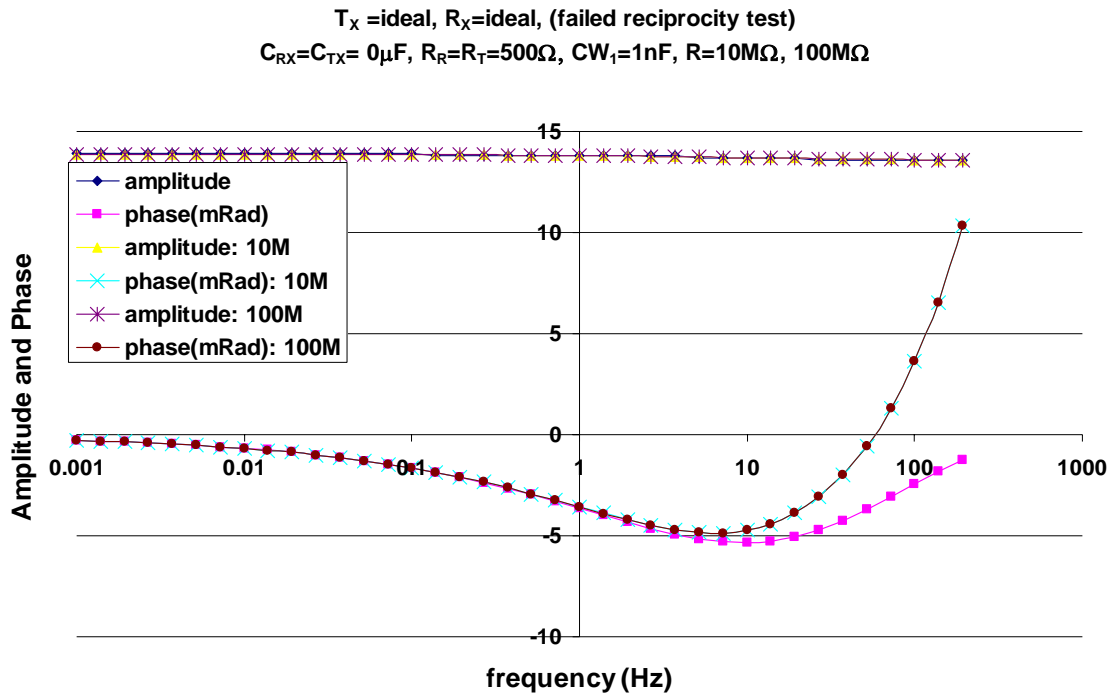


Figure 14: Spectral response of an earth modeled with Cole-Cole impedance elements, and using ideal transmitter but capacitive receiver electrodes. The receiver input impedance is 100MΩ. Note that compared to the response for the 10M receiver shown in figure 12, all the 20K distortions have disappeared and the 100k distortions are greatly reduced.

To check that this model works for the real earth, we performed tests on 27 well calibrated borehole potential electrodes that have been deployed for more than a year. The receiver electrodes were non-polarizable Ag/AgCl porous pots and the transmitter electrodes elemental copper pipes. The tests were carried out using a Zonge GDP-32

receiver and a ZT-30 transmitter. The GDP-32 has a 10M input impedance, so we designed a simple buffer of about 100M as a front end to increase input impedance of the GDP-32 as needed. The contact resistances of the electrodes were measured and a spectrum of impedance magnitude and phase were obtained for different transmitter receiver configurations with and without the 100M front end. The acquisition geometry is such that 26 electrodes distributed between four boreholes are measured against a single fixed electrode. Two electrodes (9 and 11) are found to have abnormally high impedances relative to the rest with an average impedance of 1k.

Any difference in the measured response between the 10M and 100M receiver input impedance, according to the predictions of the equivalent circuit above, suggests a capacitive coupling distortion. If the distorted responses are associated with only the high contact electrodes, then we essentially confirm the predictions of the equivalent circuit tests above. This was found to be the case, as only the responses using electrodes 9 and 11 present a difference between 10M and 100M receiver input impedance. Working on the assumption that adjacent electrodes in this geometry might be sampling the same region of the ground, and therefore present the same response, we carefully looked at the responses of the electrodes 9, 10 and 11 and is shown in Figure 15 as an argand plot. Figure 15 also shows the response of electrodes 3 and 13 which are farther away from electrodes 10 and 11.

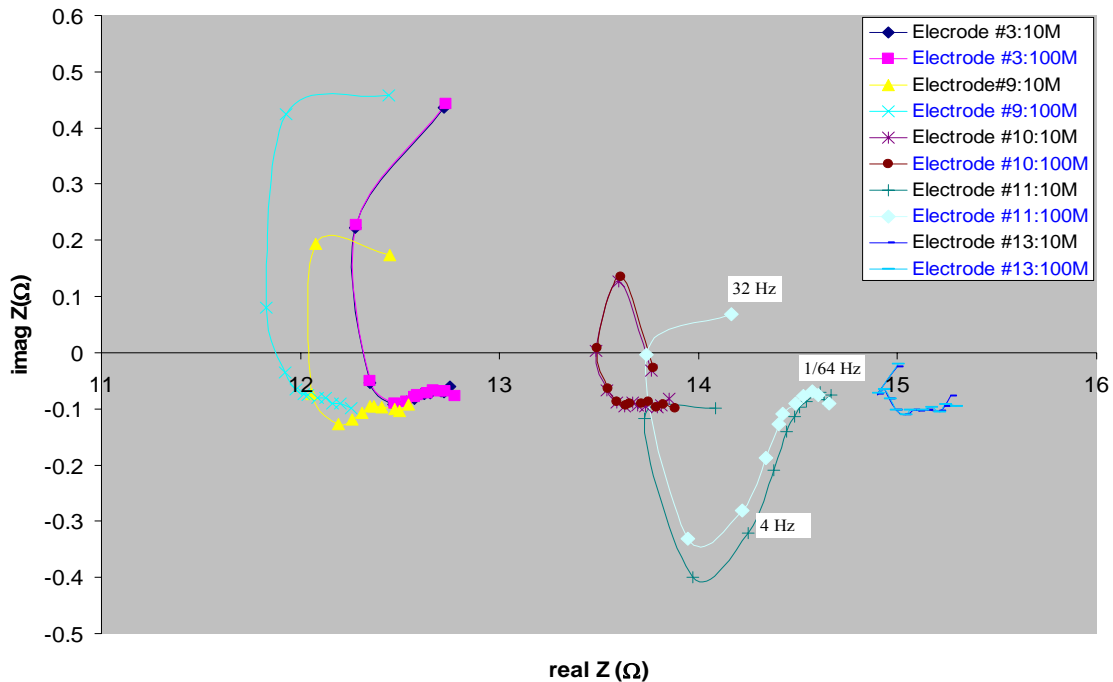


Figure 15: Argand plots of response of the earth for different borehole electrodes (measured against a single fixed electrode) and repeated for receiver input impedances of 10 or 100 MΩ. Note that only electrodes #9 and #11, the only two of twenty six electrodes with abnormally high impedances, show a difference between 10 and 100 MΩ input impedances.

Figure 16 shows the responses of two adjacent electrodes 9 and 10, as a normalized argand plot. The plot reveals that electrode 10 response remains unaffected between 10M and 100M receiver impedances. However, the 100M receiver impedance moved the response of electrode 9 nearer that of 10 in the lower part of the quadrant i.e. at the lower frequencies below 4 Hz. This result suggests that the spectral response using electrode 9 and 10 should be the same below 4 Hz if there was no capacitive distortion.

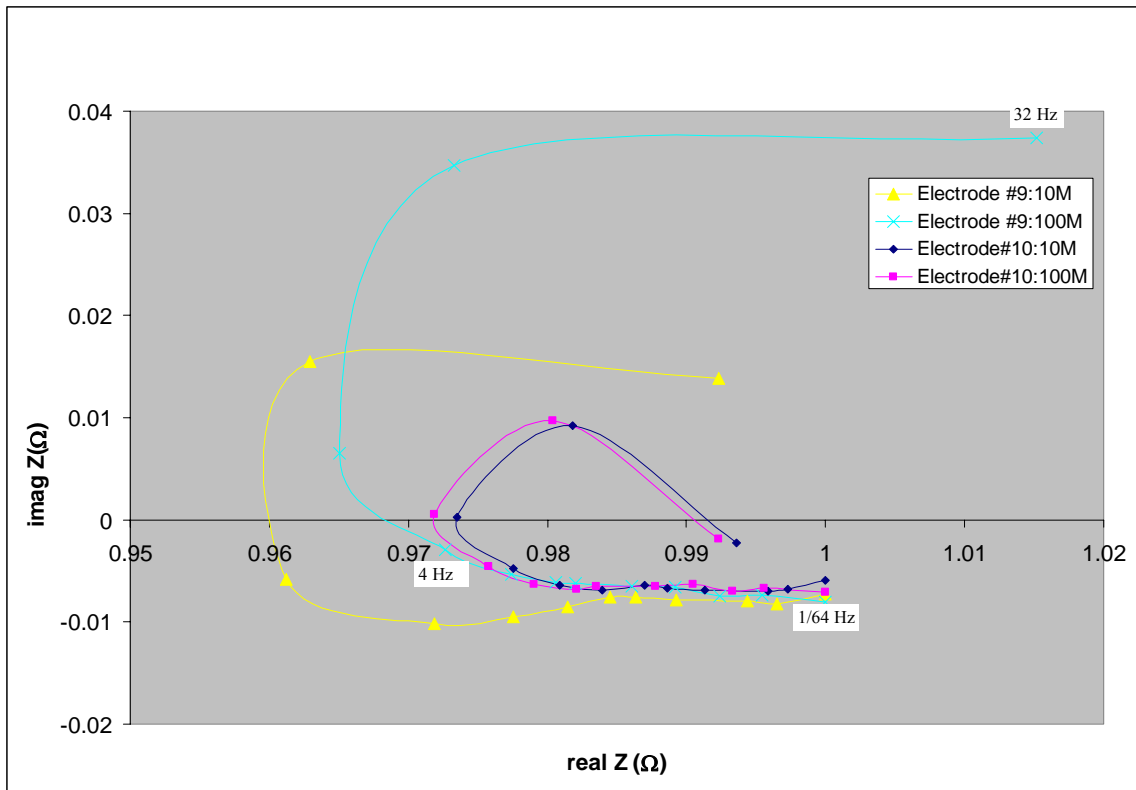


Figure 16: Argand plots of the spectral response of the earth for two adjacent borehole electrodes (measured against a single fixed electrode) and repeated for receiver input impedances of 10 or 100 MΩ. Note that the response using electrode #10 is same between 10 and 100 MΩ, and different using electrode #9. In addition, note that the 100 MΩ input impedance moved the electrode #9 response nearer that of electrode #10 in the lower quadrant.

Conclusion

In deployments of SIP that require wideband measurements, acquisition speed remains the most daunting challenge. Ideas about changes in sampling methodologies that can bring about gains in acquisition speed have been presented. In addition, inductive and coupling problems still remain elusive if DC models are used for processing wideband field data. Inductive problems are expected to be worst for cross-borehole geometries. Capacitive coupling problems can be avoided by careful wiring layouts that separate transmitter and receiver wires as much as possible. However, this scheme is limited in cross-borehole geometries, where wires are forced to be proximate. It is shown using equivalent circuit models and field measurements that increasing the receiver input impedance solves some of the capacitive coupling problems.

References

- Börner, F., Gruhne, M., and Schön, J. (1993). Contamination indications derived from electrical properties in the low frequency range. *Geophysical Prospecting*, 41:83–98.
- Dey, A., and Morrison, F.H, 1973, Electromagnetic Coupling in Frequency and Time-Domain Induced Polarization Surveys Over a Multilayered Earth, *Geophysics*, **38**, 380-405.
- Hallof, P.G., 1974, The IP Phase Measurement and Inductive Coupling, *Geophysics*, **39**, 650-665.
- Madden, T. R. and Cantwell, T. (1967). Induced polarization a review. *Mining Geophysics, Society of exploration geophysics*, 2:373–400.
- McKinley, K. S. (2003). Nonlinear complex resistivity to investigate clay-organic reactions at the savannah river site, south carolina. Master's thesis, Colorado School of Mines.
- Morgan, F.D., T.R. Madden, and Bennett, B.R., 1986, An instrument system for low frequency (10-3 -103 Hz) impedance measurements, *IEEE, Inst. and Meas.*, 35, 287–293.
- Olhoeft, G.R. (1979) Nonlinear electrical properties, in Neel, L., ed., in *Nonlinear Behavior of Molecules, Atoms and Ions in Electric, Magnetic or Electromagnetic fields: Amsterdam, Elsevier Publishing Co.*, p. 395-410
- Olhoeft, G. R. (1984). Clay-organic reactions measured with complex resistivity. 54th Ann. Internat. Mtg., Soc. Explor. Geophys., Expanded Abstracts, pages 356–357.
- Pelton, W.H., Ward, S.H., Hallof, P.G., Sill, W.R., and Nelson, P.H., 1978, Mineral Discrimination and Removal of Inductive Coupling with Multi-Frequency IP, *Geophysics*, **43**, 588-609.

- Pelton, W.H., Sill, W.R., and Smith, B.D., 1984, Interpretation of Complex Resistivity and Dielectric Data Part II, *Geophysical Transactions*, **30**, 11-45.
- Pelton, W.H., Sill, W.R., and Smith, B.D., 1983, Interpretation of Complex Resistivity and Dielectric Data Part I, *Geophysical Transactions*, **29**, 297-330.
- Seigel, H. O., 1959, Mathematical Formulation and Type Curves for Induced Polarization, *Geophysics*, **24**, 547-565.
- Sumner, J.S., 1976, *Principles of Induced Polarization for Geophysical Exploration*, Elsevier Scientific Publishing Company.
- Ward, S.H., and Hohmann, G.W., 1988, Electromagnetic Theory for Geophysical Applications, in *Electromagnetic Methods in Applied Geophysics*, Editor: Misac N. Nabighian, SEG, 131-311.